HIGH DISPERSION SPECTROSCOPY OF MOLECULES IN THE SOLAR ATMOSPHERE

by

MIRUPAMA S.

A thesis submitted to the
University of Madras
for the degree of
Doctor of Philosophy

Kodaikanal Observatory
Kodaikanal
January, 1965.

CERTIFICATE FROM THE SUPERVISOR.

I certify that the thesis entitled "HIGH DISPERSION SPECTROSCOPY OF MOLECULES IN THE SOLAR ATMOSPHERE" by Nirupama S. is a record of the research carried out by her at the Kodaikanal Observatory. The candidate has worked on this thesis under my supervision since September 1961. I declare that the thesis has not previously formed the basis for the award of any Degree, Diploma, Associateship, Fellowship or similar title. The thesis contains an account of photoelectric and photographic observations made by the candidate herself with the Kodaikanal solar tower and spectrograph along with the detailed calculations of velocities and temperatures made by her on the basis of the observations and with suitable computational aids.

M K Vainu Bappu

(M.K. Vainu Bappu)
Director
Kodaikanal Observatory.

ACKNOWLEDGEMENTS

The work reported in this thesis was carried out during the tenure of a Senior Research Scholarship kindly awarded by the Ministry of Education.

I am ever grateful to Dr. M.K. Vainu Bappu for having initiated me in the study of Astrophysics. He has been the main source of inspiration and guidance behind every aspect of work presented here. It is his deep personal interest and concern, that have made the production of this thesis possible at all.

I am much obliged to Mrs. Yamuna Bappu for having been so charmingly kind and understanding on every occasion and for the keen interest she has displayed in my welfare.

The number of things for which I am perennially indebted to Mr. A. Bhatnagar are too numerous and varied to be listed. Right from the instrumentation and observing programme down to drawings in the thesis and checking references he has lent a hand. It gives me great pleasure to look back on three years, spent in mutual co-operation.

I am thankful to Mr. K.G.A. Raheem and Mr. A.P. Jayarajan for having so readily helped me in some aspects of my observing programme.

My grateful thanks are due to Mr. T. Mark, for help rendered at the Telescope.

I must express my deep sense of obligation to the staff computer centres at Indian Institute of Technology, Kanpur and Guindy Engineering College for allowing me such a liberal use of the IBM 1620 time.

I am grateful to Mr. A.M. Ghouse for help with the drawings, to Mr. M. Jan for assisting in photographic printing and Mr. S. Vellaichamy for his help.

I am extremely obliged to the group of typists Messrs. A.L. Batcha, N. Vasudarajan and S. Sundararajan, who have made a such speedy and neat job of typing the thesis.

I am also very grateful to Mr. C.S.Veeraraghavan, Mr. & Mrs. Krishnamurthy for their valuable help.

I am obliged to Dr. A.S. Ramanathan, Messrs. D.N. Bhargava, P.I. Nayar, K.S. Ganesh, L.M. Punetha and J.V. Narayana, for the interest they have displayed in my progress.

It is a pleasure to thank the Director General of Observatories for having kindly granted permission to work at the Kodaikanal Observatory.

TABLE OF CONTENTS

TABLE OF CONTENTS

Supplement to the thesis. Paper on "An Analysis of Eruptive Prominence Motions"

SUMMARY.

In this thesis I have attempted to derive the thermal and velocity structure of the uppermost photosphere and the very low chromosphere through a study of line profiles and equivalent widths of C_2, CH and CN. This investigation was carried out at the Kodaikanal Observatory using the 36 metre solar tower telescope and the 18 metre Littrow spectrograph.

The current status of velocity and temperature determinations is outlined in Chapter I. This also considers the suitability of using molecular lines for studying the transition region between the photosphere and the chromosphere.

Chapter II specifies the observational requirements for the study and describes the observing techniques. The use of a large solar image in conjunction with high spectrographic dispersion and resolution, provides a very reliable set of data. The performance of the instruments and the details of corrections applied to the observations are also given.

Equivalent width measurements are presented in Chapter III. These are of photographically observed C_2 lines. Rotational temperatures are derived for six positions on the solar disc, representing the variation in

temperature over an optical depth range covering the region $\zeta = .04$ to $\zeta = 0.06$.

The criteria for choosing lines for the line profile analysis are listed in Chapter IV. Here I also summarize the measuring techniques of the photoelectric line profile scans. A high degree of internal consistency of the data is achieved. A detailed description of each line together with the trends in the observed centre-limb variation of profiles is also given. The dominant features of the observed variations are, that all profiles tend to become U-shaped towards the limb, and that the trends in the variations are characteristic of the strength of the line rather than the molecule.

Chapter V sets up the basic methodology and assumptions underlying the construction of a theoretical line profile. It gives details of the choice of parameters entering the calculation and the calculation of the continuous absorption coefficient and continuum intensities. It presents in full detail, the various factors required in the calculation of the line absorption coefficients.

Chapter VI briefly describes the line intensity calculations with particular reference to the doublet profiles. The results of the fitting of a computed doublet profile to the observed profile is discussed

~~is discussed~~ step by step, for different combinations of doublet separation and turbulent velocity. It is clearly seen that only a unique combination of separation and turbulent velocity would provide a satisfactory fit at the centre of the disc. However, for any given doublet separation, there is a single velocity which gives the best over all fit of a computed profile to the observed one. For three lines 3964A, CN, 4207A, CN and 5094A, C_2 of Rowland intensities ranging from 3 to -2, a perfect fit is obtained with 3 km/sec. for the radial turbulent velocity at the centre of the disc. The fits obtained for the other positions on the limb by changing the tangential turbulent velocity are, however, not good. But the most reasonable fits are obtained for ξ_{tan} =3.6 km/sec. The profiles for three other lines, 4210A, CN, 4281ACH, and 5147AC_2 are computed under the singlet assumption, and yield 4.0 and 5.05 km/sec. for the radial and tangential velocities respectively. The difference in the two sets of values obtained for the velocities is explained in terms of the differences arising out of treating the profile as singlets, while ~~as~~ in actual fact they are doublets.

An interesting feature of how a variation in the fitting factors for central intensities improves the profile fits for disc positions other than the centre is also

reported. The important point is that good fits are obtained for the same set of radial and tangential turbulent velocities i.e., 3.0 km/sec. and 3.6 km/sec. respectively for the doublet assumption and 4.0 km/sec. and 5.05 km/sec. for the singlet assumption. Also of significance is the fact that the variation of these fitting factors' from centre to limb is very similar for different lines.

This linear and parallel variation of the fitting factors seems physically very significant and points directly to deviations in partial pressures of the molecules from the conventional values.

Summarizing the results of the computations and their comparison with observation, Chapter VII examines the validity of the LTE assumption for the line profile analysis.

In conclusion, while it is almost certain that rotational line formation takes place under LTE conditions, non-LTE effects are probably indicated when the dissociation equilibrium of molecules are concerned. Inspite of the uncertainties surrounding physical constants for molecules, they offer the best hope for deriving better and better approximations to the physical structure of the highest layers of the photosphere.

CHAPTER I

THE NATURE OF THE PROBLEM

The physical structure of the solar atmosphere is assumed to be controlled by the radiation field, in the first approximation. The thermodynamic state of such an atmosphere is completely specified by the triple conditions of radiative equilibrium, hydrostatic equilibrium and local thermodynamic equilibrium fixed by the local energy density of the radiation field. In the analyses of solar spectral lines, velocity fields other than thermal, are considered only in the second order approximation where they are expressed in terms of line-of-sight velocities.

One of the most interesting problems in present-day solar physics is to study the interaction between the thermodynamic state and the velocity fields of the solar atmosphere and thereby interpret a wide variety of observed deviations from the classical picture. Direct analyses in this direction require detailed fore-knowledge of all the physical processes involved and therefore are restricted in their application to a very few cases. A more universal and flexible approach has been to obtain the thermodynamic and hydrodynamic states of the solar atmosphere independently, in classical terms in the first approximation, and consider the exact problem of interaction of the two in the next approximation.

The thermal structure as derived from continuum observations and radiative transfer theory is well established for the photosphere. Reasonable estimates of this structure for the upper chromosphere are also available from eclipse data. In the intervening region particularly in the region of transition from the photosphere to the chromosphere, the temperature distribution remains somewhat uncertain.

For the other part the velocity fields are not at all well determined and a fairly detailed review of the present status is useful.

To know the velocity structure of the solar atmosphere to the same degree of detail as P_g, P_e, T_e etc. are known as functions of optical depth, the velocity distribution over the entire observable solar atmosphere must be determined. In other words velocity should be established as an additional parameter of the model solar atmosphere.

The observed velocities in terms of line-of-sight motion are available from the following three classes of data:

(i) Small scale velocity fields tend to change the shape of the curve of growth, effectively prolonging the portion for which the equivalent width of the line varies linearly as the effective number of line-forming atoms and thus raise the transition part of the curve of growth.

(ii) The uniform motion of the entire line-forming region,

displaces the line as a whole i.e. the line is Doppler shifted. The velocity can therefore be determined by measuring the wavelength shift with respect to the undisturbed position.

(iii) The contribution of random and non-random motion which both displaces and broadens the line, is observed in the details of shape of a line profile. In such a study one determines the frequency dependence of the line absorption coefficient. The frequency dependence in the core of the line is entirely decided by the local velocity field; thus, if the thermal velocity field can be separated from the empirical velocity field derived from the ν dependence of α_ν a measure of the non-thermal velocity field is obtained.

The velocities derived from each of the above types of analysis, however, do not refer to the same physical situation. This is essentially because the field of motion in the solar atmosphere is visualised as an irregular one, capable of being described usefully only by statistical parameters. There is a hierarchy of characteristic dimensions, over which the energy of mass motion is transferred to smaller and smaller sizes, finally to be destroyed by viscosity and dissipated as heat. Thus the difference between the velocities derived by the three methods is to be understood in terms of the "scale of turbulence" most relevant to any one particular type of analysis. This may be seen in the following way.

Let L_o be the representative dimension of the range of sizes over which energy from kinetic energy of mass motion is fed into the system. This dimension L_o is generally assumed to be of the order of scale height of the atmosphere. A 'turbulent' field is classified as micro or macro-turbulent according as $L_o\chi \leq 1$ or $L_o\chi \gg 1$, χ being the absorption coefficient.

In a curve of growth analysis where one is mainly concerned with the equivalent width, the elements which are of consequence are those which have $H\chi \leq 1$. Here H is the effective height of the line forming region. These elements are small with respect to the length of the line forming region and widen the line in a manner exactly analogous to the thermal velocity field. Thus, curves of growth give microturbulent velocities from the location of the flat part of the curve of growth and pertain to the highest layers of the photosphere and hence cannot be compared directly with other velocity determinations. Further, the conventional basis of curve of growth analysis itself is being questioned in the light of possible deviations from LTE (Pecker 1957, 1959). Thus values of velocities derived from curves of growth are necessarily ill understood and offer little hope of arriving at a 'model' of velocities for the solar atmosphere.

The second class of data, where the line is displaced as a whole, should obviously be associated with motion which

is large compared to the length of the line forming region, i.e. $H\chi \gg 1$. The results derived from Doppler shifts suffer from limitations of geometrical resolution, and although recent analyses of Richard and Evans (1962a; 1962b; 1962c) give exciting results regarding the oscillatory nature of the solar atmosphere, the results do not cover the lower chromosphere in specific detail.

Finally in a line profile, one essentially observes the situation at a total optical depth of $\tau \approx 1$ so that $H\chi \gtrsim 1$. The line is thus both displaced and widened in a complicated fashion.

It is seen, therefore, that each of the types of analysis corresponds to a different region of the velocity spectrum established by the turbulent field. The values of velocities given by the different analyses should therefore be assigned to the correct scale of elements in each case. If the mean layers to which these velocities refer cover the entire atmosphere, then a consistent picture of the velocity structure could be derived.

Of the three methods, the study of line profiles offers the greatest scope for extension, to cover many aspects of the problem of determining the velocity structure of the solar atmosphere. As mentioned earlier, the primary part of the investigation consists of determining the frequency profile

of the absorption coefficient. With this as the basis, the analyses so far have proceeded along slightly different ways.

The earliest attempts equated the shape of the line profiles of weak lines to that of the absorption coefficient. Studies in this direction have mainly concentrated on selecting appropriate forms, for the absorption coefficient. Fitting with Voigt profiles has been adopted by Van de Hulst (1946), Allen (1949) and Rogerson (1957); and Allen suggests an anisotropic velocity field. All the velocities obtained by them refer to fairly deep layers of the photosphere ($\tau = 0.3$).

Synthetic profiles have been constructed by Waddell (1958) and Suemoto (1958) from detailed model atmosphere calculations. Waddell equates the source function to the Planck function at the electron temperature, while Suemoto considers the Planck function at an appropriate temperature of excitation. Waddell explains centre to limb observations of central intensity and half-half width in terms of anisotropy with $\xi_{Lam} = 3.0$ km/sec and $\xi_{rad} = 1.8$ km/sec. refering to $\tau = 0.3$ and no depth dependence. Suemoto considers ascending and descending elements so that there is both depth variation and angular dependence i.e., the velocity decreases with height as the element slows down while ascending, and when it turns to descend a horizontal motion predominates ($\tau = 0.4$), giving a marked angular dependence at this depth.

The most extensive determination of $\Delta\lambda_D$ with τ is by Unno (1959). Using Goldberg's method (1958) for determining $\Delta\lambda_D$ in terms of ratio of oscillator strengths of two lines of a multiplet, and Milne-Eddington model for fixing τ he has mapped the velocity from about -400 km. to nearly +2500 Km.

Figure I-1 sets out values of velocities derived from line profile analyses, by the various authors. We notice no determinations between -100 and +300 km. corresponding to the shaded region between the two dark lines. It should be recalled that it is precisely in this region that the temperature structure is also uncertain.

One of the main reasons for lack of data over this height range is its relative inaccessibility. This region is too high for investigation through centre-limb studies of photospheric lines and too low for eclipse analyses. The cores of strong Fraunhofer lines like that of CaII H and K and the Balmer lines of hydrogen are formed over a range of layers located among the higher layers and cannot, therefore, be used for determining effectively the physical structure of this region alone. The most useful agents for elucidating the structure of this region are the molecules. It is well known that a temperature inversion occurs in this region with $T_{min} \approx 4500^{\circ}K$ and that there is an increase in temperature on either side. Molecules tend to dissociate with increasing temperature and, therefore, are capable of existing in large

FIGURE I-1.

The known variation of turbulent velocities with height in the solar atmosphere. The shaded area is the region of interest in this investigation; triangles represent Unno's results and circles the results of other workers.

Fig. 11

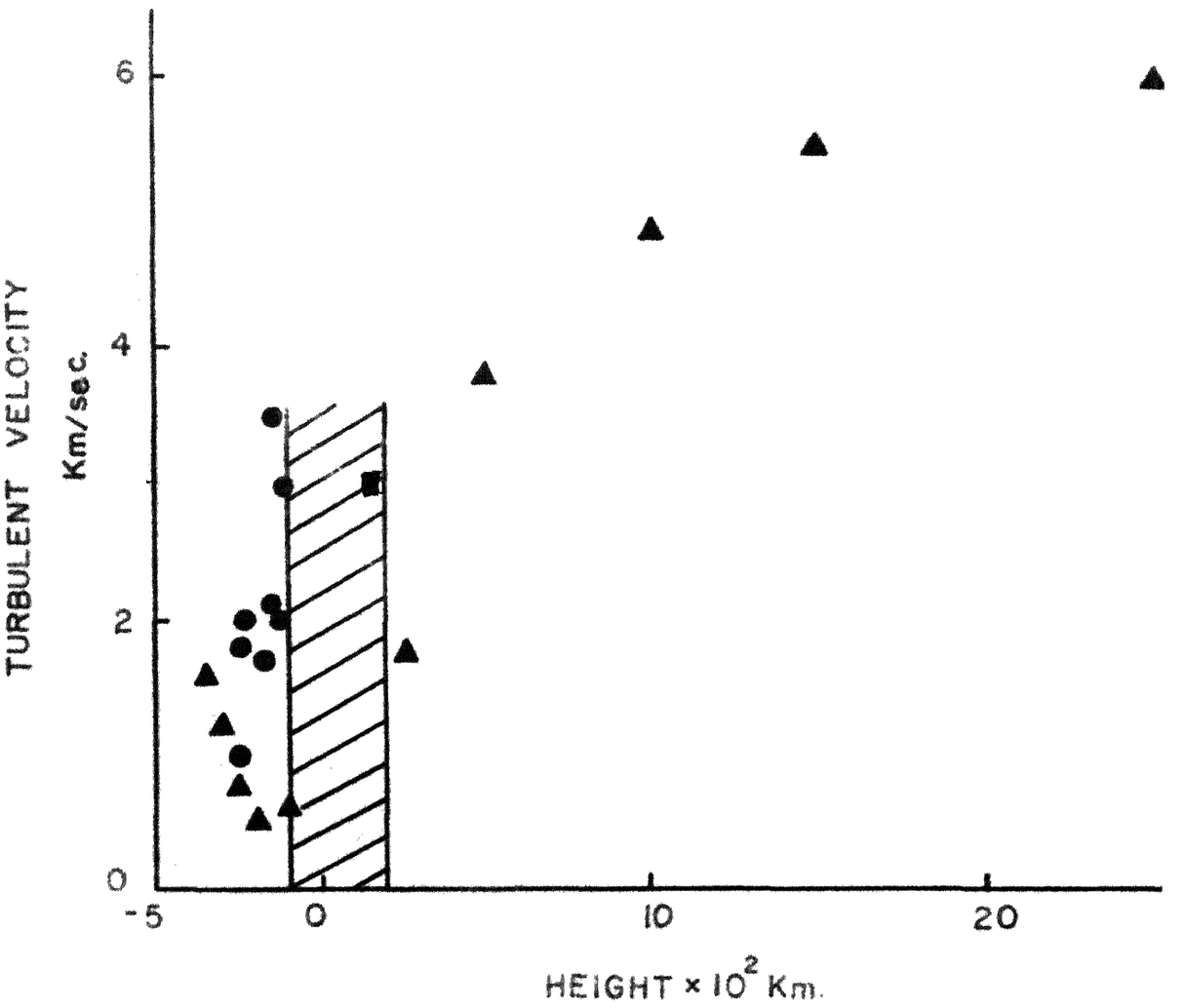

numbers, only in a narrow region around the temperature of inversion. With the molecules concentrated exclusively in this region of interest, which is not easily accessible for investigation otherwise, molecules become a natural choice for investigating the structure of this region - a point well emphasized by Oster (1957).

As mentioned at the outset, one of the possible semi-empirical approaches to the problem of coupling the velocity and radiation fields, perhaps requires as a first step, the complete specification of the temperature and velocity structures from analyses based on classical assumptions. It is realised at once that even at this stage the two problems are bodied inseparable. The absorption coefficient profile α_ν and, therefore, the local velocity field, depend strongly on the temperature structure. It would also be relevant to examine the exact mode of molecular line formation, whether deviations from LTE are already in evidence in the region where molecules are formed. Existing opinions on this point are widely divergent. In view of the very crowded nature of the rotational energy levels in a molecule it seems reasonable to expect that molecular lines are formed by pure absorption with the source function for the line being identical with the Planck function appropriate to the local electron temperature (Cowley 1964). Thus in discussing the α_ν profiles, atleast the mode of line formation is known with reasonable certainty.

there are, however, strong arguments presented, supporting non-LTE effects influencing molecular line formation in order to explain the observed centre-to-limb variations of equivalent widths of molecular lines (Becker et al 1949, 1950, 1951, 1957, 1960). This point will be discussed in detail in a later chapter.

The points raised above are common to all line profile investigations and from several standpoints molecules seem the best tools to probe into the structure of the upper photosphere and the very low chromosphere (cf. Ch. 1). However, several uncertainties characteristic of the molecular problem arise.

The first of these is an observational one, in that molecular lines are very crowded. A meaningful analysis of these lines relies heavily on having available an optimum combination of high spectrographic dispersion and resolution. The second problem is to take into consideration, in a detailed fashion, the peculiar distribution of molecules in the atmosphere. The distribution depends on:

a) Dissociation temperature of the molecules
b) Competition between the various atoms to form different molecules, as decided by the thermodynamic structure of each layer.

The most elegant treatment of this problem is due to Russell (1934), who expresses both factors in terms of the temperature

variation of the dissociation constant K_{AB} for any molecule AB. More recently de Jager and Neven (1957) and Stenger (1963) have prepared extensive tables of partial pressures of molecules at different temperatures by considering diatomic molecules alone, for six different sets of abundances.

Early investigations of molecules in the sun, concentrated primarily on their identification (Richardson 1931) (Babcock 1945), by the wavelength coincidence method and the determination of rotational excitation temperatures (Berge 1922; Richardson 1931; 1932; 1933). Roach (1939) attempted to derive abundances of C_2, CN, CH, OH and NH in the sun by calculating detailed partition functions for each of them and using the then available estimates of intensity of the molecular lines.

A centre to limb study of molecular carbon by Adam (1938) indicates an increase of temperature towards the limb. Her results, however, have rather large probable errors. Blitzer's (1940) value of $4490^{\circ} \pm 100^{\circ}$ is one of the best estimates of excitation temperature for the CH molecule.

The first systematic and accurate temperature and abundance determination is due to Hunaerts (1947). His analysis is based on the equivalent widths measured from the Utrecht Photometric Atlas and comparing them with equivalent widths computed from a Schuster-Schwarzschild model with $N_J^{\chi} \cdot f$ as the adjustable parameter. The abundances are

estimated from a molecular curve of growth.

Centre-to-limb studies of unresolved and resolved molecular lines by Becker and Peyturaux (CH, CH 1949) Becker (CH, 1950) Becker and Becker (C_2, 1950) bring to focus the problem of distribution of molecules in the top layers of the atmosphere. In the analysis of resolved lines of CH and C_2, theoretically computed centre to limb curves have been compared with observed ones.

The theoretical equivalent width is given by

$$W(\theta) = \frac{\pi e^2 \lambda_0^2}{mc^2} f \int_0^\infty y(\bar{c})\, n(\bar{c})\, h(\bar{c},\theta)\, d\bar{c} \qquad (1.1)$$

where $y(\bar{c})$ is the ratio of number of CH molecules to the number of neutral hydrogen atoms and $n(\bar{c})$ the fraction of CH molecules effective in forming the line. The weighting function $h(\bar{c})$ calculated on the basis of pure scattering compares well with observation - a conclusion opposed by Unsold on the ground that the complexity of the energy levels in a molecule ensures the formation of lines through pure absorption.

Minnaert (1949) derived theoretical excitation temperatures of molecules by applying the method of weighting function and incorporating temperature variation of the dissociation constant $K_{AB}(T)$ into an expression for equivalent

width similar to equation 1.1. He obtains temperature values too high compared to rotational temperatures, but in the same range as T_{exc} derived from central intensities of certain CH lines by Pecker and Praderie (1960) - interesting point for discussion.

Molecular lines in emission have been used to determine temperatures in the very low chromosphere (Blackwell 1953; Parker 1955; Pecker and Athay 1955; D.V. Thomas 1958) and give varied values for temperatures. Of these, Parker alone has high dispersion spectra, but is obliged to make uncertain corrections for scattered photospheric light.

Vibration-rotation bands of CO in the infra-red have been analysed (Goldberg and Muller 1953) and yield a value of 4300°K for the excitation temperature. Using the same data Newkirk (1957) obtains 4880°K for the centre and 4590°K for the limb. He finds that the centre-limb variations of CO lines can be explained by the Minnaert solar atmosphere model with pure absorption (Minnaert 1953) and that CO is concentrated in a very narrow layer at the top of the atmosphere.

The empirical approach to deviation from local thermodynamic equilibrium developed by Pecker (1959) has been applied by Pecker and Praderie (1960) to selected CH lines. The T_{exc} values obtained are around 5700°K and are very much higher than T_{rot}. This has been explained in terms of the different energy levels and the ratio of population of the

levels involved which corresponds to $^2\Pi$ and $^2\Delta$ respectively. T_{rot} corresponds to the ratio of populations of levels very near $^2\Pi$ state while T_{exc} corresponds to ratios of populations of electronic levels $^2\Delta$ and $^2\Pi$. Also the centre-limb observations are described in terms of g' weighting functions given by

$$g' = g_{pure\ absorption} + g_{non.LTE}$$

with

$$g_{non.LTE} = \frac{B(T_{el}) - B(T_{exc})}{B(T_{el})\, e^{-\tau/\mu}}$$

Even so, the agreement between the observed and computed curves is not complete.

Laborde (1961), on the other hand forwards the suggestion that it is the formation of polyatomic molecules including carbon, rather than non-LTE effects, that are more important in explaining the centre-limb variation of molecular lines. The most significant of Laborde's results is that he is able to explain centre-limb variation of certain MgI lines on the basis of equivalent widths calculated from the Minnaert-H.A.O. model but the centre-limb variation of C_2 lines cannot be explained similarly. Considerations using (i) alternate values for dissociation potential of C_2, (ii) inhomogeneities in the photosphere (iii) formation of tri-or polyatomic molecules involving carbon, fail to bring about satisfactory agreement

between observed and computed curves.

Accurate measures of equivalent widths by Cowley (1964) indicates that although pure absorption mechanism fails to explain the observed centre-limb variation correctly, the good agreement obtained for the centre of the disc confirms its validity atleast at the centre.

The work done so far covers the following ground:

1) Derivation of T_{rot} assuming a Boltzmann distribution among the rotational energy states. Equivalent widths of lines of different J values are measured and T_{rot} is determined from the relation.

$$W \propto i_J \exp(-B_0 J(J+1)hc/kT)$$

where i_J are line strength factors. The consistent results obtained for the rotational temperatures using different molecules, proves this wide range of validity of the above assumption.

2) Examination of the mode of line formation. Equivalent widths of lines at various J values are measured and the observed centre-limb variation of the ratio $W(\mu)/W(1)$ has not been explained either by the assumptions of pure absorption or pure scattering, even with non-LTE effects included. As noted earlier while the complexity of the rotational energy levels should ensure pure absorption the presence of deviations from local thermodynamic equilibrium in the upper chromosphere calls

for a re-examination of this question for the molecules. On the other hand the failure of conventional non-LTE methodology to describe centre-limb variation of equivalent widths leads one to ask if it is justified in treating non-LTE effects on molecules in the same way as in atoms, particularly in view of the good agreement between observed equivalent widths and those computed on the basis of pure absorption, obtained by Cowley (1964). It is also very crucial to bear in mind that conventional treatment explains centre-limb variation of MgH and CO and disagrees markedyonly in the case of C_2, CN and CH.

3) <u>The height distribution of partial pressures.</u> The problem of distribution of molecules has been extensively considered. The most comprehensive way in which they can be taken into account is to include the partial pressure appropriate to each layer of the model atmosphere used.

4) <u>Turbulent velocity fields inferred from molecular lines.</u> Only two investigations (Allen 1949; Wehlau and Wehlau 1956) have utilised molecular lines to determine turbulent velocities. Allen treated them along with other atomic lines and deduced an anisotropic velocity field with $\xi_{rad} = 1.9$ Km/Sec and $\xi_{tan} = 3.0$ km/sec. Wehlau and Wehlau have used the molecular lines precisely to measure velocities in the top most layers and obtain 3.5 km/sec. Details of the investigation, however, are not available.

Any fresh analysis of molecular lines must also take into account the uncertainties arising from

a) lack of knowledge of correct dissociation potentials for molecules of interest,

b) uncertainties in f values of the electronic transitions of the molecules,

c) the effect of formation of unknown molecules on the distribution of partial pressures of molecules with depth and,

d) incomplete knowledge of exact processes by which inhomogeneities of the photosphere extend into the transition region, affecting normal process of line formation.

It is seen, therefore, that five different aspects and the associated uncertainties listed below enter in a study of molecular line profiles.

(i) Temperature structure of the very low chromosphere.

(ii) Velocity structure pertaining to this region.

(iii) The distribution of partial pressures of the molecules and dissociation equilibrium appropriate to the temperature.

(iv) The exact mode of line formation.

(v) Uncertainties in the molecular constants.

The determination of the velocity structure requires that each of the above aspects be taken into consideration. The only satisfactory answer to the problem would be one that predicts the observed profiles and their centre-limb variation, after considering the question from each of these stand points.

Atleast part of the uncertainties associated with the temperature structure of the very low chromosphere may be reduced by deriving molecular rotational temperatures. Molecules provide an independent method of deducing the temperature structure of this region. The crowded nature of the rotational energy levels is an advantage in this respect in that the excitation temperature derived is most likely to be identical with the kinetic temperature. Also the determinations do not require the knowledge of f-values of electronic transitions. The intensity distribution over the rotational energy states is strictly a function of rotational transition probabilities and the statistical weight of the lower level. These intensity factors are well known functions of the rotational quantum number J and the temperatures derived are far more certain than those obtained from other techniques. A centre-limb variation of these rotational temperatures gives additional information on the depth variation.

Although it is very unlikely that any one set of physical assumptions along with a set of observations would satisfy all the conditions, it is believed that an investigation in this direction should keep in sharp focus all the constituent aspects of the problem and the conclusions drawn therefrom should be weighted in accordance with all the uncertainties that enter the problem.

THE OBSERVATIONAL TECHNIQUES

2.1. General.

The main part of the work on molecules has been aimed primarily at rotational temperature determinations. There are a few analyses which have concentrated on centre-limb variation of equivalent widths of selected lines. Table II-1 sets out the details of these analyses.

The tabular summary of the observations on molecules shows that all analyses refer to equivalent width measurements, most of which are based on photographic data. Considering the fact that simultaneous studies of several molecules have been aimed at rotational temperature determination and also due to the very complex and crowded nature of molecular spectra, photographic measurements of equivalent widths is perhaps the best possible approach. Photographically determined centre-limb variation of equivalent widths of resolved lines suffer from the inherent inaccuracies due to low quantum efficiency, non linear response and non-uniformities arising out of the processes of developing and fixing. Therefore, at best these studies are capable of providing evidence of the general trends of the results. Photographic measurement of central intensities suffer the additional distortion due to scattered light in the spectrograph, corrections to which can be made only approximately.

Table II-1

Author	Year	Description of data	Molecules studied	Type of analysis.
Dyge	1922	Photographic	CN	Intensity estimates to determine J_{max} and, therefore, T_{rot}
Richardson	1931 1932	Photographic	C_2 and CN	Intensity estimates for many J values and T_{rot} determination and pressure over a sunspot.
Roach	1939	Photographic	CH, C_2, CN, NH, OH	Calibrated Rowland intensities for obtaining molecular abundances.
Klitzer	1940	Photographic	CN	Equivalent width measurement as a function of J and therefore, T_{rot} determination.
Adam	1950	Photographic	C_2	Equivalent width measured over a range of J values and T_{rot} determination.
Munaerts	1947	Photographic	CH, CN, C_2, NH, OH	Accurate equivalent widths for determining rotational temperatures and abundances.

Table II-1 Continued.

Author	Year	Description of data	Molecules studied	Type of analysis.
Pecker and Peyturaux	1949			Approximate equivalent width estimates. Centre-limb study.
Pecker and Pecker	1950	Photographic	CN, CH and C_2	
Pecker	1957			
Goldberg and Muller	1953	Photoelectric	CO	Accurate equivalent width measurements leading to rotational temperatures.
Newkirk	1957	Photoelectric	CO	Accurate equivalent widths compared with standard models giving both centre-limb variation of equivalent widths and the rotational lines.
Pecker & Fradorie	1960	Photographic	CH	Central intensities to derive empirically, deviations from LTE. Also centre-limb variation of equivalent widths.
Laborde	1961	Photographic	C_2, CH, CN, OH, MgI and NH	Equivalent widths for T_{rot} determination in spot and disc. Also centre-limb variation of selected C_2 and MgI lines.
Cowley	1964	Photoelectric	CH	Accurate equivalent width measurements from centre to limb observations compared with synthetic singlet Doppler profiles. Rotational temperatures also determined and discussed.

The two accurate photoelectric measurements of centre-limb variation of equivalent widths deal with CO and CN (Newkirk 1957; Cowley 1964) respectively and are not an integrated study of several molecules.

In view of the survey of the molecular problem both from the observational and interpretative standpoints, the objectives of a fresh set of observations of molecular lines are fairly clear. It seems necessary to treat the problems of velocity and temperature structure simultaneously and a line profile analysis offers the best means of studying temperature and velocity effects at the same time.

Although both temperature and velocity variations affect line profiles in an analogous fashion, the thermal properties of the solar atmosphere are essentially isotropic over any volume element, while the velocity features need not necessarily be isotropic. Therefore, by studying line profiles from centre to limb it should be possible to distinguish between the two.

The most interesting feature among the centre-limb studies of molecular lines is that pure absorption and conventional models are capable of explaining observations pertaining to MgH and CO but not those of C_2, CN and CH. The good agreement between theory and observation in the case of MgH is to be expected, as the effective layer of MgH line-formation relates to fairly deep layers in the

photosphere. But CO lines are formed in the highest layers of the atmosphere. It is very significant, therefore, that CO lines can be explained in terms of pure absorption and conventional models, while, very large discrepancies prevail in explaining C_2, CN and CH equivalent widths on a similar basis. Therefore, a fresh study of the carbon constituent molecules must be a differential study of all three molecules CN, CH and C_2.

The problem that we have set ourselves calls for certain specific observational requirements. Any attempt to study depth and angular dependence of physical parameters by observing centre-limb variation, would be assured of greater accuracy by the availability of a large solar image coupled with good seeing to yield high geometrical resolution. The line profile analysis planned demands a high spectral resolution coupled with appropriately large dispersion. Again, a high degree of photometric accuracy is essential and corrections to be applied should be capable of being specified completely.

The following description of the features of the equipment used indicates that these requirements have been met to a large extent.

2.2. The instruments.

The 38 cm. solar tower telescope has been used in

this investigation. A 61 cm. fused quartz coelostat mounted on top of a 10.7 metre tower feeds a 38 cm. Grubb Parson two element achromat of 36 metre focal length. This gives a 34 cm. diameter image, having a scale of 5.5' of arc/mm. The coelostat is driven by an electronic clock, while the image is guided by an electromechanical system. The accuracy of guiding depended largely on the atmospheric seeing conditions at the time of observation. The image was guided with respect to a pattern of circles drawn at a specific set of μ values (1.0, 0.8, 0.6, 0.45, 0.35 and 0.25) and mounted at the plane of the focussed image. The spectrograph consists of a 20 cm. achromat of focal length 10.30 metres arranged in a Littrow system. The dispersing element is a Babcock grating having a 200 x 135 mm. ruled area with 600 lines/mm. and blazed in the fifth order at 5000A. In the observations presented in this work, only the fifth and sixth orders of the grating have been used.

To determine rotational temperatures C_2 lines of the Swan system were chosen. The C_2 lines are best suited for rotational temperature determinations because they are weak enough to be unaffected by saturation and strong enough for making reasonably accurate equivalent width measurements. The 5165A band of the C_2 $^3\Pi_g - ^3\Pi_u$ system was, therefore, photographed in the fifth order of the grating at μ = 1.0, 0.8, 0.6, 0.45, 0.35 and 0.25, covering a wavelength region of 50A.

To scan individual lines, a photoelectric scanner was built. It consists essentially of a housing for an unrefrigerated 1P21 photomultiplier mounted on the nut of a Hilger measuring screw, of 1 mm. thread. This screw was driven by a 1 rpm synchronous motor through a system of 1:3 gears. Thus a scanning speed of 3 mm/min was achieved. The average dispersion used in the study is 10 mm/A so that the scanning rate is 5mA per second, a speed well within the limits set by consideration of the response time of the amplifier-recording system and the resolving power of the grating.

The 1P21 photomultiplier with an S4 surface has a sensitivity curve which has a peak around 4300A. This is of particular advantage for this study which covers the range 3850-5100 A, with the majority of lines between 4200-4400A. The output of the photomultiplier is fed to a conventional D.C. amplifier with a maximum gain of 5×10^5 and the amplified output to a Brown recorder with a $\frac{1}{2}$ second time constant.

During all the observations, it was necessary to monitor the variation in sky transparency by a second photomultiplier. This photomultiplier is identical to that used for scanning but is located at some other part of the spectrum, preferably in the continuum. 10A from the

line of interest. This comparison photomultiplier is mounted on a sliding arrangement capable of moving in the focal plane of the spectrograph. This greatly facilitates in setting the monitor at the desired part of the spectrum. The output of the continuum monitor is fed to another D.C. amplifier identical to that used with the scanner. The amplifier output is recorded on an Esterline Angus chart recorder. Suitable simultaneous time marks were given both to the scanner and monitor traces which facilitates the matching of the two.

The scanner was located near the region of interest, by visual identification and the correctness of the setting checked by running several trial traces in both directions.

One of the important steps in the observing technique was to set the scanning slit exactly parallel to the line. To start with, a knife edge was made exactly parallel to an Iodine absorption line and the slit edge was made parallel with respect to this knife edge. As a later improvement a 45° mirror was placed immediately behind the second slit so that both slit and spectral line could be viewed simultaneously through an eyepiece attached at the side. One of the slit jaws was used as the knife edge and, therefore, enabled the setting of the slit directly parallel to the absorption line. A comparison of the two methods of setting

the slit showed that, both final alignments of the slit were identical.

The entrance slit of the spectrograph was always kept at 100 microns while the scanning slit was 30 microns wide. At the dispersion used the scanning slit isolated 3mA of the spectrum.

The width of the scanning slit was again decided on the basis of both resolving power of the grating and the response time of the amplifier-recorder system. Several combinations of lengths l_1 and l_2 of entrance and exit slits respectively were tried and it was found that the diffuse scattered light was least when $l_1 \propto l_2$. Therefore, both entrance and scanning slits were made 4 mm long.

To examine the effect of using wide entrance slits on the half-width of the instrumental profile the cadmium line 5085.824A was traced in the fifth order for entrance slits varying from 25 microns to 175 microns with a constant scanning slit of 22 microns. Figure II-1 is a plot of the square of geometrical slit width multiplied by dispersion $(S_g)^2$ plotted versus the square of the observed half-width in milliangstroms $(S_{eff})^2$ of the line. The linear relation satisfies the condition derived by Brodersen (1954) for emission lines.

$$S_{eff}^2 = S_g^2 + S_o^2$$

FIGURE II-1.

Slit width effects.

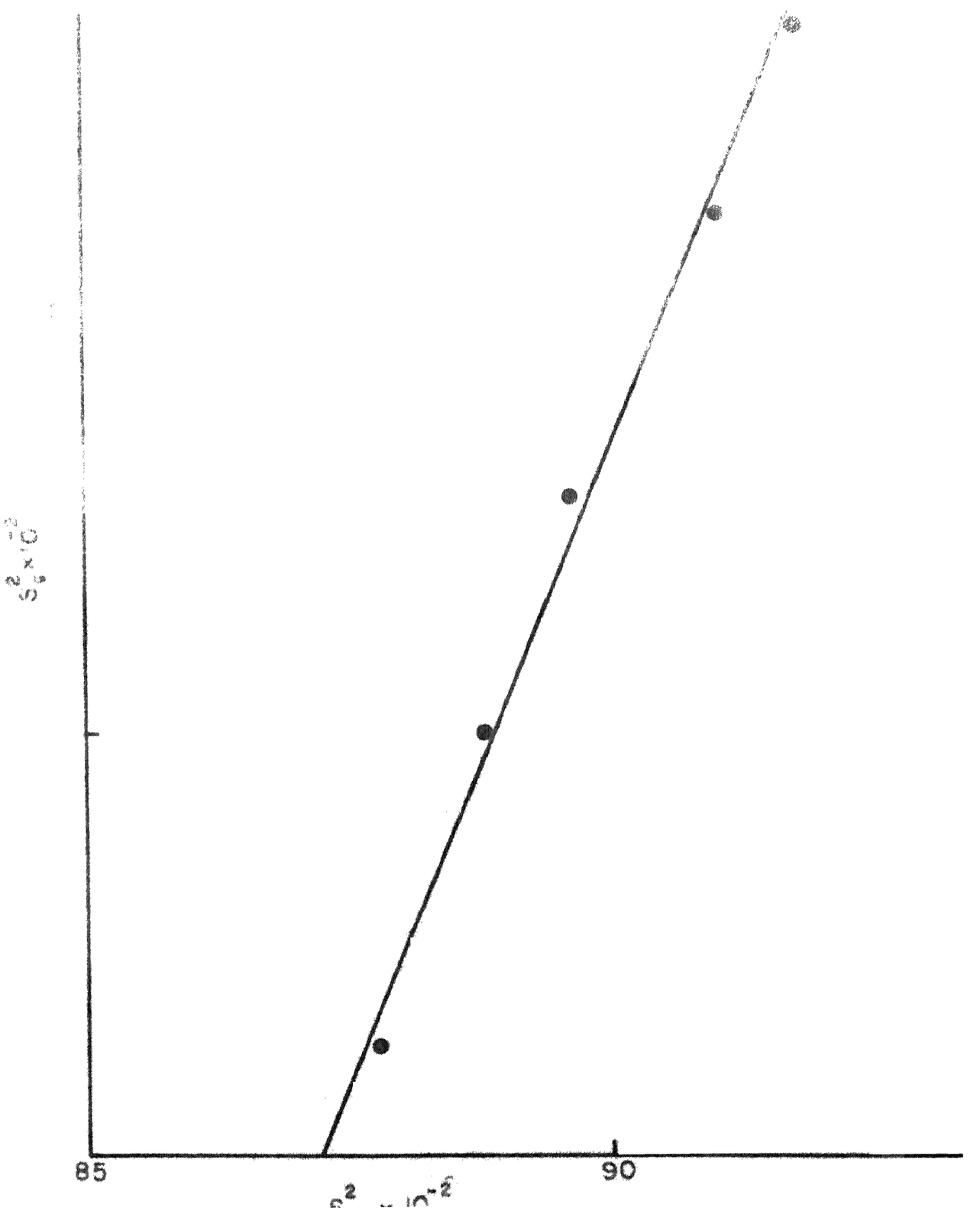
85
90

s_0^2 being the half width of the line that would have been obtained by an infinitely narrow scanning slit.

2.3. Instrumental Corrections.

For spectrographic studies directed towards line profile determinations, there are three requirements (Pierce 1957):

a) High resolving power.
b) Freedom from scattered slit.
c) Low intensity instrumental wings.

Ideally, if the entire theoretical resolving power of the grating is achieved, if there is no scattered light within the spectrograph and if the instrumental profile is that appropriate to that of the diffraction profile of the entrance slit used, the three conditions are fulfilled and no instrumental corrections are necessary. In practice, however, these are not achieved in full measure and appropriate corrections have to applied.

2.3a. Spectrograph Resolving Power.

To estimate the resolving power of the spectrograph, the absorption spectrum of Iodine was traced in the region of 5300Å in the fifth order.

A 10 cm. column of Iodine vapour was placed in the solar beam just ahead of the slit. The pressure was controlled by judicious evaluation, so that there was no pressure broadening. The optimum pressure was judged by visual examination of very close iodine doublets in the 5330A region.

With an entrance slit of 40 microns (2.4 normal slit) and a scanning slit of 22 microns, the set of doublets at 5330.10, 5330.33 and 5330.57A which are separated respectively by 9, 10 and 10mA are very well resolved as indicated in the reproduction of the trace in figure II.2. This separation corresponds to a lower limit of resolution of 600000 in the fifth order.

2.3b. Instrumental Profile.

The observed profile $g(x)$ of a line which is distorted by the finite resolving power of the instrument is given by

$$g(x) = \int_{-\infty}^{+\infty} h(x-y)\, f(y)\, dy \qquad (2.1)$$

where $f(y)$ is the true profile and $h(x-y)$ is the instrumental profile.

To evaluate the instrumental profile the Iodine single line at 5318.610A was used. This line was chosen for determining the instrumental profile because under optimum conditions of pressure in the Iodine tube, this line had a central intensity of 70% of the continuum and an equivalent width

FIGURE II-2.

A photoelectric scan of the Iodine absorption spectrum around 5330A which indicates the resolution of the spectrograph.

Fig. II 2

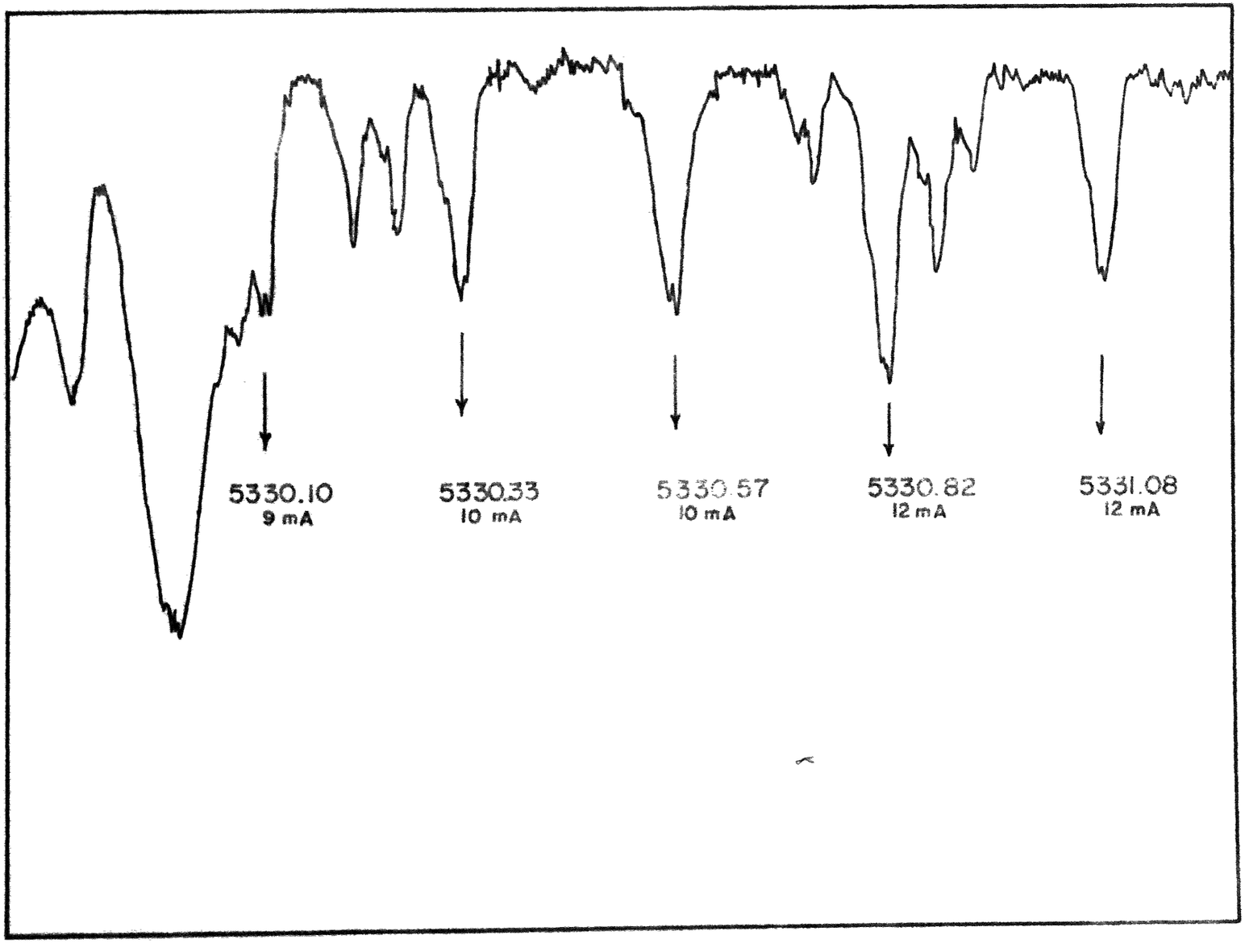

less than 5mA. The line is faint enough not to suffer from saturation effects and strong enough to provide accurate line profiles. Further the line falls in a region of the solar spectrum having a well established continuum. This line was traced in both directions several times and the mean instrumental profile derived from these traces for an entrance slit of 100 microns and scanning slit of 33 microns is given in Figure II-3.

The observed profiles have been corrected for the finite resolving power by the graphical method suggested by Bracewell (1955), which is quick and of useful accuracy. Bracewell's method essentially consists of expressing the true profiles as the sum of the observed profiles and a series of correction terms depending on the central differences of the observed profile. Multiplying equation (2.1) by $\exp 2\pi i x\delta$ and integrating from $-\infty$ to $+\infty$

$$G_1(\delta) = H(\delta) \cdot F(\delta)$$

where G, H and F are Fourier Transforms of g, h and f respectively.

Writing $$F(\delta) = \frac{G_1(\delta)}{H(\delta)} = G_1(\delta) + \left[\frac{1}{H(\delta)} - 1\right]$$

Assuming $H(\delta)^{-1} - 1$ can be expanded as a polynomial in $\sin^n \pi a\delta$ and $H(\delta)^{-1}$ an even function

$$H(\delta)^{-1} - 1 = \sum' U_n \sin^n \pi a\delta \qquad (2.3)$$

FIGURE II-3.

The instrumental profile. The dashed lines represent the diffraction profile for a 2.4 normal slit. The continuous curve is the observed instrumental profile.

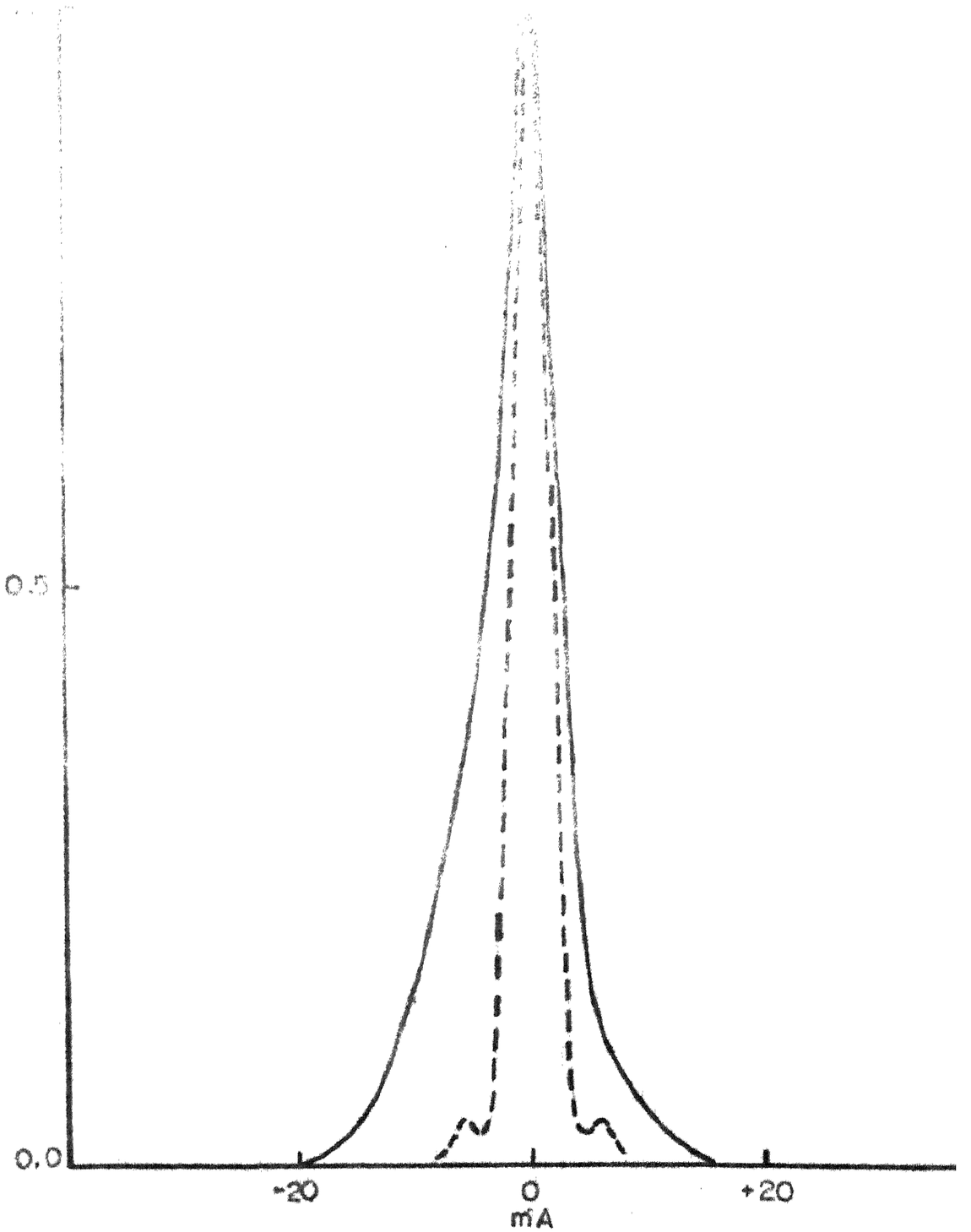
0.5
0.0
-20
0
+20
mA

n being +ve and even. Here U_n and a are to be fixed by specifying initial conditions. Substituting (3) in (2) and taking the Fourier transform again,

$$f(x) = g(x) + \sum_n U_n \Delta^n g(x) \qquad (2.4)$$

where the Fourier transform of $2_2 \sin \pi a s\, G(s)$ is $\Delta g(x)$. Δ represents the operation of central finite difference over the interval a. Considering only the first correction term

$$f(x) = g(x) - \tfrac{1}{4} U_2 \Delta^2 g(x)$$

Referring to Figure II-4 if a is known

$$f(x) = RP + \tfrac{1}{2} U_2 \delta P$$

U_2 and a are determined by noting that $U_2 \sin^2 \pi a s$ has the same curvature as $H(s)^{-1} - 1$ at $s = 0$. For small s

$$H(s) = \int_{-\infty}^{+\infty} \left[1 - \tfrac{1}{2}(2\pi x s)^2\right] h(x)\, dx$$

$$= 1 - 2\pi^2 s^2 \int_{-\infty}^{+\infty} x^2 h(x)\, dx = 1 - 2\pi^2 s^2 \sigma^2$$

$h(x)$ being the normalised observed instrumental profile

$$H(s)^{-1} = 1 + 2\pi^2 s^2 \sigma^2$$

$$H(s)^{-1} - 1 = 2\pi^2 s^2 \sigma^2 = U_2 (\pi a s)^2$$

The above condition shows that there is a certain amount of freedom of choice in fixing either U_2 or a . Usually is set equal to unity, so that $a = \sigma$ and is of the order of the instrumental half width. Chord span a for the

FIGURE II-6.

Bruceveil's method.

Fig. II 4

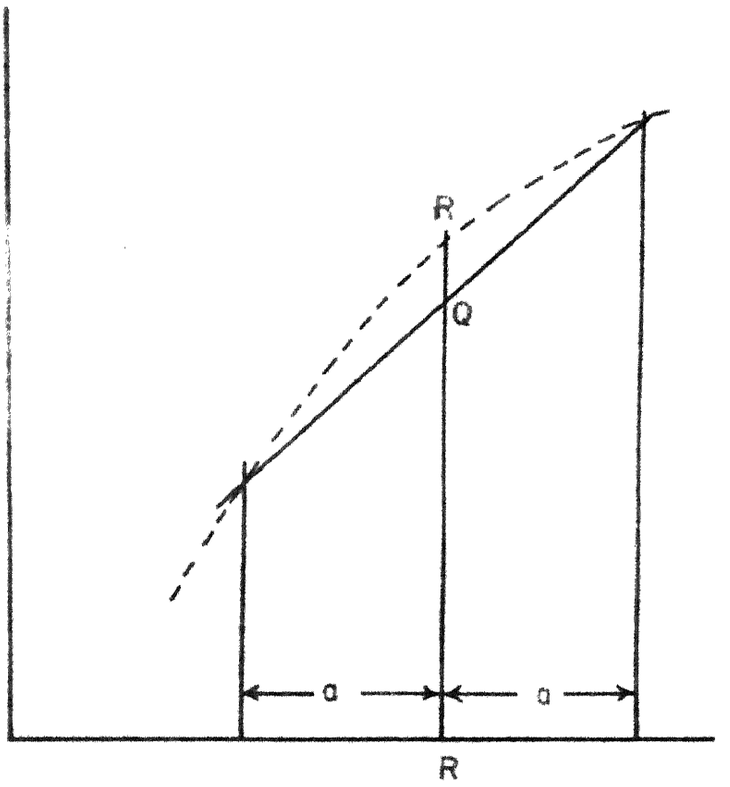

instrumental profile of the 60' spectrograph is 10.72mA and the correction in central intensities for resolving power is atmost 0.8% of the continuum intensity.

2.3c. Scattered light corrections.

The most important correction to the observations has been that for scattered light. The scattered light has two components.

1) Diffuse scattered light.
2) Rowland ghosts.

If q gives the excess scattered light, the true relative intensity at any point on the profile is given by

$$i_{true} = (i_{obs} - q) / (i_{controls} - q)$$

The diffuse scattered light was estimated by registering the signal with only the ruled area of the grating covered and the scanning slit centred at the continuum. The level of this signal was used as the dark and all measurements of the profiles were made above this 'spectrograph dark'.

To make the correction for Rowland ghosts, profiles of the standard strong lines of H_γ 4340A $Mg\,b_1$ 5184A and Na D_1 and D_2 in the sixth, fifth and fourth orders were obtained. Average profiles for each of these lines were obtained by combining measurements of atleast four traces. These average profiles were corrected for instrumental profile.

Now all these lines have published well measured profiles (White 1962, Waddell 1962a, Waddell 1962b) obtained with the Sacramento Peak double-pass system. These double-pass central intensities were taken as true central intensities and the observed single pass central intensities were corrected to give these true intensities. The necessary correction derived at the centre of the disc by the following expression.

$$\text{Ro (relative, line)} = I\,(\text{rel. doublepass})$$

$$= \frac{I\,(\text{line observed single pass}) - I(\text{scattered})}{I\,(\text{cont observed single pass}) - I(\text{scattered})}$$

solving this

$$I_{sc} = \frac{I_{obs} - I_{\text{double pass}}}{1.0 - I_{\text{double pass}}} \times 100$$

gives the scattered light in units of the continuum deflection as 100. Thus corrections obtained from H_4, Mg b, and Na D, and D_2 give the estimate of corrections for the sixth, fifth and fourth orders respectively.

To check the correctness of this approach the other points in the wings were corrected using this correction factor obtained from fitting the observed central intensity

FIGURE II-5.

The scattered light correction. Triangles represent the observed single-pass profile. Filled circles are Waddell's double-pass observations and open circles are Kodaikanal single-pass observations corrected for scattered light.

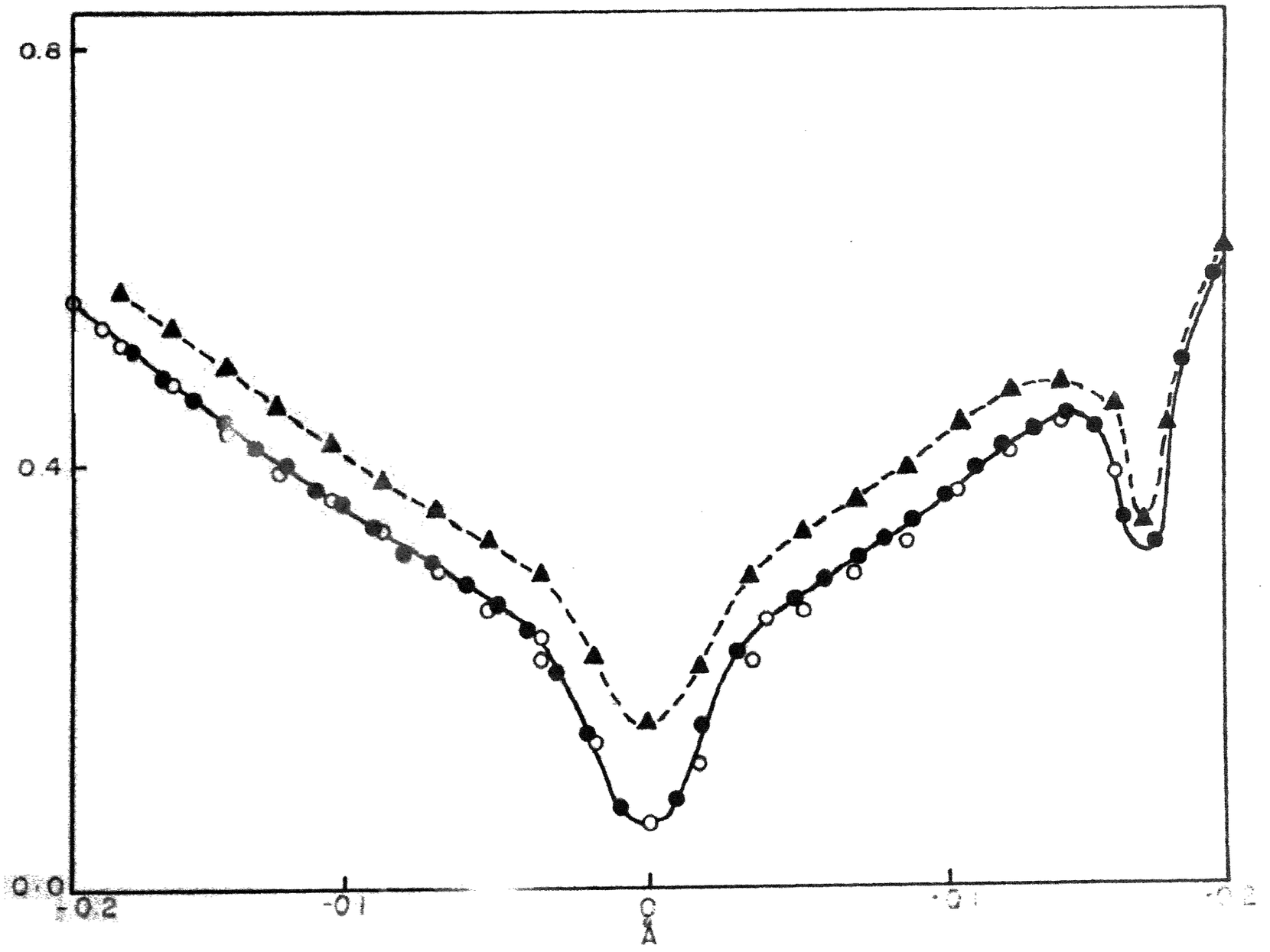
0.8
0.4
0.0
-0.2
-0.1
0
Å

Table II-2

Scattered light corrections.

Order	Standard line.	Correction.
V	5184 Mg γ_1 line	8.11%
VI	4341 H γ line	9.41%

to the double-pass central intensity. A comparison of the corrected Kodaikanal profile and the double-pass profile for Mg b$_1$ (Figure II-5) shows that they are identical within one percent. Table II-2 gives the scattered light correction factors for the various orders. As White (1961) has pointed out the observed scattered light signal is strongly dependent on the type of filter used, and the spectral response of the photomultiplier since, the output signal is the integral of the product of the total light intensity and the spectral sensitivity function of the photomultiplier.

The discussion of the corrections to be applied to the observed profiles shows that the observations are accurate in the absolute sense within two percent, while it is likely that the internal relative accuracy of the centre-limb profiles is probably within one percent.

CHAPTER III

CENTRE-LIMB VARIATION OF ROTATIONAL TEMPERATURE

3.1. Description of Data.

In order to study the centre-limb variation of rotational temperatures the rotational lines of C_2 system were chosen for analysis. The Swan system of C_2 with the band head at λ 5165A was photographed in the fifth order of the 19 metre spectrograph at the six positions μ =1.00, 0.8, 0.6, 0.45, 0.35 and 0.25 respectively, covering a wavelength range of over 60A. An entrance slit 100 microns wide and 8mm long was used. An Ilford 624 filter was used to cut out the overlapping orders. The exposure times varied from 20 seconds at the centre to 40 seconds at the limb on a fine grain plate. The plates were developed in D11 for 7 minutes at 68°F.

The plates were calibrated with a Hilger step wedge with six steps, using the centre of an out-of-focus solar image. The plates were microphotometered with a modified Cambridge microphotometer at a magnification of 23 and the final trace dispersion was 0.0093A/mm.

3.2. Measurement.

The C_2 lines in the solar spectrum are some of the weakest molecular lines and it was, therefore, decided to

measure the equivalent width by approximating the line contours to triangles. The list of lines selected for measurement together with their J values and intensity factors and log (W/i) are set out in Table III-1.

3.3. Rotational temperatures.

The derivation of rotational temperatures from equivalent width measurement is based on classical formulae. The rotational energy of a molecule in the initial rotational level of quantum number J'' is given by

$$E_r = hc\, B(J''+1)J''$$

where h is Planck's constant, c the velocity of light and B_v the rotational constant for the particular vibration level. The population of a level of rotation is proportional to exp (-Er/kT), T being the temperature corresponding to the Boltzmann distribution of molecules in the initial state.

The effective number of molecules that are responsible for any rotational line is given by

$$N = \text{Constant} \times c \times \exp(-Er/kT)$$

TABLE III-1.

Line	Wavelength	1	Log (W/1)					
		μ	=1.0	0.8	0.6	0.45	0.35	0.25
R_3 (15)	5143.307	12.7	-4.78	-5.04	-4.92	-	-5.14	-4.91
R_3 (16)	5138.094	15.7	-4.71	-5.34	-4.98	-5.05	-5.11	-5.11
R_3 (17)	5136.426	16.8	-4.76	-5.27	-5.02	-4.85	-4.96	-4.94
R_2 (17)	5136.256	16.9	-4.80	-5.05	-4.66	-4.90	-4.85	-4.89
R_3 (23)	5124.059	23.6	-4.71	-5.00	-4.43	-5.11	-4.79	-5.31
R_{23}(37)	5086.234	73.9	-5.06	-5.15	-5.58	-5.13	-4.98	-5.09
R_1 (25)	5119.364	25.0	-4.86	-5.28	-5.22	-5.21	-5.15	-5.09
P_{23}(29)	5159.467	55.8	-5.02	-5.46	-5.40	-5.33	-5.29	-5.21
P_1	5120.702	52.0	-5.31	-5.44	-5.31	-5.75	-5.62	-5.51
$P_1+P_2+P_3$ (62)	5094.095	185.9	-5.75	-5.86	-5.89	-5.94	-5.81	-5.58
Temperatures			4350°K	4600°K	4000°K	4530°K	4590°K	4510°K
Range in temperature determination.					± 350°K			

i being the intensity factor for the line in question. This intensity factor is a function of the statistical weight of the lower level of the transition and the rotational transition probabilities for the line.

In the weak-line approximation, the intensity of a line is proportional to the effective number of molecules in the initial level. The intensity is given by

$$W = \text{Constant} \times i \times \exp(-E_r/kT)$$

$$= \text{Constant} \times i \times \exp(-hc B_v J''(J''+1)/kT)$$

Therefore,

$$\log_{10}(W/i) = \text{Constant} - \frac{hc}{kT} B_v J''(J''+1) \text{ Mod}$$

$$\text{Mod} = 0.43429$$

Thus, a plot of log (W/i) versus $J''(J''+1)$ is a straight line having a slope proportional to $1/T$. This gives a convenient method for determining the temperature that is characteristic of the population distribution in the rotational energy levels.

For the C_2 lines chosen for study the weak line approximation is fairly reasonable and once the intensity factors and rotational quantum numbers are known, rotational temperatures can be derived from the measured equivalent width.

The laboratory wavelength of the lines and the assignments of rotational quantum numbers are from Johnson (1927). The calculation of intensity factors requires the knowledge of the mode of coupling appropriate to the transition. Budo (1937) has made elaborate calculations for the case where the two electronic states are near Hund's coupling case b. The values obtained from Budo's formulae are very nearly equal to those obtained from Höni - London's simple formula given by

$$P(J) = \frac{J^2 - \Omega^2}{J}$$

$$R(J) = \frac{(J+1)^2 - \Omega^2}{(J+1)}$$

where $\Omega = |\Lambda + \Sigma|$. For the $^3\Pi_g$ state $\Lambda = 1$ and $\Sigma = 3$ and, therefore $\Omega = 1, 2$ or 3, giving respectively the (P_1, R_1), (P_2, R_2) and (P_3, R_3) branches. In view of the gross nature of the analysis, the Höni-London formulae were used to calculate intensity factors as function of J.

Table III-1 presents the results for the six positions on the disc. The value ± 350°K is not a probable error, but represents the upper limit of the range of temperatures obtained, when points with large scatter are accommodated in the straight line fits. Although the probable errors are not too large, the measurements for low J values scatter badly around the mean. In fact it is this factor that is mainly responsible for the uncertainty of ± 350°K in the temperature determinations. The measurements at μ =0.60 have the largest scatter and the significance of the low temperature value of 4000°K obtained for this μ position is lost.

3.4. Discussion.

The results presented indicate that the rotational temperatures derived from C_2 measurements have no significant variation from centre to limb. A probable error of 350°K would conceal any small change in the temperature. Contribution function calculations for C_2 show that the mean level of formation of C_2 changes from τ =0.06 to τ =0.04 on going from centre to limb. In this range, the temperatures derived here merely set an upper limit of 500°K to the change in temperature.

An important point to note is that, a rotational temperature, derived on the basis of existence of LTE

can be obtained even at the limb. This suggests that, deviations from pure absorption mechanism of line formation, to explain centre limb variation of equivalent widths are not indicated.

CHAPTER IV

THE ANALYSIS OF LINE PROFILE SCANS

4.1. General.

The first consideration in choosing individual lines for intensive study is that they be unblended lines as far as possible with a well defined local continuum on either side of the line. The presence of rotational fine structure due to spin doubling in molecular lines makes it impossible to choose singlet lines in the true sense of the word. At best, it is possible to choose almost superposable doublets and lay more stress on the second criterion, of the line wings reaching the local continuum. In order to be able to study the general trends, if any, for each molecule atleast four lines must be chosen for each molecule. The third criterion is to choose lines of similar intensity in each group so that variations in behaviour from line to line in any one group, would not be due to saturation effects. Also, it would perhaps be useful if we choose lines having widely different J values to examine level effects if any (Richardson 1932, Cowley 1964).

In practice, it has not been possible to fulfill the first and third conditions entirely. As regards the first condition, except probably for one line 5147.106A all other lines are almost superposable doublets. The choice was restricted to lines which reached the true local continuum at least in one wing.

While all the C_2 lines chosen are weak and all CH lines are medium strong, of the CH lines chosen, three are strong lines and two are weak lines. Among the lines under study there are three well resolved doublets and one resolved triplet. It is believed that fitting a resolved doublet profile would provide a critical test for both the adopted velocity and temperature models. Table ~~III~~ IV-1 sets out the details of observations.

4.2. Specification of reference continuum.

The reference continuum over an absorption line is defined by a straight line fitted to the continuum on both sides of the line. To locate this continuum a straight line was defined with respect to scans over 10A only. Therefore, the reference is strictly to a local continuum. It has, however, been compared with the Utrecht Atlas and in all cases it is close to the general continuum specified therein, except for the CH lines 3864A and 3879A. To standardise all measurements with respect to the general continuum, the profile measurements of 3864A and 3879A were multiplied by the ratio of the local continuum to general continuum as measured from the Utrecht Atlas. The factor is 0.95 changing the central intensities by 2.5%. Column 8 of Table ~~III~~ IV-1 gives the wavelength of the local continuum with reference to which the measurements have been made.

IV

Table III-1.

Details of the photoelectric observations included in this study.

Date of Observation	Wavelength.	Molecule.	Transition.	Rowland Intensity.	Seeing	Transmission.	Location of local continuum
1 April 1964	3864.307A	CH	$^2\Sigma^+ - \Sigma^+$	3	Average	V. Fair	3863.25
2 April 1964	3879.578A 3879.661A 3879.716A	CH	$^2\Sigma^+ - \Sigma^+$	1 0 0	2 ~ 3	Good	3880.55
30 March 1964	4192.917A	CH	$^2\Sigma^+ - \Sigma^+$	-1	2 ~ 3	V. Fair	4192.80
11 March 1964	4297.409A	CH	$^2\Sigma - \Sigma^+$	1	2 ~ 3	Good	4297.65
14 March 1964	4212.236A 4212.407A	CN	$^2\Sigma - \Sigma^+$	-1 -1	~ 2	Fair	4212.50
18 March 1964	5086.251A 5086.399	C_2	$^3\Pi_g - ^3\Pi_u$	-1 -2	~ 2	V. Fair	5086.15
17 March 1964	5094.029A	C_2	$^3\Pi_g - ^3\Pi_u$	-2	< 3	Good	5093.90
24 March 1964	5147.106A	C_2	$^3\Pi_g - ^3\Pi_u$	-2	2 ~ 3	Good	5145.05
26 March 1964	5159.467A 5159.609A	C_2	$^3\Pi_g - ^3\Pi_u$	-3	2 ~ 3	Fair	5158.25

Table III-1 - continued.

Date of Observation	Wavelength.	Molecule.	Transition.	Rowland Intensity.	Seeing.	Transmission.	Location of local continuum
14 March 1964	4219.370A	CN	$A^2\Delta - X^2\Pi$	3	2 ~3	Fair	4212.50
15 March 1964	4218.726A	CN	$A^2\Delta - X^2\Pi$	3	~2	V. Fair	4218.60
16 March 1964	4281.374A	CN	$A^2\Delta - X^2\Pi$	2	~2	V. Fair	4281.65
20 March 1964	4378.915A	CN	$A^2\Delta - X^2\Pi$	2	2 ~3	Good	4378.75

4.3. Measurement.

After fixing the 'spectrograph dark' as described in Chapter II, copies of each of the observed profiles were made on a transparent millimetre graph sheet. On an average there were atleast six traces of the profile, three each in one direction, for every fe position on the solar disc. The average dispersion on the trace was .006A/mm. Corresponding to each such trace of the line, there is a sky transparency monitor trace. The variations in sky transparency were changed to the scale of the scanner traces and plotted over the profile from instant to instant as variations in the continuum. For a majority of the traces, corrections for sky transparency were unnecessary. For the very few cases wherein transparency corrections were required the magnitude of such rectification was well within one percent.

After plotting the continuum above the traced copy of the line profile, deflections were measured correct to 0.5mm above the spectrograph dark, for every millimeter of the profile along the direction of dispersion, starting from the centre of the line. The corresponding continuum deflection was also measured. The ratio of the two gives the residual intensity at that point of the profile. The average residual intensities for six observed profiles were thus obtained. Each of these average residual intensities were corrected for the general scattered light appropriate to the order and wavelength as taken from Table II-2.

Thus the corrected average profiles for the six positions on the solar disc were plotted to a large working scale. These profiles (listed in table IV.1) were then corrected graphically for finite resolving power by Bracewell's method as outlined in Chapter II, ~~Table III-1 to III-1b~~, to give the corrected observed profiles. (Figures IV.3 – IV.15)

4.4. Evaluation of accuracy of observing and reduction techniques.

In order to test the reproducibility of the wavelength scale on the traces, the hyperfine structure of the Hg 5461A line was traced several times both in the direction of increasing and decreasing wavelengths. The traces when superposed, matched completely both in intensity and wavelength indicating that the scanning was uniform within limits of detection and that no wavelength distortion is present.

The amplifier-recorder system was put to extensive tests for stability and linearity of response at various light levels. Deflections corresponding to any one light signal were reproduceable within one-tenth of a small Brown recorder division, this being the measure of the accuracy of the recording. The measuring technique used in the present analysis has probable errors in the measurement of central intensities ranging from 0.1% to 0.6%. Also, the accuracy is consistent with the over all accuracy

capable of being achieved in view of the correction to be applied to the observed profile. The larger probable errors obtained for some measurements, all certain to observations made under conditions of less than average seeing and transparency. The effect is particularly noticeable for profiles at μ=0.35 and μ=0.25, as poor seeing meant, uncertainties in guiding, and limb observations are naturally sensitive to the location of the image with respect to the slit. Although a larger number of traces were always used to obtain the average profile when seeing and transparency conditions were below average, the probable errors obtained were slightly larger than otherwise.

As mentioned in Chapter II the final figure of accuracy is strongly determined by the scattered light correction rather than any other single factor. It is the uncertainty in the magnitude of this correction together with uncertainties in fixing the continuum that limits the accuracy to as high a figure as 1.5 per cent. However, the relative accuracy of the variations in profiles observed from centre to limb is of the order of the probable error of measurement and well within 1 per cent. Therefore, the trend of variations of the profiles from centre to limb is much more reliable than the absolute value of central intensity at any point on the disc.

4.5. Description of the observed line profiles.

The CN line at 3864.307A belongs to the 0-0 vibrational transition of the $^2\Sigma^+ - ^2\Sigma^+$ system. It has a Rowland intensity of 3 and is a very close spin doublet of the R branch having a rotational quantum number $K=14$. The spin doublet separation is around 15mA, just at the limit of the resolving power of the spectrograph. This is one of the narrowest observed profiles and displays a very slight asymmetry. At the centre, this line had a central intensity of 28.75 per cent. The central intensity increases from centre to limb, slowly at first and steeply later, giving a central intensity of 38 per cent at μ =0.25. The half width also increases from centre to limb. The profiles take on a characteristic U-shape while going from centre to limb. This is evident most strikingly at μ =0.35 and μ =0.25.

The CN triplet lines at 3879.579A, 3879.661A and 3879.716A also belong to the 0-0 sequence of the $^2\Sigma^+ - ^2\Sigma^+$ system, having Rowland intensities of 1,0 and 0 respectively. All three lines belong to the P branch having J = 9½, 47½ and 48½ respectively. At the centre of the disc all three are distinctly resolved. At μ =0.6, the spin doublet with $K=48$ cease to be resolved. Although it is not possible to draw quantitative conclusions about the centre-limb variation of central intensities, it is evident that minimum intensity of the profile increases from centre to limb in the same fashion as in the line 3864.307A. The fact that profiles broaden

towards the limb is also obvious. At μ =0.25 it is shallow and broad. As a measure of the energy absorbed, by the three lines in combination from the continuum, the area under the curve was measured and the ratio of equivalent widths W(A)/W(C) was plotted versus μ. Figure ~~III-2~~ IV-2 shows this variation.

The CN line at 4192.917A comprises of 4192.898A, 4192.898A, and 4192.962A of the $^2\Sigma^+ - {}^2\Sigma^+$ transition and has a Rowland intensity of -1. The two components at 4192.898A and 4192.962A are the spin doublets ~~of the~~ (K=40) of the second band $\Delta v = -1$ sequence belonging to the P branch with K=41. while the other at 4192.898A belongs to the R branch. The observed central intensity of this line is 92.65 per cent. The line reaches the continuum on both wings. The profile has a pronounced red asymmetry, as is only to be expected in view of the presence of a long wavelength blend at 4192.962A. The variation of minimum intensity in the profile follows a different pattern in that it decreases on going from centre to limb. The half widths, however, increase. The profiles themselves show the same characteristic U-shaped profile on going to the limb.

The CN line at 4207.409A comprises of the two lines 4207.399A and 4207.468A, also belonging to the $\Delta v = -1$ sequence of the $^2\Sigma^+ - {}^2\Sigma^+$ transition. It is a spin doublet of the P branch with rotational quantum number and has Rowland intensity of 1. The minimum intensity at the centre of the disc is 53 per cent. This minimum intensity decreases slightly until μ =0.45 and thereafter increases

FIGURE IV-1.

The observed centre-limb variation of central intensities. (a) Strong lines (b) Weak lines.

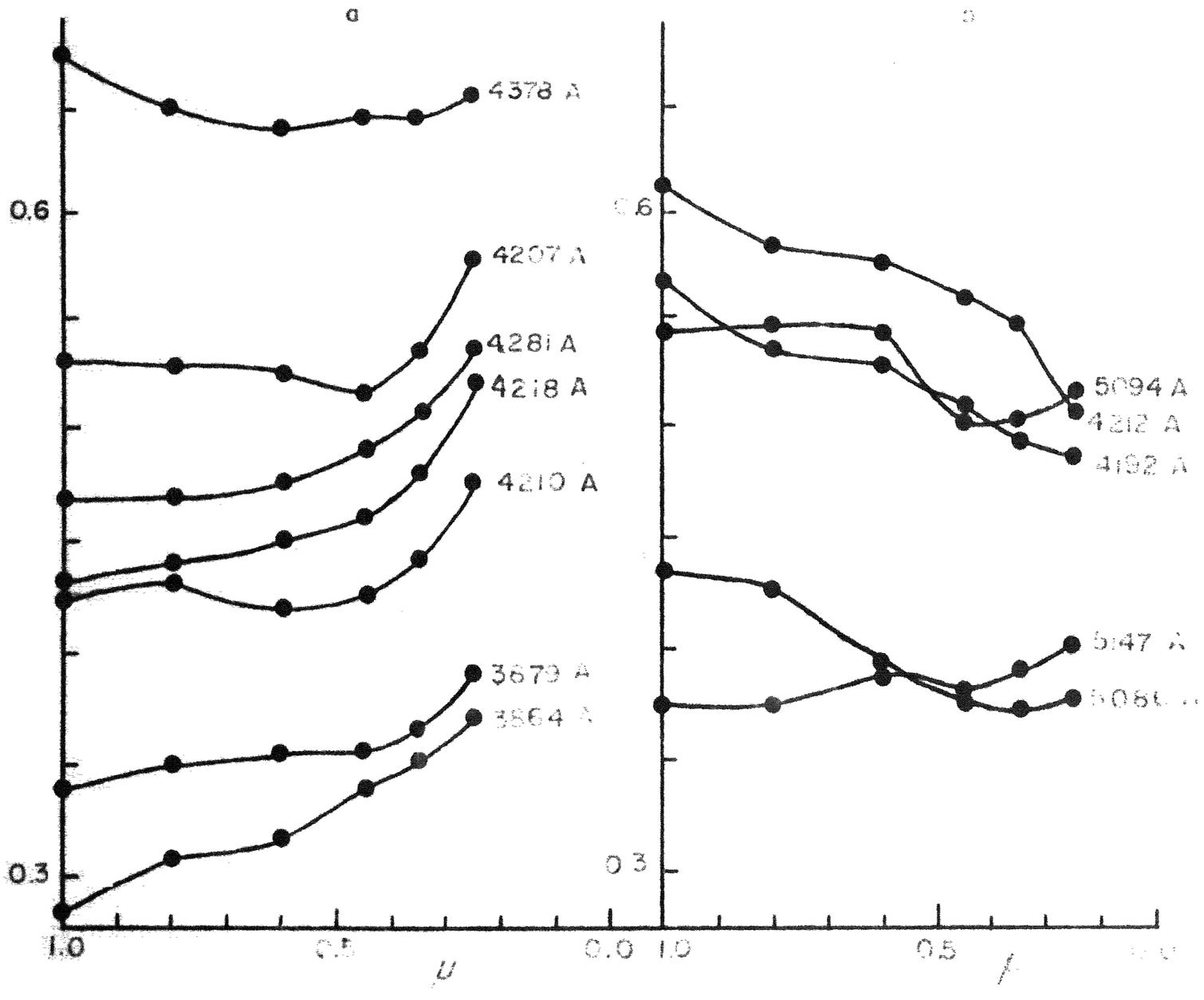
a
4378 A
4207 A
4281 A
4218 A
4210 A
3679 A
3664 A
0.6
0.3
1.0
0.5
0.0
u
b
5094 A
4212 A
4192 A
5147 A
0.6
0.3
1.0
0.5

FIGURE IV-2.

The observed variation of

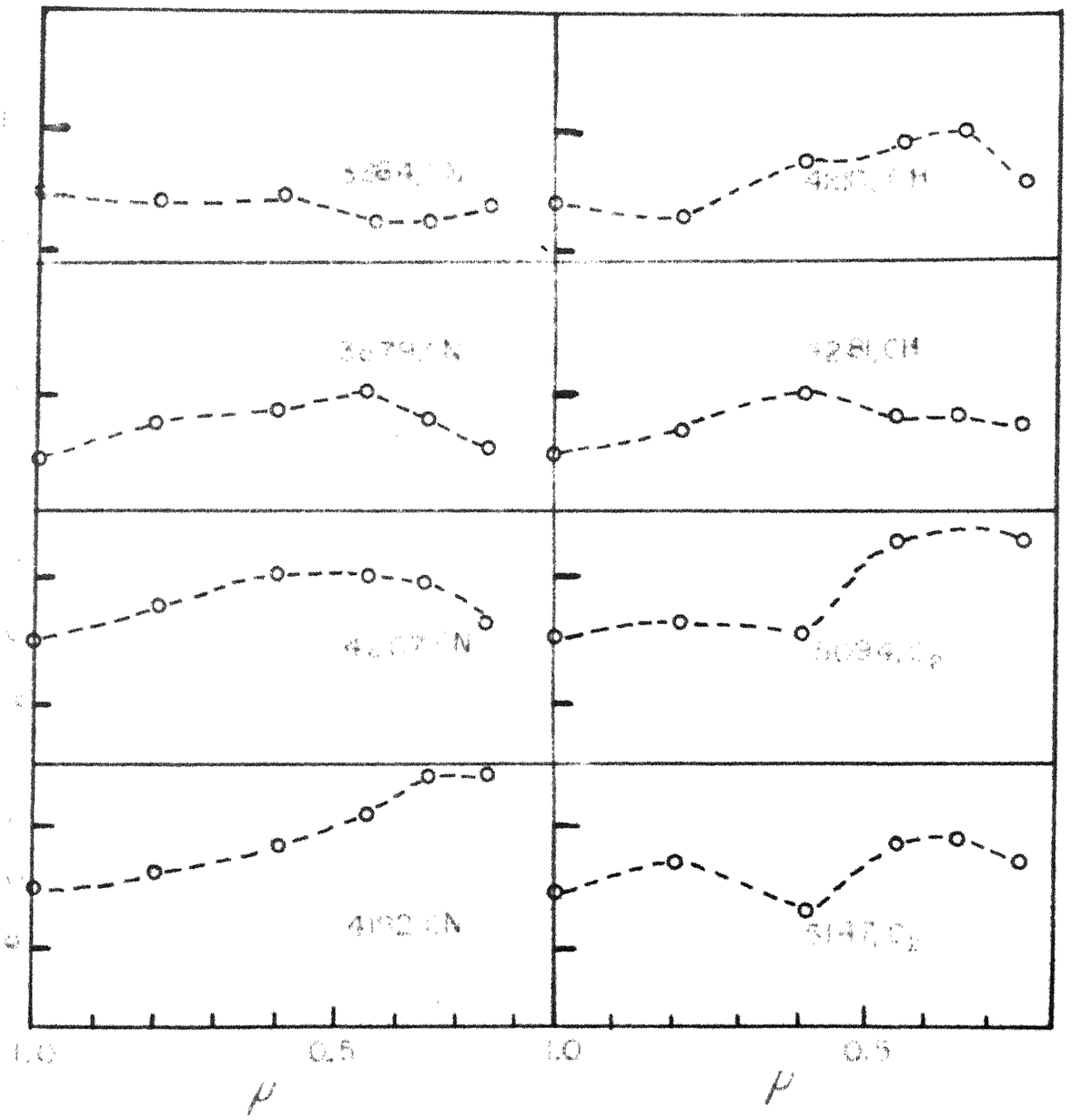
1.0
0.5
μ
1.0
0.5
μ

quite steeply. The profiles are broader and shallower, those at the limb being U-shaped.

The lines at 4212.215A, 4212.275A and 4212.399A are CN lines of the $\Delta v = -1$ sequence, 4212.275A and 4212.215A being spin doublets of the P branch having $K = 38$, while 4212.399A also belongs to the P branch with $K = 7$. The two lines have Rowland intensity of -1. The central intensities of both these lines decrease from centre to limb. For the spin doublet, however, the decrease is steeper while for the 4212.399A it is much more gradual. Both lines display the familiar feature of broadening towards the limb although they do not become very pronouncedly U-shaped.

4210.970A is a CH line belonging to the complex band due to $A^2\Delta - X^2\Pi$ transition. It belongs to the R branch of the 0-0 sequence being a very close spin doublet of R_{2cd} / R_{1cd} having rotational quantum number $K = 16$. This line has a Rowland intensity of 3. There is a distinct asymmetry in the violet, which has its origin probably in the doublet nature of the line. The central intensity at the centre of the disc is 42.5 per cent. The centre-limb variation of central intensity follows the same general pattern followed by 3864.307A, i.e., a slow increase upto $\mu = 0.8$ and a steep increase thereafter. However,

there is a slight decrease at $\mu = 0.6$. In view of the somewhat large probable error characterising the observation at this position it is difficult to conclude on the reality of this dip.

4218.726A is also a close spin doublet of the CH $A^2\Delta - X^2\Pi$ transition. Belonging to the R branch of the 0-0 sequence it is a superposition of $R_{1d} + R_{2d}$ having $K = 15$. The spin doublet separation in wave numbers is $\Delta 0.25 cm^{-1}$. Being very similar to 4210.970A, this has a Rowland intensity of 3 and a central intensity at the centre of the disc of 43 per cent. This line displays a red asymmetry. The centre-limb variation of the central intensities follow the pattern of behaviour exhibited by 3864.307A more closely than does 4210.970A. The increase in half width and the dramatic change from V to U shaped profiles is once again noticed.

4281.974A is another close spin doublet of the same CH electronic transition. 4281.974A is, however, a member of the Q branch of 0-0 sequence being a combination of $Q_{1d} + Q_{2d}$ with rotational quantum number $K = 22$. The separation between the spin doublet wave numbers is $0.9 \Delta 0.25 cm^{-1}$ The Rowland intensity of the line is 2. Here the asymmetry is in the violet wing, which wing also reaches the continuum. The central intensity at the centre of the disc is 47.0 per cent

FIGURES IV-3 TO IV-12.

The observed profiles for six μ values.

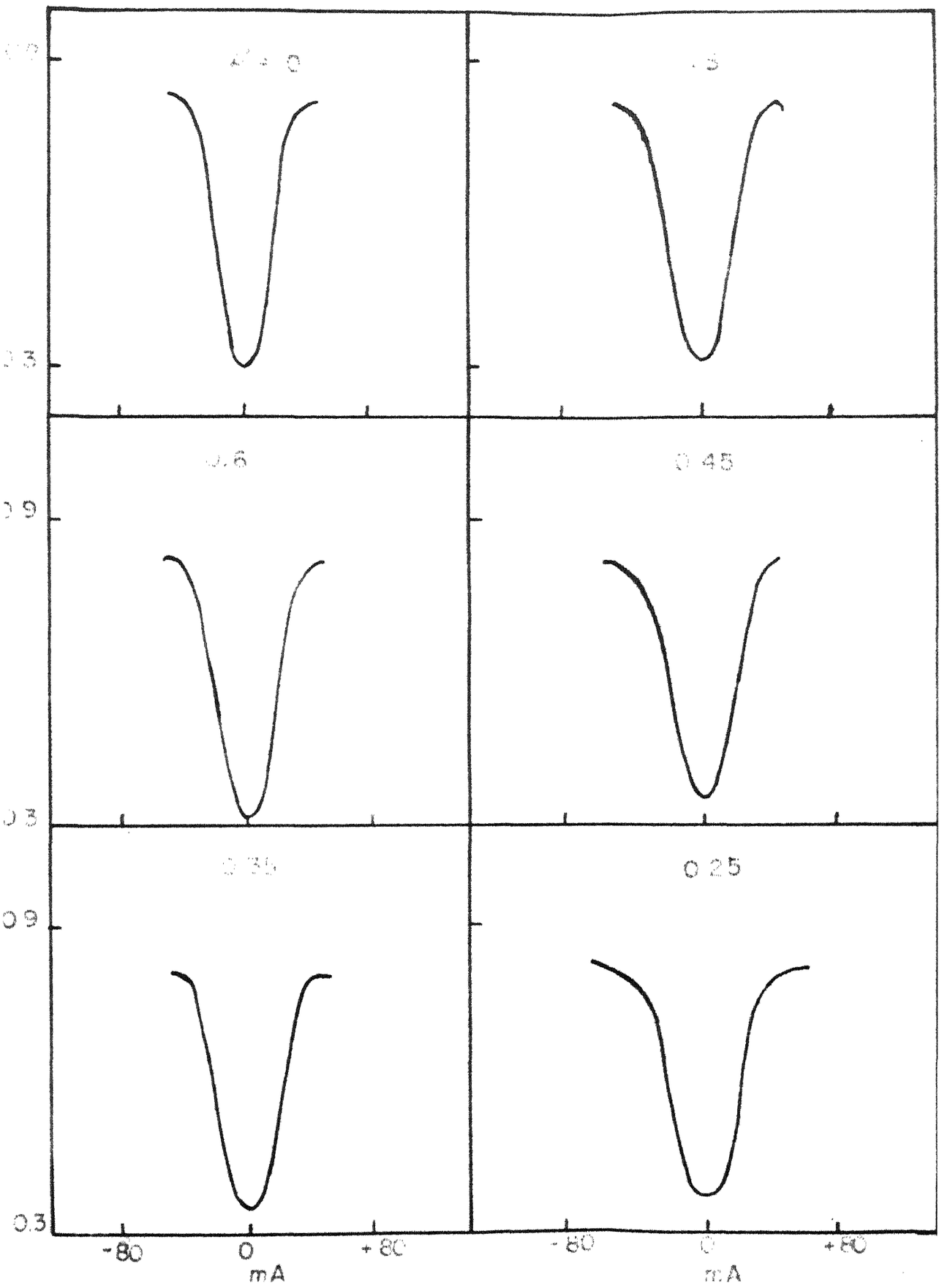
0.9
0.3
0.6
0.45
0.9
0.3
0.35
0.25
0.9
0.3
-80
0
+80
mA
-80
0
+80
mA

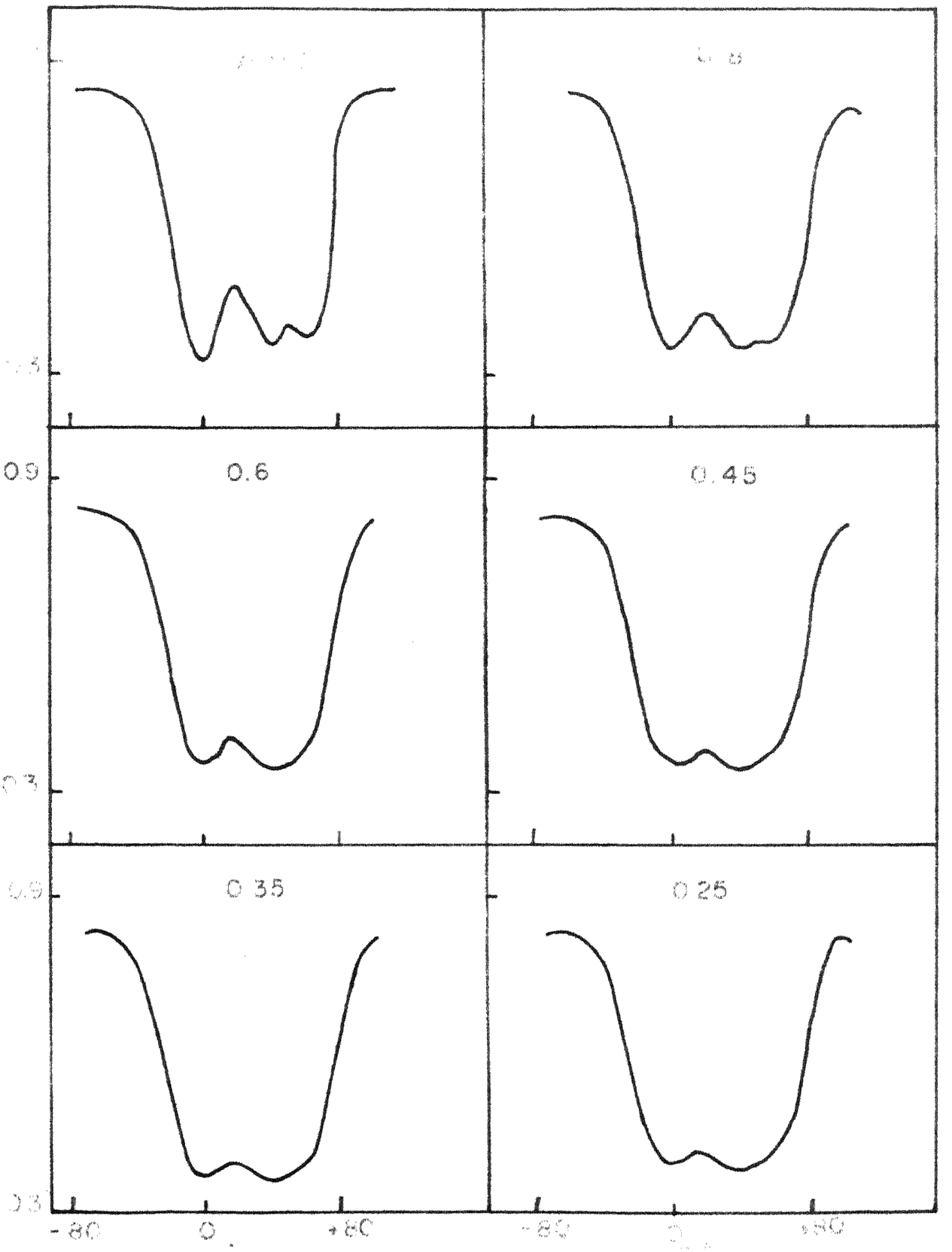
0.6
0.45
0.35
0.25
-80
0
+80

4192, CN

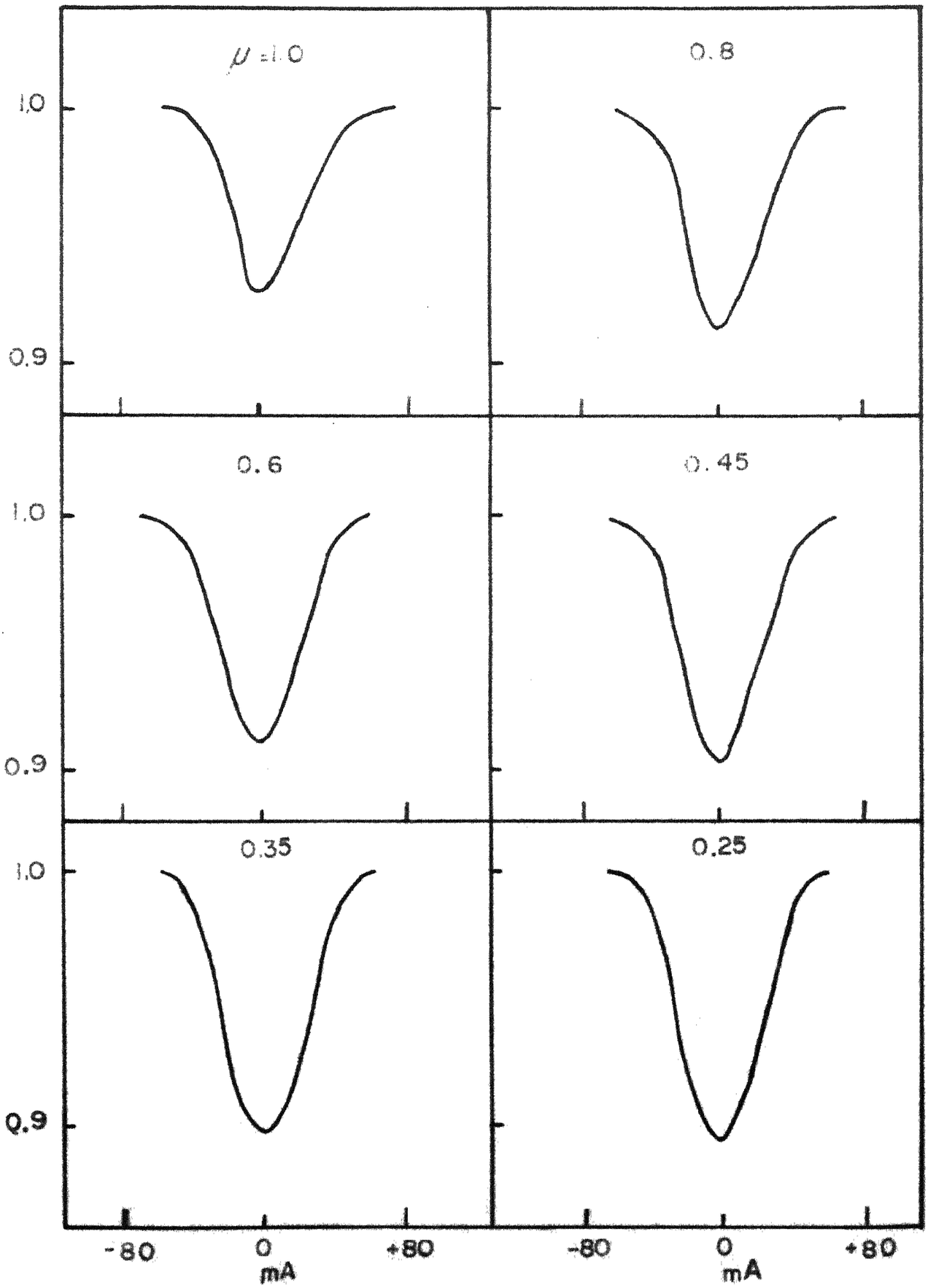

4207, CN

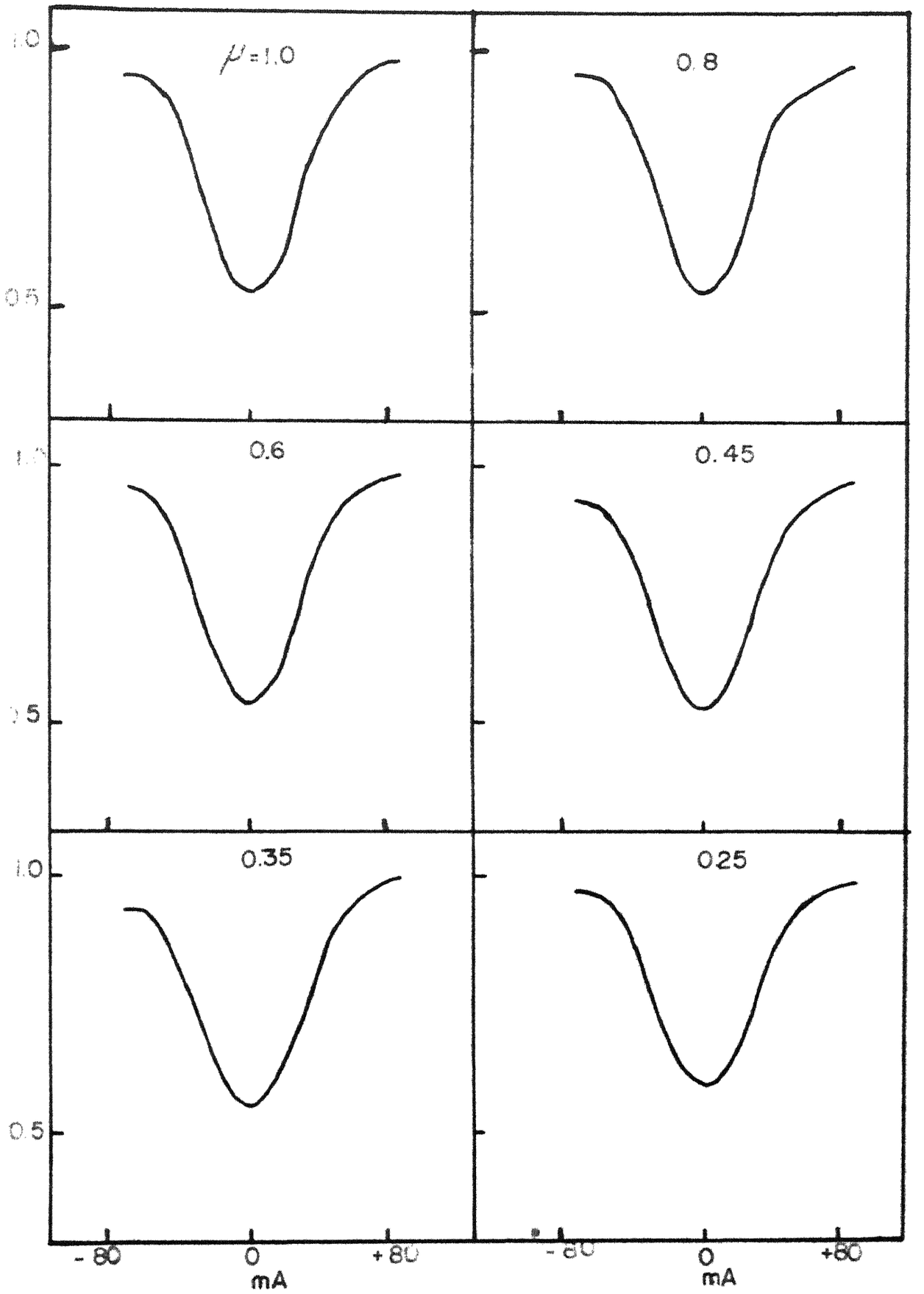

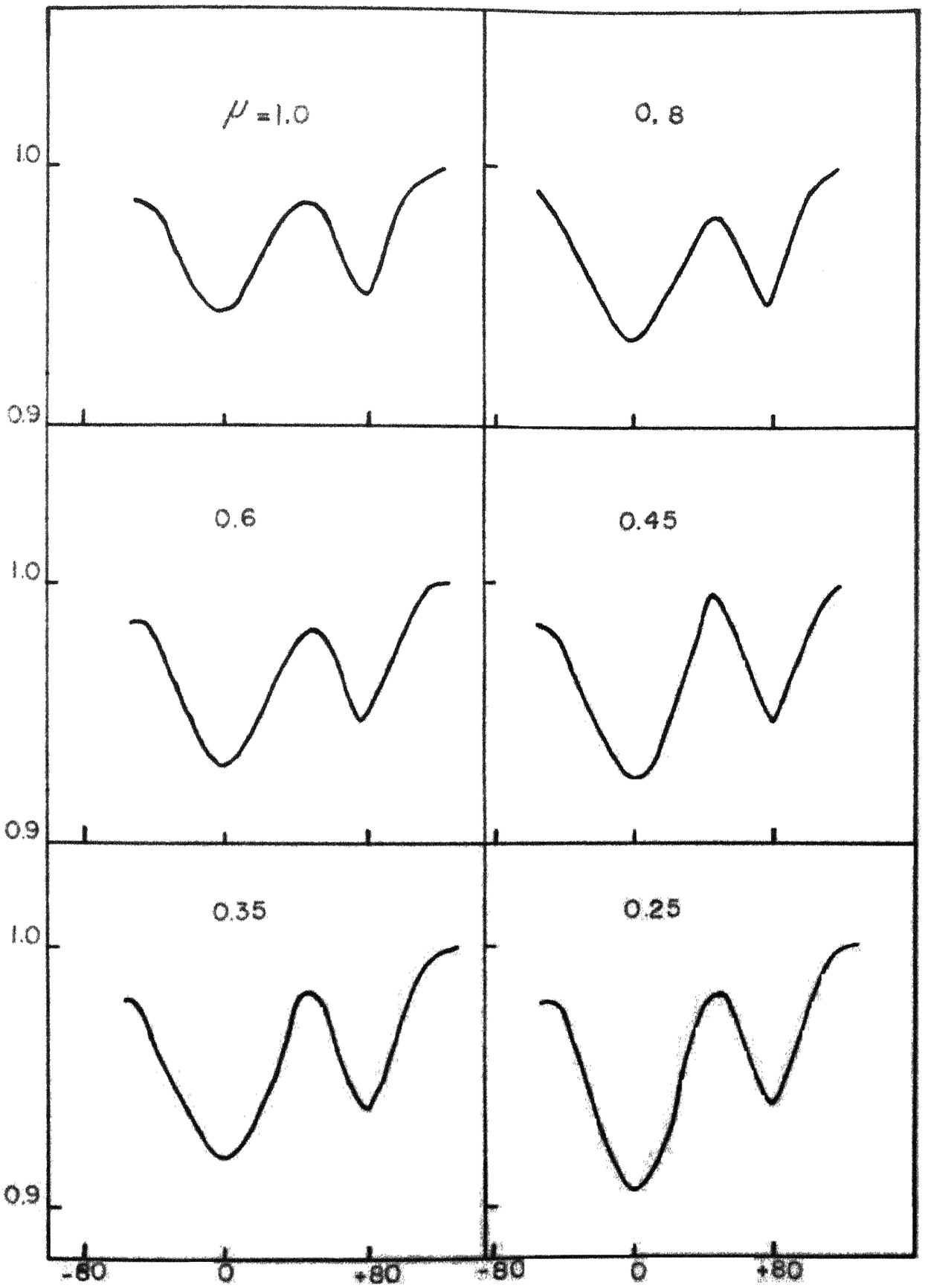
4212, CN
μ = 1.0
0.8
0.6
0.45
0.35
0.25
1.0
0.9
-80
0
+80

4210, CH

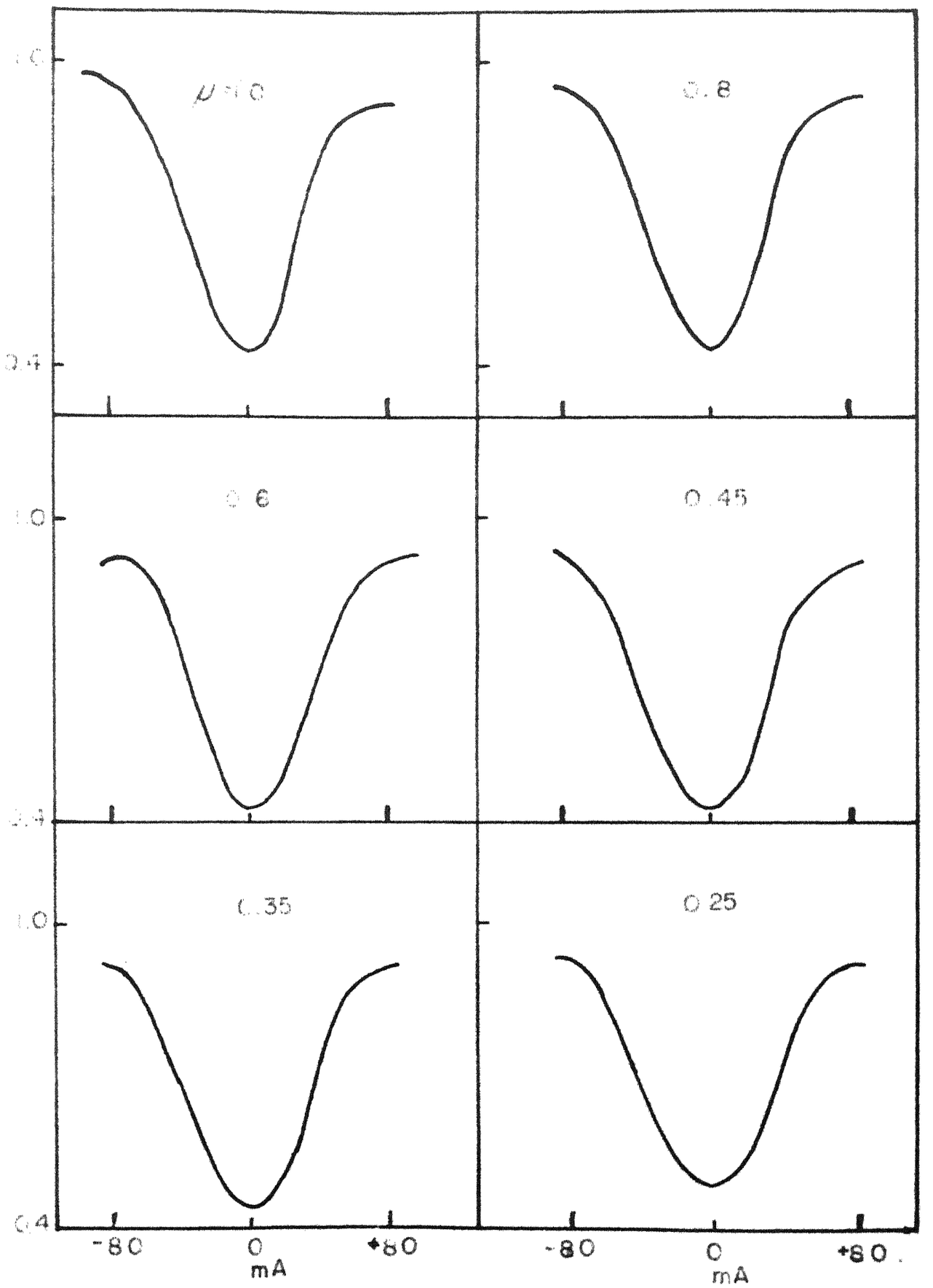

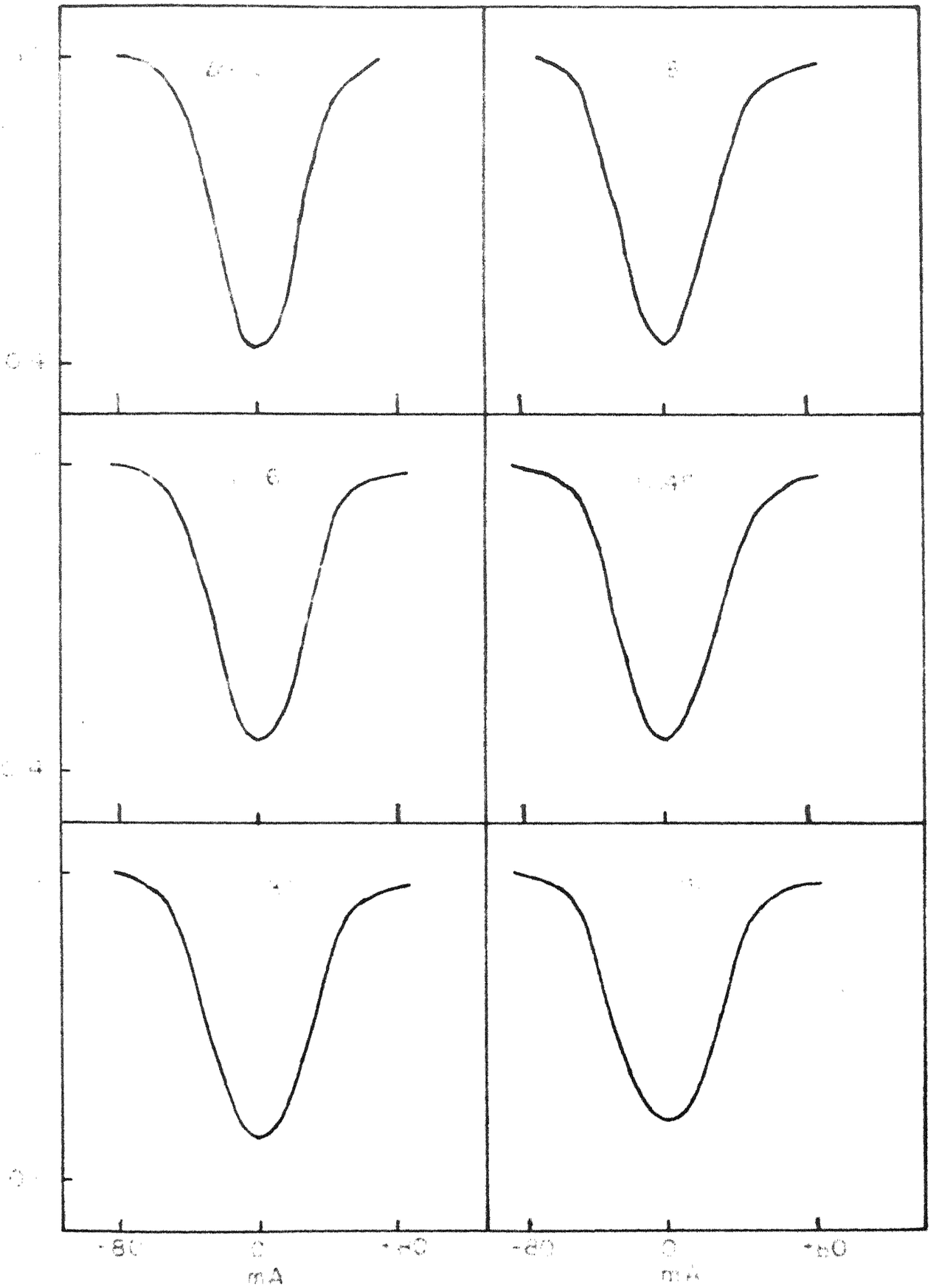
mA
mA

4281, CH

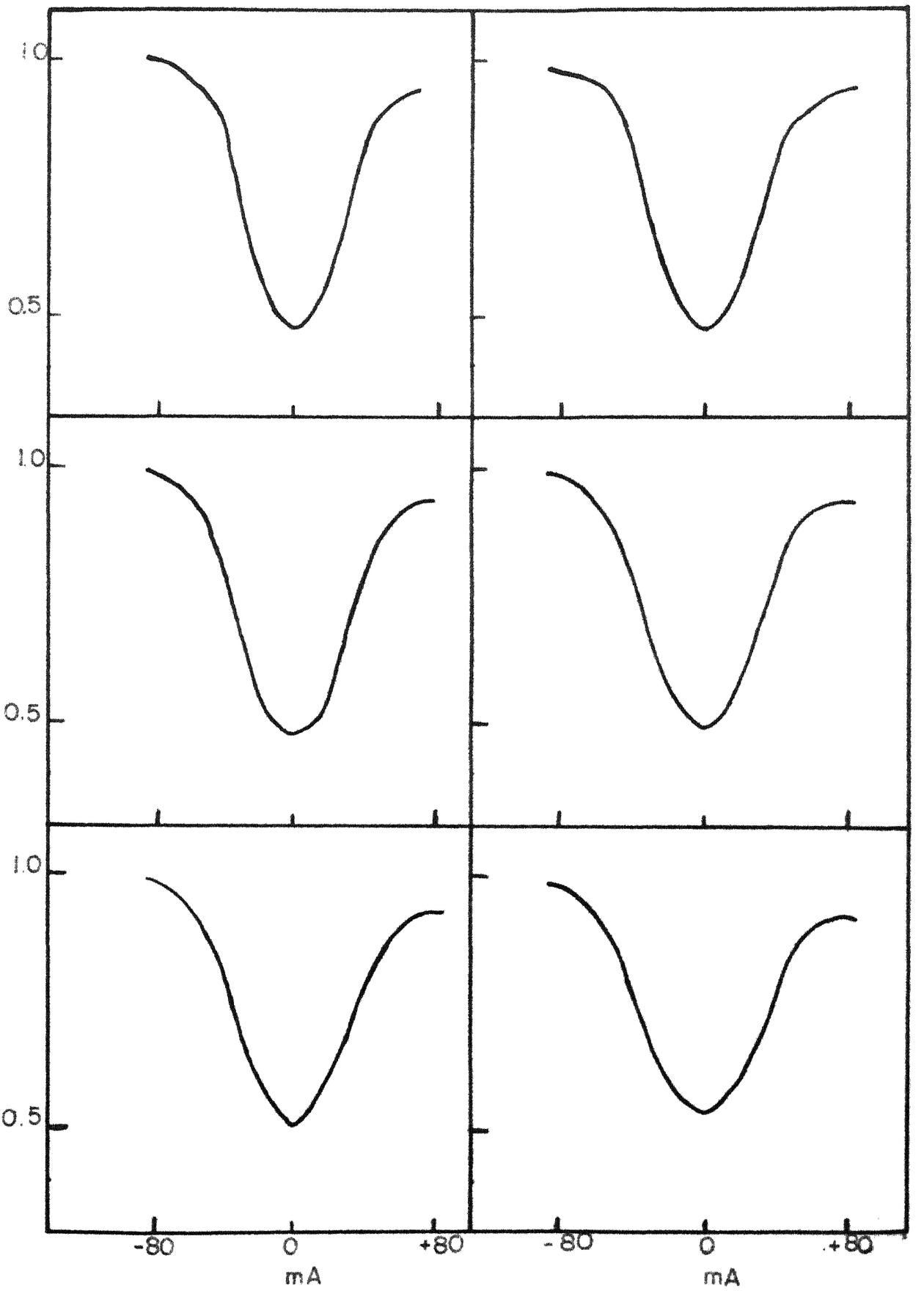

4378, CH

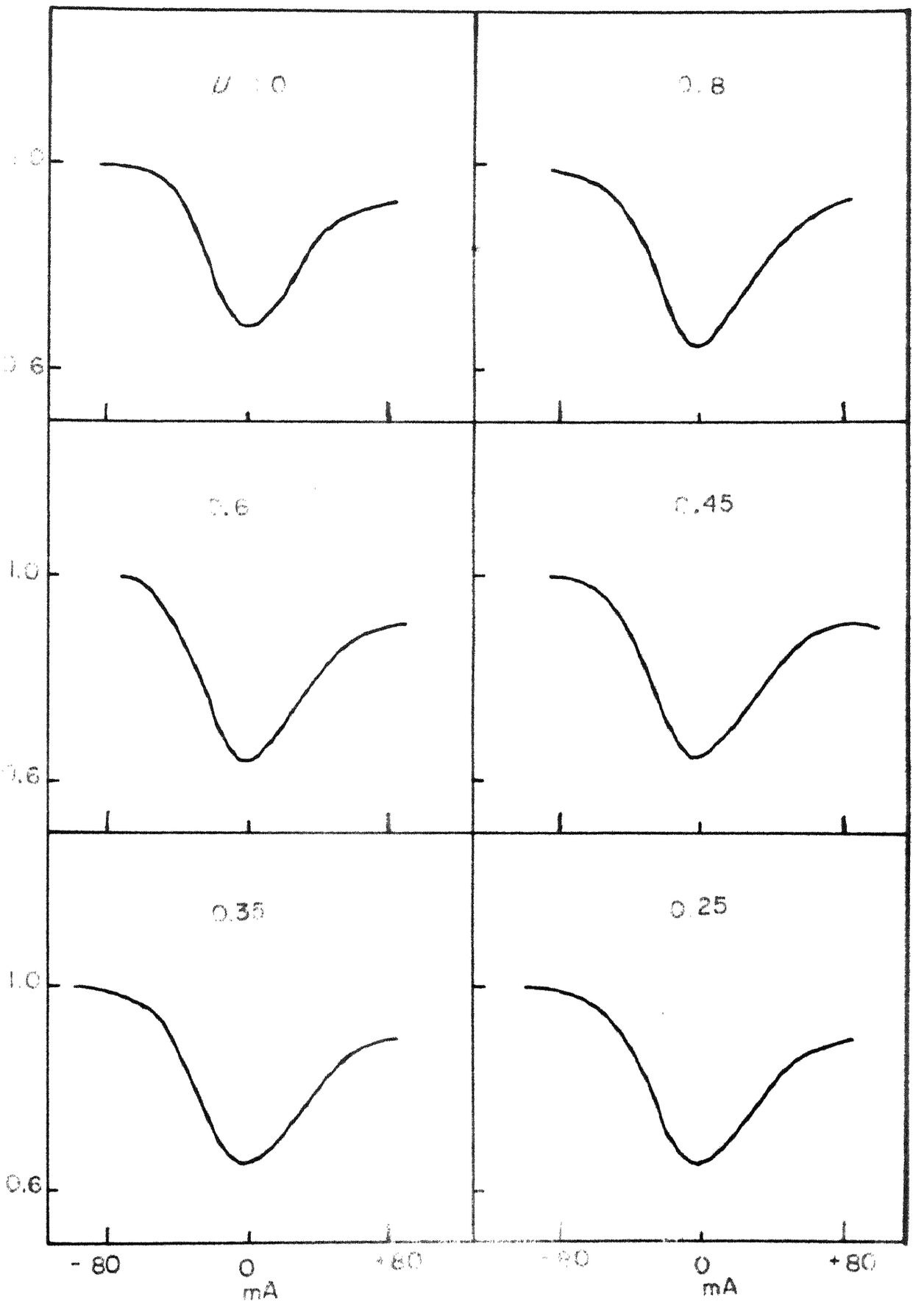

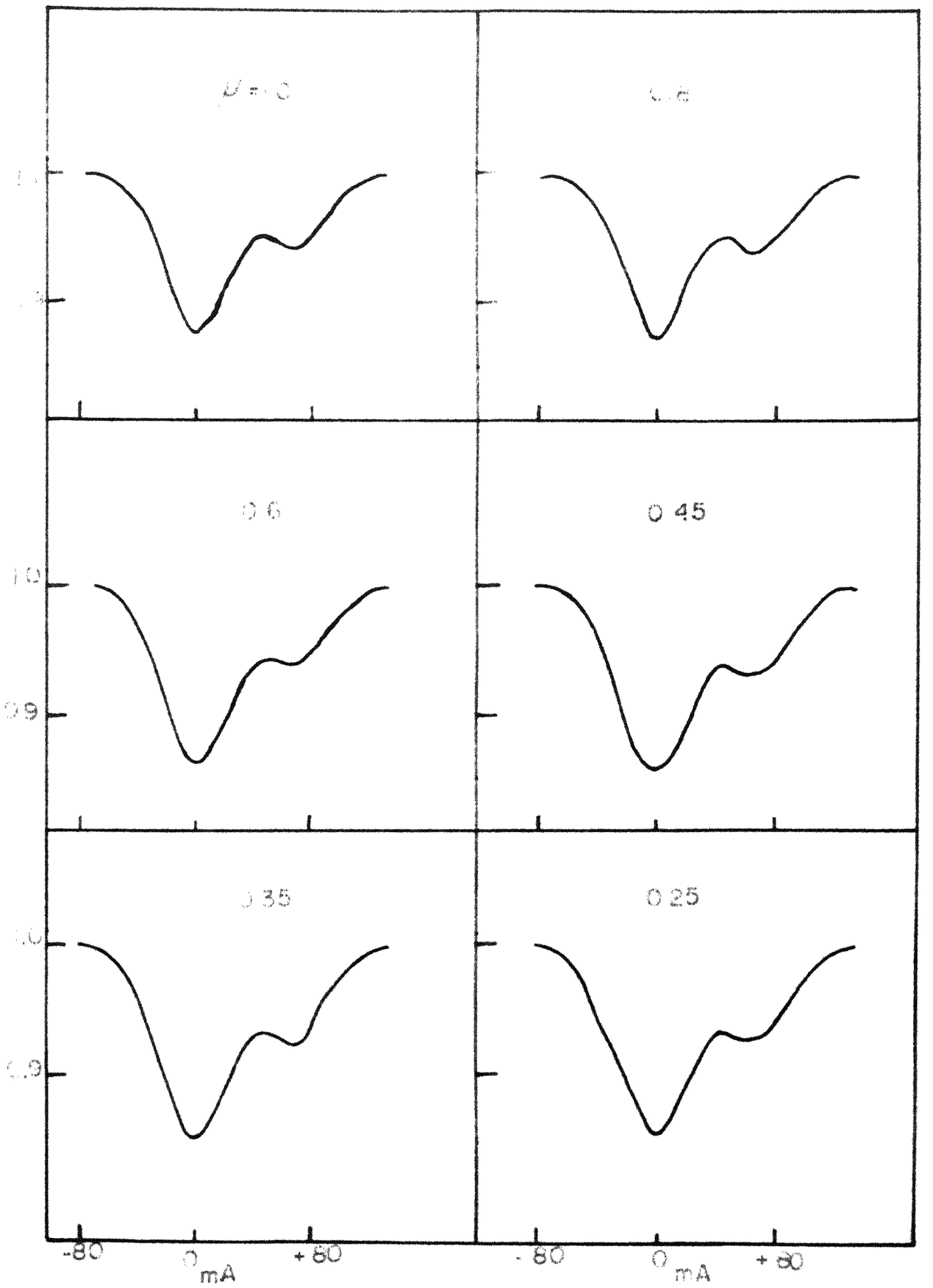
0.6
0.45
0.35
0.25
-80
0
mA
+80
-80
0
mA
+80

5094, C_2

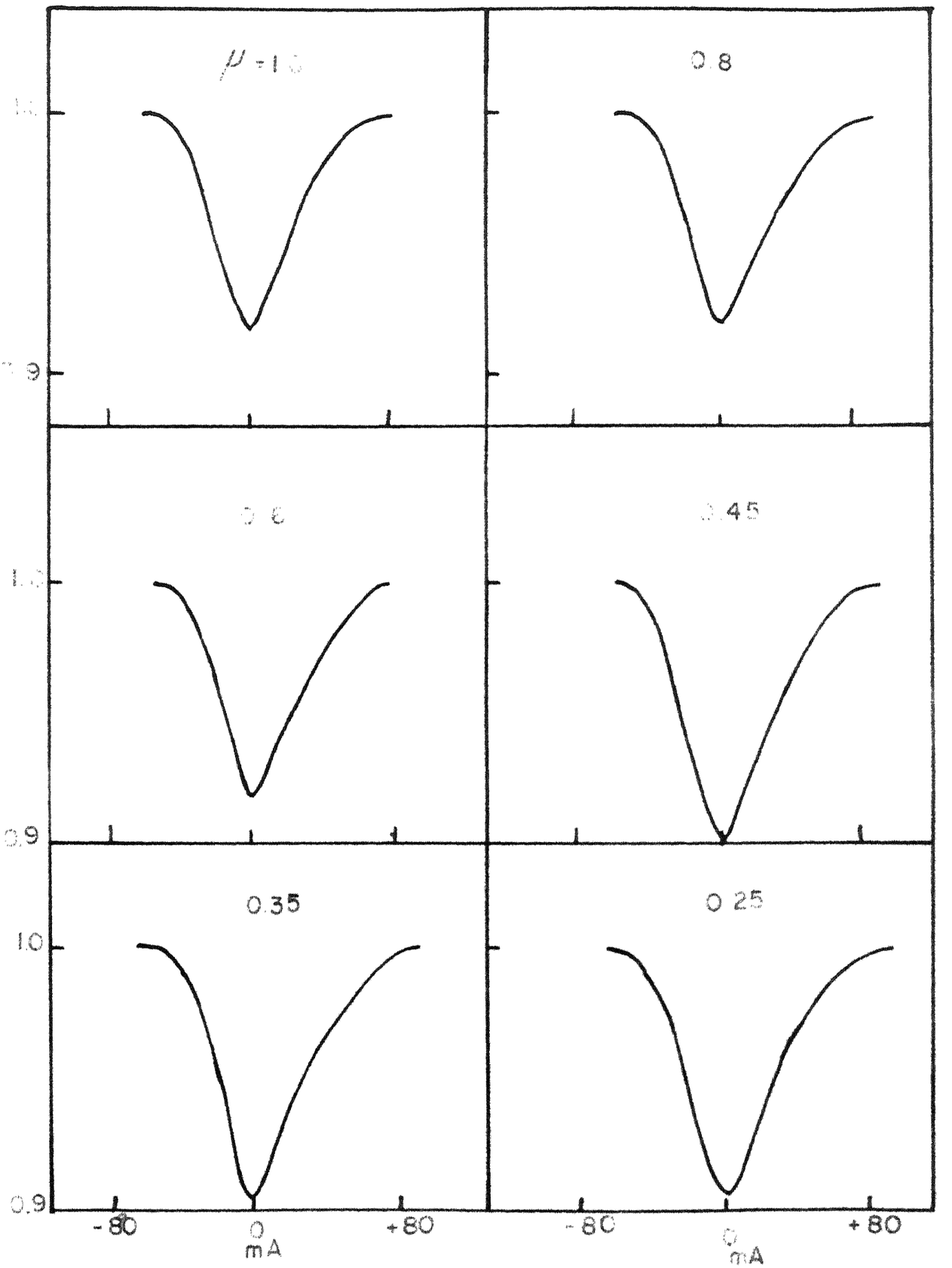

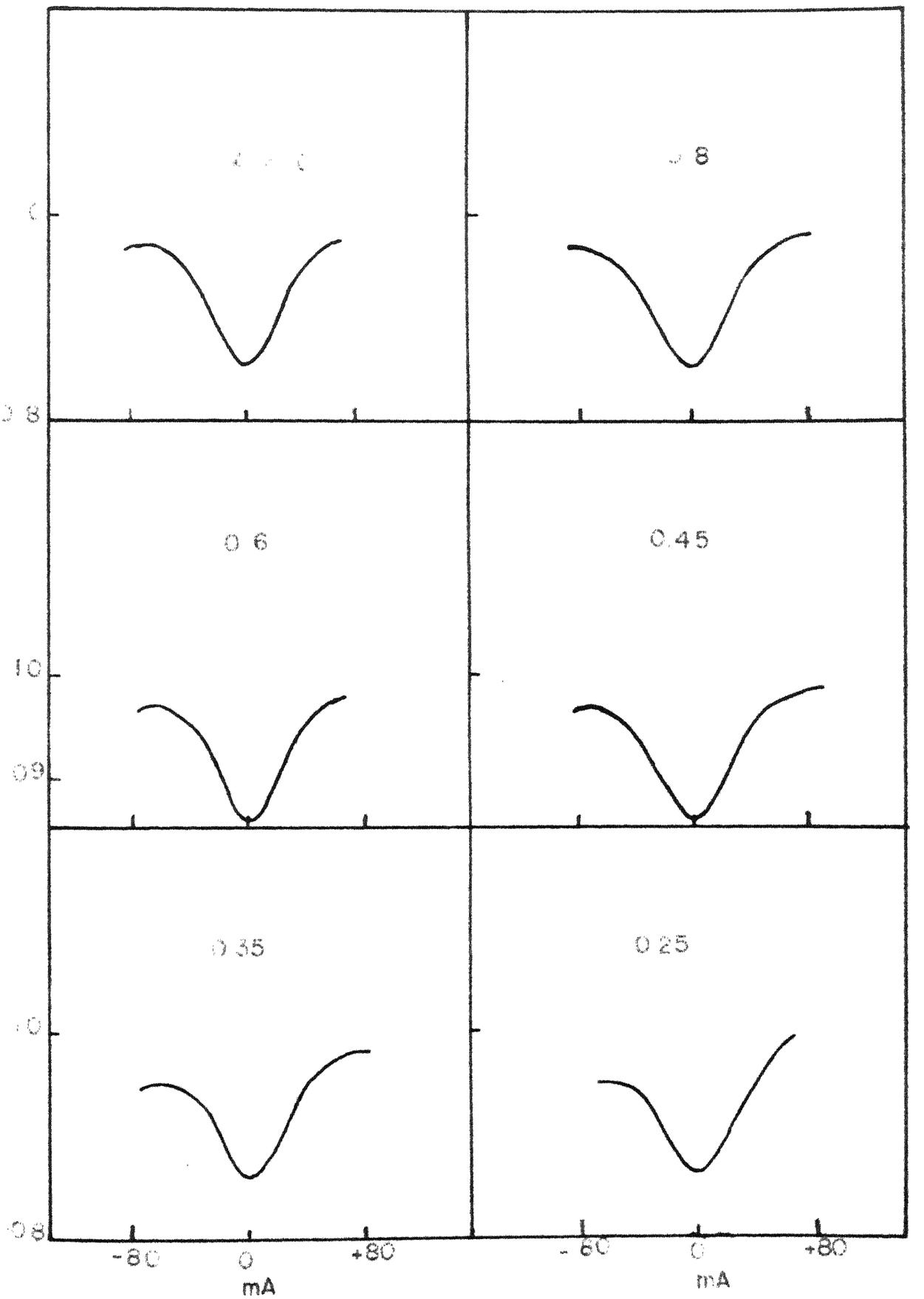
0 8
0 6
0.45
0 35
0 25
-80
0
+80
mA
-80
0
+80
mA

5159, C_2

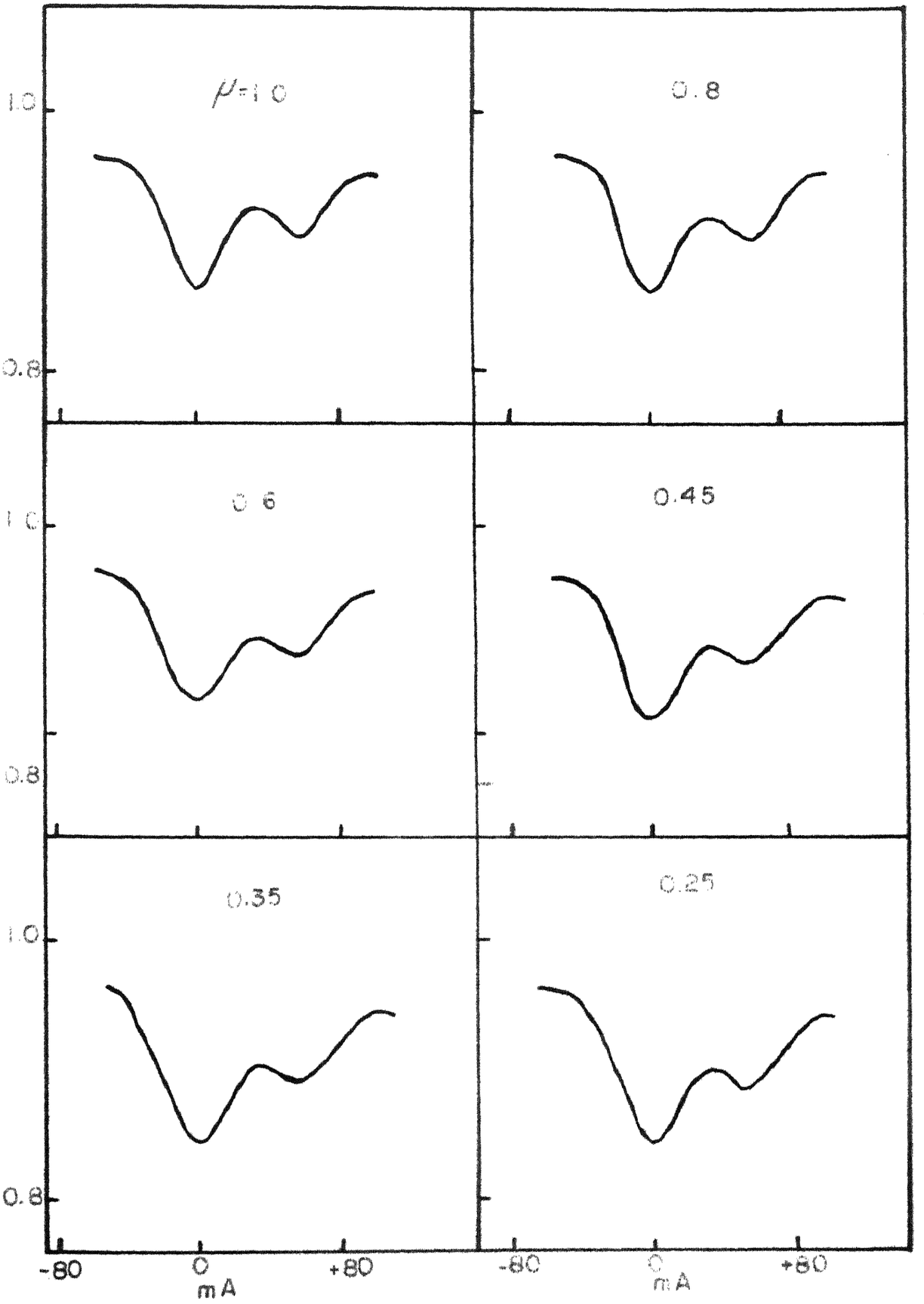

and the centre-limb variations of central intensity has the same characteristic trend of gradual increase followed by a rapid one. The change of the line profiles from relatively narrow V shaped profiles to broad shallow profiles is again present. This line also exhibits broadening towards the limb.

4378.915A belongs to the P branch of 1-1 sequence of the $A^2\Delta - X^2\Pi$ transition. It is an unresolved combination of the spin doublet P_{1dl} and P_{2dl} lines having rotational quantum number $K=15$. The wave number separation of the spin doublets is $<0.2cm^{-1}$. It reaches the continuum on the violet side, but is blended quite badly in the red wing. The Rowland intensity is given as 1 and the line has a central intensity of 68 per cent in the centre of the disc. In the centre-limb variation of central intensities, 4378.915A behaves like 4192, 4212 etc. In other words the central intensity decreases slowly upto $\mu = 0.6$ and then shows a slight increase. The profiles show the common behaviour of broadening and become quite pronouncedly U-shaped towards the limb.

The lines 5086.251A and 5086.399A are C_2 lines of a partially resolved triplet of $^3\Pi_g - {}^3\Pi_u$ transition with 5086.251A being the unresolved $R_{23}(37)$ line and 5086.399A the $R_1(37)$ line. The Rowland intensities of these lines are -1 and -2 respectively. The central intensity of the

unresolved R_{23} line 5086.251A seems to be unaffected by blending from the 5086.399A line and has a value of 87.4 per cent at the centre of the disc. This value decreases on going towards the limb in a very similar fashion to the central intensities of the 4192A and 4212A lines of CN. The common feature of broadening of the profile is also present.

5094.029A is a composite line of unresolved $P_3(62)$ at 5094.002 and $P_1(62)$ at 5094.095, belonging again to the $C^1\Pi$ sequence of Swan bands of C_2. The line has a Rowland intensity of -2 and reaches the continuum on both sides. The line displays a red asymmetric wing. The central intensity at the centre of the disc is 91.7 per cent and decreases to 90.1 per cent at μ =0.45. It then rises to 90.6 per cent thereby showing a trend similar to the foregoing faint lines. Also evident is the increase in half width together with the profile becoming markedly less steep on going from μ =0.35 to μ =0.25.

5147.106A is a C_2 line belonging to the R_1 branch of the $C^1\Pi$ sequence of the 5165A Swan system. The rotational quantum number has the value J=11. This line has a Rowland intensity -1 and is blended on both wings. It is unlikely that this blending affects the central intensity. There is, however, a slight violet asymmetry, which may be an atomic blend effect. Starting with a central intensity

of 85 per cent at μ =1.0, the central intensity changes very little until μ =0.35 and then increases to 96 per cent. The increase in half width is not very pronounced, nor do the profiles assume very distinct U-shapes at the limb.

The lines 5159.467A and 5159.609A form a partially resolved triplet of the P branch of the C_2 Swan system. 5159.467A is the unresolved P_{23} line with J = 28 while 5159.609A is the resolved $P_1(28)$ line.

Both in regard to the variation in minimum intensity from centre to limb and in the width and shape of profiles the combination of these lines show the same general trend as the other weak lines considered.

Thus, summarising the general trends, we find that all the lines are broader at the limb than at the centre, irrespective of line strengths. As for central intensities, all the weak lines show a decrease upto μ =0.45 and then a tendency to increase at μ =0.25.

All strong lines show the identical trend of a small increase in central intensity upto μ=0.7 and then a steep increase upto μ =0.25, irrespective of the molecule.

The generality of the trend emphasizes that it is highly likely that the centre-limb variations are characteristic of the physical structure of the solar atmosphere

rather than a property of the particular molecule concerned. However, any factor arising out of the depletion or augmentation of the available carbon supply could affect all three molecules simultaneously and this possibility cannot be ruled out.

In the succeeding two chapters the methodology of constructing synthetic molecular line profiles and then matching with selected observed profiles are presented.

CHAPTER V

THE CALCULATION OF THE CONTINUOUS ABSORPTION, CONTINUUM INTENSITIES AND LINE ABSORPTION COEFFICIENTS

5.1. Introduction.

In this chapter we investigate the significance of constructing synthetic molecular line profiles, the basic assumptions underlying such a construction and the choice of related physical parameters entering the problem.

One of the fundamental problems in stellar atmospheres is to derive the physical structure of the outer layers of the star from a study of the intensities of the absorption lines formed in this layer. The outline of the current status of the molecular problem given in Chapter I indicates clearly that a completely rigorous theoretical approach will be impossible. Thus, in deriving the physical structure from the line spectrum, we pose the reverse problem i.e. given the physics of the outer layers of the sun, through which a certain energy flux is transported by radiation in the first approximation, how can we derive the profile of an absorption line ? Comparing such a derived profile and the observed profile, the degree of agreement between the two, gives a measure of the correctness of the original specification of the physical structure. In other words we must have a reasonable fore-knowledge of

the physical structure that we have set out to determine and arrive at the correct structure by its ability to predict the observed profiles. Therefore, together with a rough idea of the likely structure of the outer layers we must also know the basic theory of line formation.

5.2. Basic theory of line formation.

In computing theoretical line profiles a simple model atmosphere stratified in plane parallel layers is assumed. These layers are not subjected to large scale turbulence, i.e. hydrostatic equilibrium is postulated, in the first approximation. The methodology of now obtaining the line profile consists of,

a) Absorption coefficient for the line of interest - an aspect partly in the realm of atomic and molecular physics.

b) The process of outward flow of radiation through layers that have their physical and chemical structure specified by the model atmosphere assumed.

The line intensity calculations could be made to any degree of sophistication depending on the starting conditions.

Consider a narrow beam of monochromatic radiation $I_\nu(\theta)$ passing through an elemental volume of thickness ds, at an angle θ to the normal to the atmosphere.

The differential change in the intensity as it passes through this layer is

$$\left.\begin{aligned} dI_\nu &= -(K_\nu + l_\nu + \sigma + \sigma_\nu)\rho I_\nu \frac{dZ}{\cos\theta} \\ &\quad + (K_\nu + l_\nu + \sigma + \sigma_\nu)\rho S_\nu \frac{dZ}{\cos\theta} \end{aligned}\right\} \qquad (5.1)$$

where $d\delta = -dz/\cos\theta$ and S_ν is the source function i.e. the ratio of the total emissivity of the layer to total absorptivity.

Defining optical depth t_ν as

$$dt_\nu = (K_\nu + l_\nu + \sigma + \sigma_\nu)\rho\, dz$$

where K_ν and σ are the absorption and scattering coefficients in the continuum respectively and l_ν and σ_ν are those corresponding to the line.

Therefore, (5.1) may be written as

$$\cos\theta \frac{dI_\nu(t_\nu,\theta)}{dt_\nu} = I_\nu(t_\nu,\theta) - S_\nu(t_\nu,\theta) \qquad (5.2)$$

We are concerned about determining the 'profile' of a line i.e. $I_\nu(t_\nu,\theta)$ in the small range of frequency over which l_ν and σ_ν change steeply. The continuum processes are relatively slow functions of frequency and are essentially

constant over this small range of frequency where line processes are so strongly frequency dependent.

To obtain a line profile, therefore, we must solve (5.2) simultaneously for different frequency ranges of the profile. In the case of a semi-infinite plane parallel atmosphere the formal solution of (5.2) is

$$I_\nu(0,\theta) = \int_0^\infty S_\nu(t_\nu,\theta)\, e^{-t_\nu/\cos\theta}\, dt_\nu/\cos\theta \qquad (5.3)$$

It is now clear that the problem of constructing theoretical line profiles is solved if S_ν, b_ν, K_ν, σ_ν and σ are known as functions of an arbitrarily chosen optical depth.

From the empirical model of the solar atmosphere, adopted as an initial assumption, the variations of temperature, total gas pressure and electron pressure are known as functions of the optical depth at 5000Å. Knowing the model atmosphere and the sources of continuous opacity and the atomic or molecular parameters characteristic of the line, it is possible to obtain K_ν σ, b_ν and σ_ν for each of the optical depths of the model atmosphere.

If there is local thermodynamic equilibrium every where in the atmosphere

$$S_\nu \equiv B_\nu$$

where B_ν is the Planck function for the local temperature and is given by

$$B_\nu = \frac{2h\nu^3}{c^2} \frac{1}{\exp(h\nu/kT)-1}$$

we, therefore, now have

$$I_\nu(0,\theta) = \int_0^\infty B_{\nu'} e^{-t_{\nu'}/\cos\theta} dt_{\nu'}/\cos\theta \qquad (5.4)$$

The integrand is known for a set of t_ν values, so that a numerical solution for $I_\nu(0,\theta)$ is both straightforward and feasible.

At this stage it is interesting to look at the principle underlying the analysis of a line profile and how an extensive study of the line profile gives a clearer picture of the atmosphere. A rough approximation to (5.4) is

$$I_\nu(0,\theta) \sim B_\nu\left(T_e(t_\nu = \cos\theta)\right)$$

This relation shows that the line profile is completely

analogous to $dT_e/d\tau$ because the line profile simply corresponds to looking at different depths in the line and the continuum. Therefore, a T_e increasing inwards gives an absorption line and a T_e increasing outwards gives an emission line.

Since the assumed model atmosphere temperature distribution, enters in the determination of $I_\nu(\cos\theta)$ and J_ν for a fixed $\cos\theta$, we can investigate the dependence of t_ν and, therefore, α_ν and in the core of the line α_ν has a frequency dependence fixed by the velocity field. Thus by forcing an agreement between observed and predicted line profile cores, we have an empirical method of arriving at the velocity field. The residual intensity at any point on a line profile is given by

$$R_{\Delta\lambda}(\mu) = I_{\Delta\lambda}(0,\mu) / I_\lambda(0,\mu)$$

where $\cos\theta = \mu$, $I_{\Delta\lambda}(0,\mu)$ is the intensity in the line at a distance $\Delta\lambda$ from the line centre and $I_\lambda(0,\mu)$ is the continuum intensity at the wavelength of the line centre.

Therefore, to compute numerically the residual intensity at each point of a line profile, the following have to be specified:

1) Model solar atmosphere giving the temperature, electron pressure and total gas pressure as function of optical depth at one specific wavelength.

2) The sources of continuous opacity in the solar atmosphere and the calculation of the continuous absorption coefficient corresponding to the model atmosphere adopted.

3) The calculation of continuum intensities appropriate to the model used, for all wavelength regions of interest and for different angles of emergence of the radiation.

4) The calculation of line absorption coefficient, which involves the knowledge of molecular constants, atomic abundances, nature of physical processes other than thermal in the atmosphere and the distribution of molecules over the solar atmosphere.

In what follows each of these points will be dealt with in detail.

5.1. The Model Atmosphere.

In choosing the appropriate model atmosphere for studying molecular lines, two factors must be borne in mind. Firstly carbon constituent molecules are formed in the very superficial layers of the photosphere and all three molecules chosen for this study have been observed in emission.

Therefore, a model atmosphere covering very small values of optical depth is required. Secondly, the ability of standard photospheric models to explain the observations relating to CO (Dewaire 1957) and OH (Laborde 1961) indicates that very cold models with a minimum temperature around 3500°K advocated by Becker (1957) are probably ruled out.

In a semi-empirical study of this kind it was felt that an analytical model based on accurate observations is more suitable than an entirely theoretical model. To represent the photosphere from log τ = -1.6 to log τ = +0.6 the Pierce-Waddell (1961) model was chosen. In view of the need to consider layers of the atmosphere much higher than that corresponding to log τ = -1.6, this model was extended by combining it with the model given for the lower chromosphere by Thomas and Athay (1961). This extends upto log τ = -5.0.

~~Figure V-1 shows the temperature and pressure distributions of the combined model~~ and Table V-1 gives the numerical values of the parameters as a function of log τ_0 for the wavelength 5000A.

5.4. Calculation of continuous absorption coefficient.

It is well known that hydrogen, by far the most abundant element in the sun, is the principal absorber either in a neutral state or as negative hydrogen ion.

Table V-1.

Morse-Haddell HAW Model

log τ_5	T in degrees K	P_g in 10^5 dynes/cm	P_e in 10^2 dynes/cm	K_o in 10^{-25} per neutral hydrogen atom.
-5.0	6150	0.0071	0.0040	0.1482
-4.8	6060	0.0089	0.0039	0.1537
-4.6	5940	0.0123	0.0038	0.1616
-4.4	5820	0.0182	0.0038	0.1753
-4.2	5675	0.0275	0.0039	0.1954
-4.0	5505	0.0427	0.0038	0.2064
-3.8	5400	0.0646	0.0036	0.2106
-3.6	5380	0.0977	0.0035	0.2200
-3.4	5230	0.1413	0.0037	0.2505
-3.2	5140	0.2130	0.0040	0.2903
-3.0	5050	0.3167	0.0045	0.3642
-2.8	4955	0.4365	0.0054	0.4700
-2.6	4870	0.5957	0.0062	0.5863
-2.4	4780	0.7943	0.0072	0.7316
-2.2	4720	1.0720	0.0087	0.9407
-2.0	4680	1.4150	0.0108	1.2110
-1.8	4630	1.8620	0.0132	1.4605
-1.6	4740	2.3990	0.0164	1.7394
-1.4	4842	2.9240	0.0211	2.0457
-1.2	4976	3.7760	0.0288	2.4831
-1.0	5141	4.8870	0.0404	3.0148
-0.8	5339	6.3100	0.0593	3.7945
-0.6	5575	8.0540	0.0944	5.1547
-0.4	5805	10.0000	0.1660	7.6028
-0.2	6130	11.9900	0.3206	12.0060
-0.0	6469	15.9300	0.6622	20.5280
+0.2	6858	15.6700	1.4660	36.2100
+0.4	7362	17.2200	3.5240	56.9560
+0.6	8005	18.4500	9.3760	131.2600

The two modes of interaction of radiation with the hydrogen atom which are of importance to the continuous opacity, are the bound-free and free-free transitions. Kramers has shown that the absorption cross section per atom in the n^{th} level is proportional to $1/\nu^3$ beginning at the Balmer limit

$$k_\nu(\nu) = \frac{64\pi^4 e^{10} m}{3\sqrt{3}\, ch^6 m^{5/3}}$$

The contribution of the various energy levels to the absorption coefficient depends on the populations of the levels. This is given by the Boltzmann distribution corresponding to the temperature,

$$\frac{N_n}{N} = \text{constant} \cdot n^2 \exp(\chi/n^2 kT)$$

where N is the number of neutral atoms N_n is the number in level n and χ the ionisation potential of hydrogen. Quantum mechanical calculations for the absorption cross sections for neutral hydrogen by Menzel and Pekeris show that Kramer's formula must be corrected by a Gaunt factor g which is generally very near unity. In this study the exact values of Gaunt factors are not included and are set equal to unity.

In the calculation of absorption coefficient due to

bound-free transitions, the recombinations or stimulated emission has been corrected for by introducing the factor $(1 - \exp(-h\nu/kT))$ in the absorption coefficient.

Therefore, the expression for continuous absorption coefficient due to bound-free transitions from level n of the hydrogen atom is given by

$$K_n(\nu) = \frac{64 \cdot \pi^4 e^{10} m}{3\sqrt{3} c h^6 \nu^3} (1 - e^{-h\nu/kT}) e^{-\chi/kT} \frac{e^{\chi/n^2 kT}}{n^3}$$

The total absorption coefficient per atom of neutral hydrogen at a particular temperature is the sum of the absorptions from all the levels capable of absorption at the wavelength of interest. Since the regions of interest in this study fall between the Paschen and Balmer limits, transitions from 3,4,5 ... levels must be considered. Noting that for any given wavelength the lowest levels considered are the main contributors to absorption, the remaining terms may be replaced by

$$\frac{e^{\chi/N^2 kT} - 1}{(2\chi/kT)}$$

In this study N = 9 giving

$$K_\nu = \left(\sum_{n=3}^{8}{}' \frac{e^{+\chi/n^2 kT}}{n^3} + \frac{e^{\chi/81 kT} - 1}{(2\chi/kT)} \right) \frac{64\pi^4 e^{10} m}{3\sqrt{3} c h^6 \nu^3} (1 - e^{-h\nu/kT}) e$$

The absorption cross-section for the free-free continuum is

$$K(\nu) = \left(\frac{c}{\nu^3}\right) \cdot \frac{1}{(2\chi/kT)} \cdot \left(1 - e^{-h\nu/kT}\right) e^{-\chi/kT}$$

$$c = \frac{64}{3\sqrt{3}} \frac{\pi^4 e^{10} m}{ch^6}$$

Therefore, the atomic absorption coefficient for both bound-free and free-free part is

$$K_\nu(H) = \left(\frac{c}{\nu^3}\right)\left(1 - e^{-h\nu/kT}\right) e^{-\chi/kT} \sum_{n=3}^{9} \frac{e^{\chi/n^2kT}}{n^3} + \frac{e^{\chi/81k}}{(2\chi/kT)}$$

The contribution to the continuous absorption coefficient by the negative hydrogen ion has been extensively calculated.

The most recent of these calculations is by Gingerich (1961) who has computed a polynomial approximation to the Chandrasekhar-Breen (1946) values with new values for the free-free component derived by Ohmura and Ohmura (1960). The values of the absorption coefficient due to negative hydrogen ion per neutral hydrogen atom per unit electron pressure, were adopted from the detailed tables published by Gingerich.

To obtain the total continuous absorption coefficient per neutral hydrogen atom for each level of the model

atmosphere a programme was written to evaluate the expression.

$$K_\nu = k_\nu(H) + K_\nu(H^-) \cdot P_e$$

$$K_\nu = \frac{c}{\nu^3}\left(1 - e^{-h\nu/kT}\right) e^{-\chi/kT} \sum_{n=3} \frac{e^{\chi/n^2kT}}{n^3} + \frac{e^{\chi/81kT}}{(2\chi/kT)}$$

These computations were carried out for all the 29 levels of the adopted model and for wavelength regions 3660Å, 4200Å, 5000Å and 5100Å.

5.5. Calculation of continuum intensities.

Solving the time-independent transfer equation for a semi-infinite plane parallel atmosphere, the intensity in the continuum is given by

$$I_c(\nu, \mu) = \int_0^{\infty} S_\nu \, e^{-\tau_\nu/\mu} d\tau_\nu/\mu$$

Replacing S_ν by B_ν on the assumption of local thermodynamic equilibrium

$$I_c(\nu, \mu) = \int_0^{\infty} B_\nu \, e^{-\tau_\nu/\mu} d\tau_\nu/\mu$$

By definition, the optical depth τ_ν at any frequency is related to the optical depth τ_0 at the standard frequency corresponding to λ 5000Å by the relation,

$$d\tau_\nu = \frac{K_\nu}{K_0} d\tau_0$$

$$\tau_\nu = \int_0^{\tau_0} \frac{K_\nu}{K_0} d\tau_0$$

Thus, the numerical evaluation of the continuum involves the following steps:

1) Numerical integration over the ratio of absorption coefficients to obtain the optical depth at the wavelength of interest for each level of the model atmosphere.

2) Evaluation of the Planck function for each level corresponding to one wavelength region.

3) Integration of $B_\nu e^{-\tau_\nu/\mu} \frac{K_\nu}{K_0} \cdot \frac{d\tau_\nu}{\mu}$ over all the levels of the atmosphere.

Since the model is known at equal intervals in log τ_0 rather than τ_0 and considering also the fact that log τ_0 is physically closely related to geometrical heights in the atmosphere, we perform the integration over the log τ_0 scale.

Putting

$$y = \log \tau_0$$

$$dy = \frac{d\tau_0}{\tau_0} \cdot Mod$$

$$d\tau_0 = \frac{10^y dy}{Mod}$$

$$\tau_\nu = \int_{-\infty}^{y} \frac{K_\nu}{K_0} \frac{10^y dy}{Mod} \qquad (5.5)$$

$$\text{and } I_0(\nu,\mu) = \int_{-\infty}^{y_1} \frac{B_\nu}{Mod} e^{-\tau_\nu/\mu} \frac{K_\nu}{K_0} \frac{10^y dy}{\mu} \qquad (5.6)$$

For numerical integration Gregory's formula up to the first difference has been used. The integral $I = \int_a^b X_n dx$ is given by

$$I = \frac{1}{2} X_0 + X_1 \cdots X_{n-1} + \frac{1}{2} X_n + \frac{1}{12} (\Delta X_n - \Delta X_1$$

$$\Delta X_1 = X_1 - X_0$$

$$\Delta X_n = X_n - X_{n-1}$$

From (5.5) it is seen that in order to obtain the optical depth τ_ν corresponding to a level of the model atmosphere, it is necessary to integrate over all overlying levels. Therefore τ_ν's have been calculated only from $\log \tau_0 = -4.2$ and downwards.

Table V-2.

Continuum Intensities, $I^c_\lambda \times 10^{-5}$

Wavelength	μ=1.00	μ=0.80	μ=0.60	μ=0.45	μ=0.35	μ=0.25
3860A	2.037	1.861	1.599	1.340	1.159	0.915
4220A	2.403	2.195	1.892	1.603	1.381	0.134
5000A	3.059	2.799	2.438	2.115	1.869	1.595

In calculating the integral (5.6) integration to infinity is required. Layers above log $\tau_0 = -4.2$ contribute negligibly to the continuum intensity. Below log $\tau_0 = 0.6$ the contribution was again small and, therefore, not included in the present computations.

The calculation of continuum intensity was made for the wavelength regions 3360A, 4220A, and 5000A ~~and 5190A~~ for μ values 1.0, 0.8, 0.6, 0.45, 0.35 and 0.25. Table V-2 gives the computed continuum intensities.

5.6. Determination of line absorption coefficient.

From the classical theory of electron for the vibration of a linear harmonic oscillator in a fluctuating electric field of a light wave, the absorption coefficient is given by

$$\alpha_\nu = \frac{\pi e^2 N}{mc} \frac{\gamma}{[(\omega-\omega_0)^2 + (\gamma/2)^2]} \qquad (5.7)$$

Equation (5.1) is the 'damping profile' where ω is the characteristic frequency of the line and γ is the classical damping constant. The damping profile is symmetrical with respect to $\omega = \omega_0$. In the quantum mechanical picture N is replaced by Nf, f being the oscillator strength and γ_R is now the radiation damping factor.

Expression (5.7) relates to a situation in which absorption takes place in a stationary atmosphere. In an atmosphere with a characteristic temperature and having turbulent velocities which follow a Maxwellian distribution, and negligible damping the line absorption coefficient per neutral hydrogen atom expressed in wavelength units is

$$\alpha_\lambda = \frac{\sqrt{\pi}\, e^2}{mc^2} f \lambda_0^2 \frac{N}{\Delta\lambda_D} \exp -(\Delta\lambda/\Delta\lambda_D)^2 \quad (5.8)$$

where N is the total number of molecules capable of absorbing the line of interest $\Delta\lambda_D$ is the 'Doppler width' given by

$$\frac{\Delta\lambda_D}{\lambda} = \frac{\xi}{c}$$

and $$\xi^2 = \frac{2RT}{\mu} + \xi_t^2$$

ξ_t being the line of sight turbulent velocity. The assumption of a Maxwellian distribution for turbulent velocities is one of convention. It is very probable that the approximation is reasonable in so far as it provides numerical estimates of turbulence velocity fields having eddy sizes of the order of the length of the line forming region.

Therefore, in calculating the line absorption

coefficient three quantities, besides physical constants, must be known:

N - which includes the abundance of the molecule concerned at any particular temperature and pressure and the condition of excitation of the available molecules.

$\Delta \lambda_D$ - which requires the specification of ξ_t as a function of an angle of emergence and/or depth and

f - the oscillator strength of the molecular transition concerned.

The abundances given by Goldberg, Aller and Muller (1959) for carbon, nitrogen and oxygen have been adopted in this study.

The f- values to be used for the $^2\Sigma^+ - {}^2\Sigma^+$ transition of CN, $^3\Pi_g - {}^3\Pi_u$ transition of C_2 and the $A^2\Delta - X^2\Pi$ transition of CH have always been under discussion. In a critical summary of the molecular situation in the sun de Jager and Neven (1957) give 0.044, 0.040 and 0.060 as the respective f values of CH, C_2 and CN, which form a self consistent set. Cowley (1964) has been able to predict the correct equivalent width of CH lines at the centre of the disc by adopting f = 0.029 and a dissociation energy of 7.5 ev. In this investigation White's (1940) original f

value of 0.026 has been used for CH along with the dissociation energy of 7.2 ev. The ratio of f values of C_2 to CH has been given by Lyddane, Rogers and Gaunch (1941) as 0.92. Therefore, the f value chosen for C_2 is 0.024. Central intensity calculations for CH using f = 0.060 give absorption coefficients that are too high by a factory of 100. Thus we were forced to adopt an arbitrarily low f value for CH. Following Keeler and Praderie (1960) this was chosen to be 0.0005.

The problem of calculating the total number of molecules of a particular kind capable of absorbing a certain frequency of radiation consists of two steps. We determine for this purpose the distribution of partial pressure of the particular molecule with height as well as the fraction of all the molecules of this kind that are in the vibrational and rotational level appropriate to the line absorption in question.

The distribution of partial pressures of a molecule corresponding to the assumed model atmosphere can be obtained by considering the dissociation equilibrium of all the important diatomic molecules simultaneously. The partial pressures $p(H)$, $p(C)$, $p(N)$ and $p(O)$ of free atoms H, C, N and O and the fictitious pressures $P(H)$, $P(C)$, $P(N)$ and $P(O)$ that would occur if the elements were completely

dissociated are related by the system of equations.

$$P(H) = p(H)\left[1 + \frac{2p(H)}{2K(H_2)} + \frac{p(C)}{K(CH)} + \frac{p(N)}{K(NH)} + \frac{p(O)}{K(OH)}\right]$$

$$P(C) = p(C)\left[1 + \frac{p(H)}{K(CH)} + \frac{2p(C)}{K(C_2)} + \frac{p(N)}{K(CN)} + \frac{p(O)}{K(CO)}\right]$$

$$P(N) = p(N)\left[1 + \frac{p(H)}{K(NH)} + \frac{p(C)}{K(CN)} + \frac{2p(N)}{K(N_2)} + \frac{p(O)}{K(NO)}\right]$$

$$P(O) = p(O)\left[1 + \frac{p(H)}{K(OH)} + \frac{p(C)}{K(CO)} + \frac{p(N)}{K(NO)} + \frac{2p(O)}{K(O_2)}\right]$$

Here $K(AB)$ is the dissociation constant for the molecule AB. The system of equations given above is a set of four equations of the second degree in four unknowns. They may be solved directly by iteration, but the solution is made much simpler because a number of terms are vanishingly small in view of the dominating abundance of hydrogen. For the assumed abundances the system of four equations reduces to

$$P(H) = p(H)\left[1 + 2p(H)/K(H_2)\right] \qquad (5.9)$$

$$P(C) = p(C)\left[1 + \frac{p(H)}{K(CH)} + \frac{p(O)}{K(CO)}\right] \qquad (5.10)$$

$$P(N) = p(N)\left[1 + \frac{2p(N)}{K(N_2)} + \frac{p(H)}{K(NH)}\right] \qquad (5.11)$$

$$P(O) = p(O)\left[1 + \frac{p(C)}{K(CO)} + \frac{p(H)}{K(OH)}\right] \qquad (5.12)$$

The solution of these equations is straight forward. Equation (5.9) is a second degree equation in $p(H)$ and the solution $p(H)$, of this substituted in (5.11) gives $p(N)$, while (5.10 and (5.12) are linear equations in $p(O)$ and $p(C)$ and may be solved simultaneously.

Prior to the calculation of partial pressures the dissociation constants K_{AB} for H_2, N_2, NH, C_2, CH, CO, CN and OH must be known as functions of temperature. The dissociation constant of a molecule is given by (Aller 1953).

$$K(AB) = \frac{g_A g_B}{g_{AB}} \frac{(2\pi mkT)^{3/2}}{h^2} \frac{h^2}{8\pi^2 I} \left(1 - e^{-\omega hc/kT}\right) e^{-D_0/k}$$

where g_A , g_B and g_{AB} are statistical weights of the ground levels of atoms A and B and the molecule AB, μ is the reduced mass of the molecule, I is the moment of inertia of the molecule, ω the wave number corresponding to the vibrational frequency, and D_o is the dissociation energy. All the molecular constants have been adopted from Herzberg (1951) except for D_o . The D_o values published by Wilkinson (1953) have been used. The more important molecular constants used are set out in Table V-3.

The partition function for a molecule is given by

$$Z = Z_{rot} \cdot Z_{vibr} \cdot Z_{ele} \cdot Z_{sym}$$

the standard approximations being

$$Z_{vibr} = \sum_{v=1}^{\prime} e^{-v\omega hc/kT}$$ v being the vibrational quantum number.

Hence, $$Z_{vibr} = \left(1 - e^{-\omega hc/kT}\right)^{-1}$$

$$Z_{rot} = \sum_{J}^{\prime} (2J+1)\, e^{-B_v J(J+1)hc/kT}$$

$$\simeq kT/hcB$$

$$Z_{ele} = D(2S+1)(2\Lambda+1)\, e^{-T_e hc/kT}$$

Table V-3.

Dissociation Potentials and Oscillator Strengths.

Molecule	Dissociation potential.	Oscillator Strengths.
CN	7.5 e.v.	0.026
C_2	6.25 e.v.	0.024
CH	3.47 e.v.	0.0005

where for $\Lambda = 1, D = 1$ and for $\Lambda = 1,2,3$ etc $D = 2$

$2\Sigma + 1$ is the multiplicity of the electronic level.

$Z_{sym} = \frac{1}{2}$ for homonuclear molecules and 1 for hetero nuclear molecules.

In the calculation of partition functions only the ground levels of molecules have been considered.

In the computation of partial pressures the partition function and the dissociation constant were calculated for each level of the assumed model atmosphere and then used in solving the system of equations (5.9) to(5.12).

Knowing the partial pressures of $p(C)$, $p(H)$ and $p(N)$ the partial pressures of C_2, CN and CH are given by

$$p(C_2) = \frac{p(C) \times p(C)}{K(C_2)}$$

$$p(CN) = \frac{p(C) \cdot p(N)}{K(CN)}$$

and $$p(CH) = \frac{p(C) \cdot p(H)}{K(CH)}$$

The computations were made using a IBM 1620 computer and a common programme was written in the FORTRAN II language, for all the three steps, to obtain all the relevant partial

Table V-4.

Relative Partial Pressures - Cl, Cl and C_2.

Log C_0	$p_{(N)}/p_g$	$p_{(H)}/p_g$	$p_{(C_2)}/p_g$
-5.0	3[illegible]8.3[illegible]-14	106.0[illegible]-12	162.1[illegible]-14
-4.8	590.7[illegible]-14	170.2[illegible]-12	245.6[illegible]-14
-4.6	915.5[illegible]-14	266.5[illegible]-12	437.7[illegible]-14
-4.4	226.2[illegible]-13	481.9[illegible]-12	844.8[illegible]-14
-4.2	513.7[illegible]-13	948.1[illegible]-12	178.8[illegible]-13
-4.0	102.4[illegible]-12	157.7[illegible]-12	344.2[illegible]-13
-3.8	206.4[illegible]-12	273.1[illegible]-11	660.1[illegible]-13
-3.6	440.3[illegible]-12	409.7[illegible]-11	132.7[illegible]-12
-3.4	105.3[illegible]-11	900.0[illegible]-11	238.2[illegible]-12
-3.2	212.0[illegible]-11	158.2[illegible]-10	562.7[illegible]-12
-3.0	429.6[illegible]-11	273.0[illegible]-10	108.3[illegible]-11
-2.8	936.7[illegible]-11	446.1[illegible]-10	199.4[illegible]-11
-2.6	156.9[illegible]-10	711.4[illegible]-10	355.0[illegible]-11
-2.4	294.6[illegible]-10	110.2[illegible]-09	611.9[illegible]-11
-2.2	505.6[illegible]-10	170.0[illegible]-09	103.7[illegible]-10
-2.0	770.8[illegible]-10	241.7[illegible]-09	155.9[illegible]-10
-1.8	979.2[illegible]-10	311.1[illegible]-09	196.8[illegible]-10
-1.6	102.0[illegible]-09	362.9[illegible]-09	214.0[illegible]-10
-1.4	944.5[illegible]-10	364.7[illegible]-09	187.6[illegible]-10
-1.2	661.0[illegible]-10	368.8[illegible]-09	159.6[illegible]-10
-1.0	478.9[illegible]-10	359.2[illegible]-09	127.1[illegible]-10
-0.8	321.9[illegible]-10	336.7[illegible]-09	950.5[illegible]-11
-0.6	199.9[illegible]-10	301.8[illegible]-09	663.7[illegible]-11
-0.4	129.9[illegible]-10	272.6[illegible]-09	479.2[illegible]-11
-0.2	676.9[illegible]-11	216.7[illegible]-09	285.6[illegible]-11
0.0	359.5[illegible]-11	171.1[illegible]-09	172.2[illegible]-11
0.2	180.9[illegible]-11	129.2[illegible]-09	986.8[illegible]-12
0.4	795.3[illegible]-12	901.1[illegible]-10	501.9[illegible]-12
0.6	309.4[illegible]-12	594.7[illegible]-10	230.9[illegible]-12

pressures. The details of the programs are given in the appendix.

Given the partial pressure of a molecule, the fraction of this molecule that are in a rotational level J capable of absorbing the line of interest is obtained from

$$N_{AB} = p(AB) \cdot \frac{(2J+1)}{Z(AB)} e^{-BJ(J+1)hc/kT}$$

and the statistical weight (2J+1)

The rotational transition probabilities are given in terms of line strength factors i which are functions of the rotational quantum number. Therefore, the total number of molecules capable of absorbing the line at a particular temperature is given by

$$N_{AB} = \frac{p(AB)}{Z(AB)} \cdot i \cdot e^{-BJ(J+1)hc/kT}$$

The line absorption coefficient, per neutral hydrogen atom at a temperature T has, therefore, the form

$$\alpha_\lambda = \frac{\sqrt{\pi} e^2}{mc^2} f \frac{\lambda_o^2}{\Delta\lambda_D^2} \frac{p(AB)}{p(H)} \frac{i}{Z(AB)} e^{-J(J+1)hc/kT}$$

The line strength factors for C_2, CH and CN were calculated from the following formula.

The $^3\Pi_g$ and $^3\Pi_u$ states are closer to Hund's coupling case b and the six branches from two sets of triplets $P_1(J+1)$, $P_2(J)$, $P_3(J-1)$ and $R_1(J+1)$, $R_2(J)$, $R_3(J-1)$. The intensity factors of the triplets under this condition have been given by Budo (1937).

$$\therefore i[P_1(J)] = \frac{(J-2)J(J+1)}{(J-1)(2J-1)}$$

$$i[P_2(J)] = \frac{(J-1)^2(J+1)^2}{J^3}$$

$$i[P_3(J)] = \frac{J(J+2)(2J-1)}{(J+1)(2J+1)}$$

$$i[R_1(J)] = \frac{(J-1)(J+1)(2J+3)}{J(2J+1)}$$

$$i[R_2(J)] = \frac{J^2(J+2)^2}{(J+1)^2}$$

$$i[R_3(J)] = \frac{(J+1)(J+3)(2J+1)}{(J+2)(2J+3)}$$

For CH, the rotational energy levels of $^2\Delta$ state are subject to spin doubling into two sub-levels but Λ type doubling of each of these is practically zero, the doubling into c and d levels being latent. The $^2\Pi$ state has of course four sub-sub-levels corresponding to Wirm Dahlen $T_{1c}, T_{1d}, T_{2c}, T_{2d}$. Intensity factors for the predicted branches of the $A^2\Delta$-$X^2\Pi$ band, without taking into account Λ type of doubling are as follows:-

$$i\,[P_{1d_1}] = i\,[P_{1cd}] = \frac{(K+1)(K-2)(K-1)}{2K(2K+1)}$$

$$i\,[P_{2d_1}] = i\,[P_{2cd}] = \frac{(K-1)(K-2)(K-1)}{2K(2K-1)}$$

$$i\,[R_{1d_1}] = i\,[R_{1cd}] = \frac{(K+1)(K+2)(K+1)}{2K(2K+1)}$$

$$i\,[R_{2d_1}] = i\,[R_{2cd}] = \frac{(K-1)(K+2)(K+1)}{2K(2K-1)}$$

Since Λ type components of a given sub-level have equal statistical weights, lines which differ only in the subscript have the same strength factors and their common intensity factor for the corresponding branch.

For the CN lines in a $^2\Sigma$ state there is case b spin doubling of each rotational level but no Λ type of doubling, for each value of K, $J = K \pm \frac{1}{2}$. The intensity factors for four of the six branches to be expected are given by

$$\epsilon[R_1] = \epsilon[P_1] = \frac{2K(K+1)}{(2K+1)}$$

$$\epsilon[R_2] = \epsilon[P_2] = \frac{2K(K-1)}{(2K-1)}$$

The only remaining parameter to be specified is the Doppler width. The choice of a model of turbulence has been based on the following considerations. Firstly, depth-independent models with anisotropy have been able to explain atomic line profiles to a large extent (Wadiell 1958). Secondly, the effective layer of molecular line formation is probably narrower than that for atomic lines. So a depth-independent anisotropic turbulence model is chosen in the first approximation, the values of the velocities being obtained by fitting the central intensity and half width of an observed line at the centre of the disc and at $\mu=0.25$. If ξ_{rad}, and ξ_{tan}, are the assumed radial and tangential velocities then

$$\xi_t^2 = \xi_{tan}^2 - \mu^2(\xi_{tan}^2 - \xi_{rad}^2)$$

$$\Delta\lambda_D^2 = \frac{\lambda_0^2}{c^2}\left(\frac{2RT}{M} + \xi_t^2\right) \qquad (9\text{-}13)$$

The form of equation (5.13) indicates that ξ_{rad} may be obtained by fitting central intensities and half widths at the centre of the disc and ξ_{tan} by fitting those at $\mu = 0.25$, together with being able to predict the correct centre-limb variation of central intensities.

Recent work by Schmidberger (1963) indicates that a depth-dependent anisotropic turbulence model in which the line of sight velocity remains constant, fits the observations much better. Therefore, a suitably extended form of Schmidberger's model of turbulence could also be tested in constructing synthetic line profiles to match observed ones.

CHAPTER VI

THE CALCULATION LINE PROFILES.

6.1. The methodology.

In chapter V we have assembled all the physical parameters needed for the evaluation of line intensity,

$$I_{\Delta\lambda}(0,\mu) = \int_0^{\infty} B_\lambda e^{-t_\lambda/\mu} dt_\lambda/\mu$$

The calculation of line intensity is essentially the same as for continuum intensity, except that the optical depth in the continuum is replaced by that in the line. Because scattering is unimportant for molecular lines, the line optical depth t_λ is defined as,

$$dt_\lambda = (\alpha_\lambda + K_\lambda)\rho dz$$

α_λ being the line absorption coefficient and K_λ the continuous absorption coefficient at that wavelength.

$$dt_\lambda = \left(\frac{\alpha_\lambda}{K_\lambda} + 1\right)\frac{K_\lambda}{K_0} \cdot K_0 \rho dz$$

$$= (\eta_\lambda + 1)\,\frac{K_\lambda}{K_0}\,d\tau_0$$

$$= \frac{\alpha_\lambda + K_\lambda}{K_0}\,d\tau_0$$

$$= \left(\frac{\alpha_\lambda}{K_0} + \frac{K_\lambda}{K_0}\right) d\tau_0$$

Changing over to the $\log \tau_0$ scale with $Y = \log \tau_0$

$$t_\lambda = \int \frac{\alpha_\lambda + K_\lambda}{K_0}\,\frac{10^Y}{Mcd}\,dy \qquad (6.1)$$

The line intensity at a distance $\Delta\lambda$ from the line centre becomes

$$I_{\Delta\lambda}(0,\mu) = \frac{1}{\mu}\int_{-\infty}^{+\infty} B_\lambda\, e^{-t_\lambda/\mu}\,\frac{(\alpha_\lambda + K_\lambda)}{K_0}\,\frac{10^Y}{Mcd}\,dy \qquad (6.2)$$

Here again B_λ and α_λ were evaluated at each level of the model atmosphere adopted, while K_0, $\frac{K_\lambda}{K_0}$ partial pressures, partition functions and model atmosphere parameters were read in as input data.

For the numerical integration of both (6.1) and (6.2) Gregory's formula as given in chapter V was used

up to the first difference. As in the calculation of continuum intensity the first four levels could not be used in line intensity calculation, because the evaluation of t_λ at each optical depth involved integration over all the overlying regions. The residual intensity

$$R_{\Delta\lambda} = \frac{I_{\Delta\lambda}(0,\mu)}{I^c_\lambda(0,\mu)}$$

the intensity in the continuum having already been evaluated. $R_{\Delta\lambda}(0,\mu)$ is calculated for different values of $\Delta\lambda$, on an average at eight points on each wing, to obtain the intensity profile of the line. Again, the profile is computed for as many positions on the solar disc, as were required to indicate the trend of the computed results. With an IBM 1620 computer the calculation of a single residual intensity took 225 seconds for a singlet and 290 seconds for a doublet.

The calculation of line contours for doublets or triplets was essentially the same, except that for each level, the appropriate absorption coefficients of the constituent lines were added with the appropriate wavelength shift. If $\Delta\lambda_\delta$ is the separation in wavelength between the two lines at λ_1 and λ_2 the total line absorption coefficient $\alpha_{\Delta\lambda}$ at a distance $\Delta\lambda$ from λ_1 is given by

$$\alpha_{\Delta\lambda} = \alpha_1 e^{-(\Delta\lambda/\Delta\lambda_D)^2} + \alpha_2 e^{-[(\Delta\lambda+\Delta\lambda_S)/\Delta\lambda_D]^2}$$

where α_1 and α_2 include all factors other than $e^{-(\Delta\lambda/\Delta\lambda_D)^2}$ of the absorption coefficient defined by equation (5.8) and relate to the individual lines at λ_1 and λ_2 respectively. This can be completely generalised to include any number of molecular lines blending together.

In treating blends of lines of dissimilar excitation, a completely rigorous method would involve taking into account the fact that the two lines are formed at different layers of the solar atmosphere and that the line formed at the higher layer absorbs from the residual intensity of the line formed in the lower layer and not from the continuum. The situation is much simpler in the case of two lines of the same molecule blending with each other. In most cases components of molecular blends are from almost identical energy levels, these being spin doublets or triplets with the same rotational quantum number. Therefore, the blending lines have identical conditions of excitation and the total line absorption

coefficient at any wavelength is the sum of the absorption coefficients at that wavelength, due to all the component lines

$$\alpha_{\Delta\lambda} = \sum_i \alpha_{\Delta\lambda_i}$$

It is important to note that $\Delta\lambda$ is not measured from the central wavelength of the blend, but from the centre of one of the constituent lines.

6.2. The computed profiles.

The trends in the observed centre-limb variations emphasizes that these variations are very similar for the strong lines on the one hand and weak lines on the other, irrespective of the molecule of their origin. Therefore, computations were restricted to a selected set of lines so that the characteristic features of the observed variations may be studied. The CH lines, 3864.307A and 4207.403A, the C_2, lines 5094.029A and 5147.106A and the CH lines 4210.970A and 4291.974A were selected for extensive computation.

As noted in chapter IV, each one of these lines is a doublet, 5094.029A of C_2 being a triplet. It is well known that hyperfine structure of atomic lines widens the line considerably and simulates the effect of turbulent velocities

and if unaccounted for, give rise to spuriously large turbulent velocities. An important part of calculating molecular line profiles, therefore, is to properly take into account the fine structure associated with spin coupling, in which the wavelength separations are of the same order of magnitude as in atomic hyperfine structure - well within 0.1Å.

The construction of an unresolved doublet profile to which an appropriate turbulent velocity must be fitted is complicated. The contour is very sensitive to the separation between the two lines and a very small change in this separation changes the profile considerably. Preliminary calculations also indicated that the use of the rigorous doublet approach is necessary for separations larger than about 25mÅ. This value, for which the use of a separation in wavelength becomes necessary, depended very strongly on what values of turbulent velocities were assumed initially. The lower the turbulent velocity, the lower is the upper limit of effective separation. This is very reasonable, because in a turbulence broadened line, the effective number of absorbing molecules are shifted away from the central frequency of the line and two line centres separated by a very small amount are not resolved and only larger separations are effective in changing the line contour. Also, the relative intensities of the two component lines is very important in reproducing exactly

the asymmetries observed and the location of the central wavelength.

In view of the aspects mentioned above, two restrictions served as guide lines in planning the strategy of calculations. Firstly, that published separations for spin doubling are probably accurate up to 10mA which corresponds to 0.75 km/sec. at 4000A. Secondly, the spectrographic resolution used in this study gives 15mA for the smallest resolvable separation in wavelength. Therefore, a spin doublet with a separation of 15mA or less may be treated as a coincident doublet - a singlet with the identical absorption coefficients of the two lines added. The fitting of this line with its observed counterpart would fix velocity values which may be used in the other doublet contour calculations.

The 3864.307A line of CH is a line having a spin separation of less than 15mA. In this region of the solar spectrum the local continuum is depressed below the general continuum by ten per cent. In order to compare theoretically computed profiles with observed ones, the computed profiles were referred to an arbitrarily depressed continuum.

With an initial value of ξ_{rad} the computed central intensity at the centre of the disc was fitted to the

observed value of 28.75 per cent. With this fitting factor the entire singlet profile was calculated and the half width of the profiles at the centre of the disc was computed and compared with the observed half width. ξ_{rad} was changed iteratively to fit the observed half width. However, changing ξ_{rad} from the initial value changes the computed central intensity. Therefore, ξ_{rad} and the fitting factor were changed alternately to obtain the right combination of central intensity and half width. The best fit was obtained for a radial turbulence velocity ξ_{rad} =3.0 km/sec.

With ξ_{rad} and the fitting factor - which is a measure of the uncertainties in the transition probabilities used - fixed, the observed half width at μ =0.25 was fitted by changing ξ_{tan} iteratively. A good fit was difficult to obtain because, if the tangential velocity was increased arbitrarily to fit the central intensity the profile at μ =0.25 was too broad and the tangential velocities obtained were improbably large. On the other hand, velocitiesgiving reasonable half width fits gave central intensities that were too low. A compromise value had to be chosen for ξ_{tan} which was atleast capable of predicting the correct trend of the centre-limb variation. The optimum value found was ξ_{tan} = 3.6 km/sec. The profiles

with the combination of ξ_{rad} and ξ_{tan} were computed for disc positions corresponding to μ =0.80, 0.60, 0.46 and 0.35. Except for μ =1.00 the computed profiles are too deep and broad, having therefore, larger equivalent widths than observed ones. This is a discrepancy encountered in all studies of centre-limb variation of equivalent widths of the CH, C_2 and CN lines.

In order to investigate whether there was any other effect at play in making the observed profiles, shallower and narrower than computed ones, a different fitting factor was used, to fit the central intensities of the profile at each one of the different disc positions. With these fitting factors, the combination of ξ_{rad} =3.00 km/sec. and ξ_{tan} =3.6 km/sec. fits the observed profiles remarkably well. The variation of these fitting factors from centre to limb was very linear. The fact that by varying the fitting factor the optimum combination ξ_{rad}=3.0 km/sec. and ξ_{tan}=3.6 km/sec. fits the profiles very well indeed, indicates that the turbulent velocity field derived is not the cause for the lack of agreement between the observed and predicted profiles. Therefore, this velocity field may be taken to be the most appropriate velocity field in computing doublet contours.

For making detailed doublet profile calculations

the lines 4297.403A of CH and 5094.029A of C_2 were chosen as it was believed that these had the most reliable published doublet separations. 4297.403A of CH consists of the spin doublets at 4297.339A and 4297.463A of rotational of rotational quantum number $K=4C$, as assigned by Heurlinger (1918)* and adopted to current molecular spectroscopic notation. The wavelength separation between the two lines is given as 69mA. This separation was included in the calculation of line absorption coefficient. To start with, a radial turbulent velocity of 3 km/sec. was assumed and the doublet intensity contour was computed for the centre of the disc. The computed profile had a half width 20mA larger than the observed one. A reduction of the velocity to 2.5 km/sec. gave a profile that was well resolved, clearly indicating that 2.5 km/sec. was too low a value for velocity. Further the computed profile was broader than the observed one, essentially because the width of the resolved doublet comprised of not only the intrinsic Doppler widths of the lines, but also the effective separation between the two. A velocity of 2.75 km/sec. again gave a resolved doublet profile, but narrower than the one obtained for 2.5 km/sec; the increase

---

* I am very grateful to Mrs. Moore Sitterly for kindly loaning a copy of Heurlinger's thesis.

FIGURE VI-1.

The observed and computed profiles of CN 3864A. The filled circles are the computed points. The continuous curve is the observed profile. ξ_{rad} and $\xi_{t...}$ are 3 km/sec and 3.6 km/sec respectively.

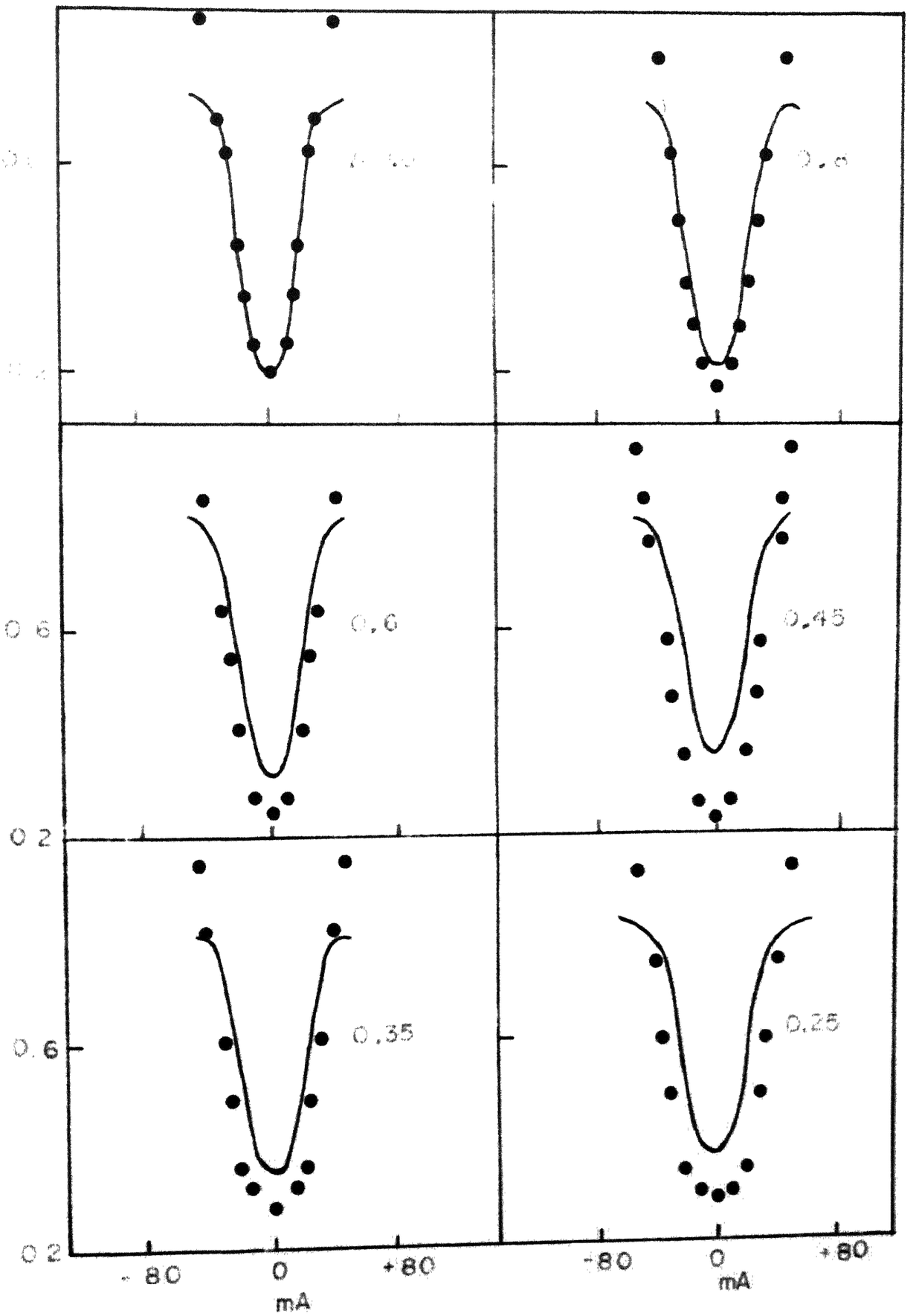
0.6
0.45
0.35
0.25
0.6
0.2
0.6
0.2
-80
0
+80
mA
-80
0
+80
mA

in turbulence while increasing the intrinsic width of the component lines, causes an apparent decrease in the effective sum of the half widths of the two lines. An increase in the velocity to 3.1 km/sec. showed that this increase caused the total half width of the line to be larger than the one computed for 3.0 km/sec. It was then evident that 3.0 km/sec. represented the optimum value for the radial turbulent velocity and the lack of a perfect fit with the observed profile for this value of velocity, pointed out to a decrease in the assumed separation between the two lines. Successive decrease in the separation and recomputation of the profile gave for 60km separation and 3.0 km/sec. radial turbulent velocity, a very good fit with the observed profile at the centre of the disc. This fit is illustrated in Figure VI-2. That a decrease of 9km in the separation improved the fit to such a large extent emphasizes the need for knowing these separations very accurately.

The fit for the tangential velocity at $\mu = 0.35$ could not be made as satisfactorily as for $\mu = 1.0$. The central intensities computed were all too low. The tangential velocities required to obtain a central intensity fit gave profiles that were too broad. 3.6 km/sec. was chosen for the tangential velocity as being the

FIGURE VI-2.

The observed and computed profiles of C_2 5054A and CH 4207A on the doublet assumption.

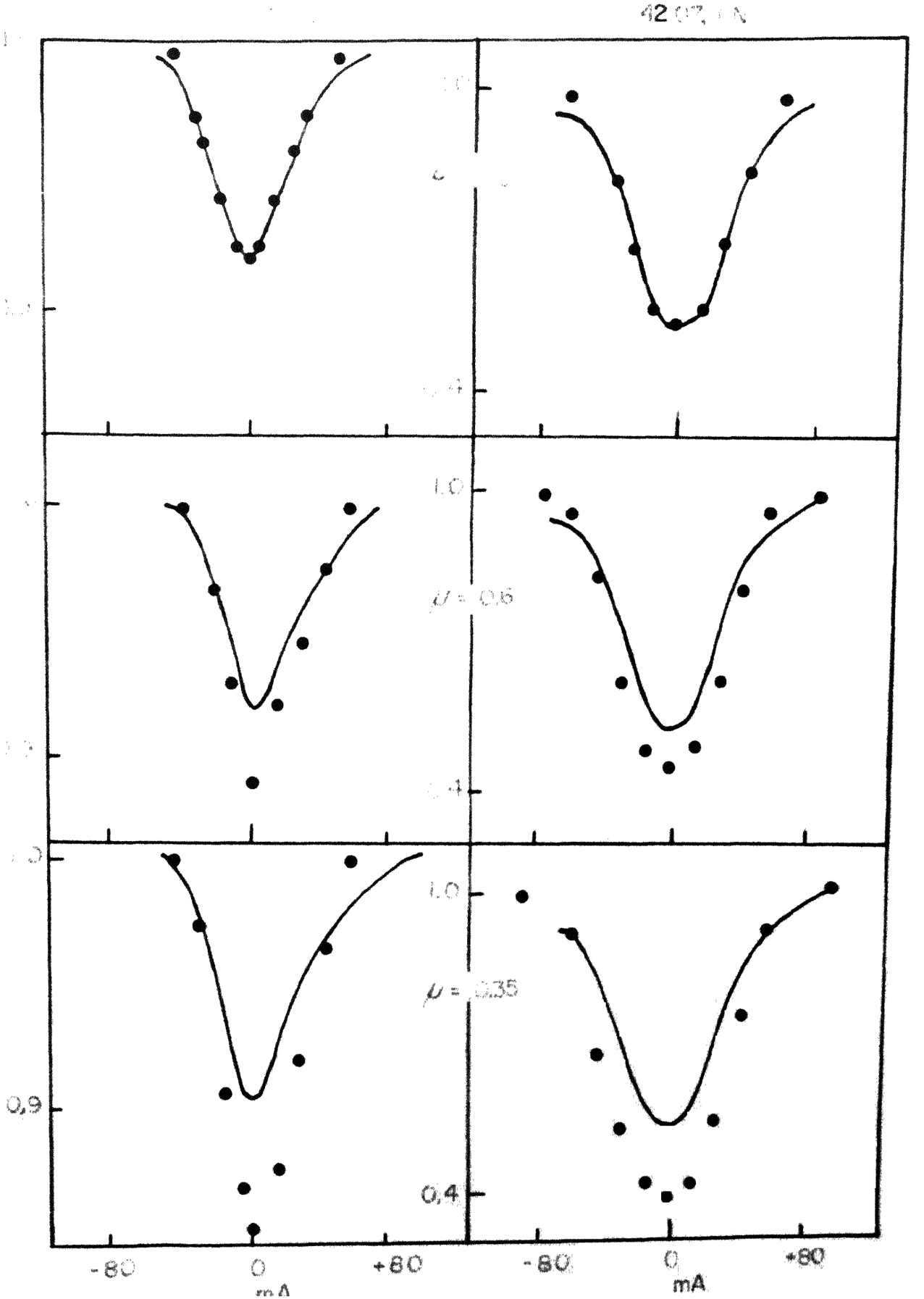
1.0
0,9
1.0
0,4
-80
0
+80
mA
-80
0
+80
mA

velocity giving atleast the correct trend of centre-limb variation of central intensities. While the turbulence radial velocity of 3.0 km/sec. is highly reliable, the value of the tangential velocity derived is less certain, and the poor limb fits show that factors other than turbulence are important there.

The 5094.029A line of C_2 consists of a triplet of the P branch with rotational quantum number $J=62$. $P_2(62)$ and $P_3(62)$ lines are coincident for all practical purposes and $P_1(62)$ is 93mA away. The respective wavelengths of the $P_{2,3}(62)$ and $P_1(62)$ components are 5094.002A and 5094.035A.

Again, theoretical line contours were computed with a radial turbulent velocity of 3 km/sec. and a separation of 93mA, for the centre of the disc. This combination of separation and velocity gave at once a very good fit with the observed profile. To examine the effect of a decrease in the separation, a new profile was constructed, with 65mA separation; the profile obtained disagreed distinctly in the red wing, although the fit in the inner core and violet wing remained more or less unaffected. This confirmed that the 93mA and 3.0 km/sec. combination for separation and radial turbulent velocity is the correct combination. A fit for the tangential velocity was attempted at $\mu = 0.35$ and once again this could not be done effectively. The computed

profiles for 5094.029Å at μ =0.60 and μ =0.35 are shown in Figure VI-2 while Figure VI-3 gives the centre-limb variation of central intensities.

The detailed calculations of doublet profiles showed that the width and shape of such profiles were fixed by a unique combination of velocity and separation. It was further realised that the actual value of the separation between the lines was very critical, only when it was of the same order of magnitude as the assumed Doppler width, which is approximately 50mÅ. Separations greater than 80mÅ do not affect the half width of the line, although they decide the asymmetry in the wings. Separations smaller than 20mÅ, lead to a situation wherein turbulence effects dominate and the line may be treated as a singlet.

In view of the above points, together with the great deal of uncertainty that surrounds the wavelength separations, it was felt that the time consuming doublet calculations on a medium-speed computer for each of the selected lines was not justified. Therefore, singlet calculations were made for the rest of the selected lines. As a tie-in with the doublet calculations, the singlet calculations were repeated for the 4207.402Å CN line and the 5094.029Å C_2 line. Adopting the same fitting procedure as outlined

FIGURE VI-3.

The observed and computed centre-limb variations of central intensities. The continuous curve indicates the observed variation. The dashed curve represents the computed variation.

Fig VI.3

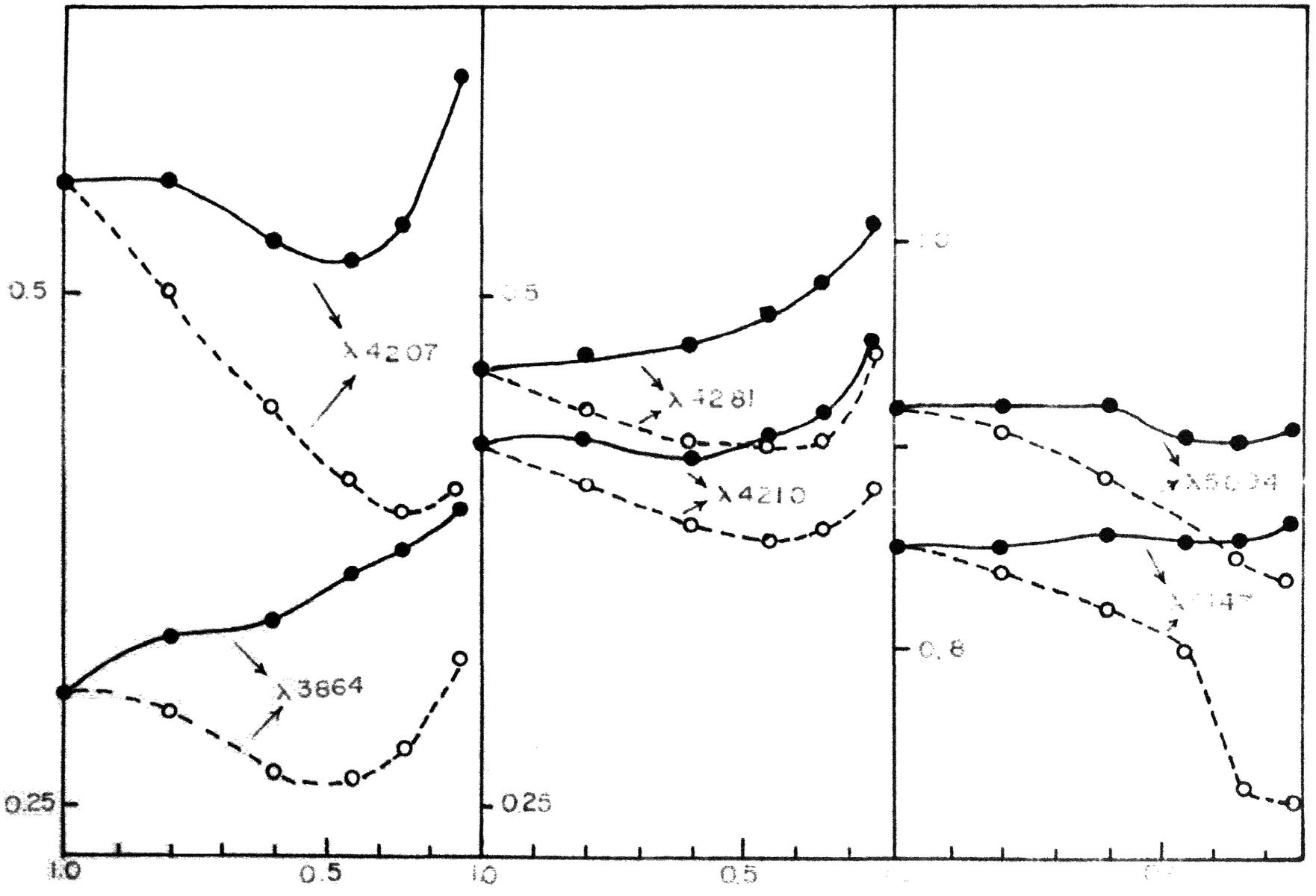

for the doublet with separation set equal to zero, the values of ξ_{rad} and ξ_{tan} obtained were 4.0 and 5.05 km/sec. respectively. The fits at the centre of the disc were naturally poorer than that for doublet profiles, particularly for the 5094.029A line. The fits for the limb profiles were poor as in the other case. These results are shown in Figures VI-4 and VI-5.

The increase in the turbulent velocity required to fit the observations at the centre, from 3.0 km/sec. to 4.0 km/sec., is a direct measure of the effect of the doublet nature of the lines. The values of the velocity derived from the singlet assumption were not critical as in the doublet case. A velocity of 4.1 km/sec. or 3.9 km/sec. would have provided equally good fits at the centre of the disc.

In order to examine whether factors other than turbulence, could improve the fits at positions other than at the centre of the disc, different fitting factors were used for different positions on the disc, so that the observed and computed central intensities agreed. The profiles computed for these fitting factors for the various disc positions revealed that the combination of 4.0 km/sec. and 5.05 km/sec. for radial and tangential turbulent velocities, gave very good profile fits in every case as seen in

FIGURE VI-4.

Computed and observed profiles of CH 4207A on the singlet assumption.

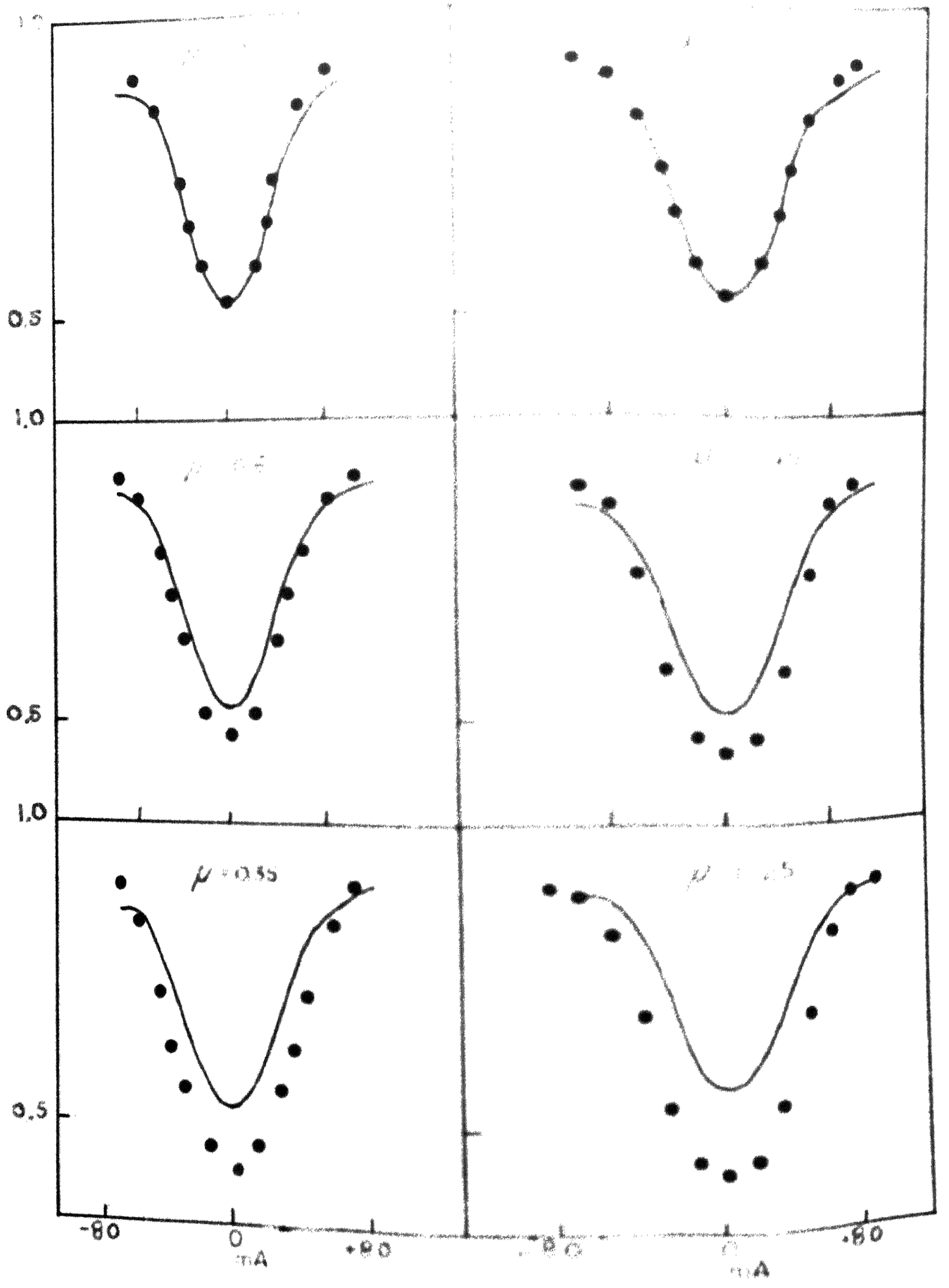
0.5
1.0
0.5
1.0
μ = 0.55
0.5
-80
0
+80
mA
-80
0
+80
mA

FIGURE VI-5.

Computed and observed profiles of C_2 5074A on the singlet assumption.

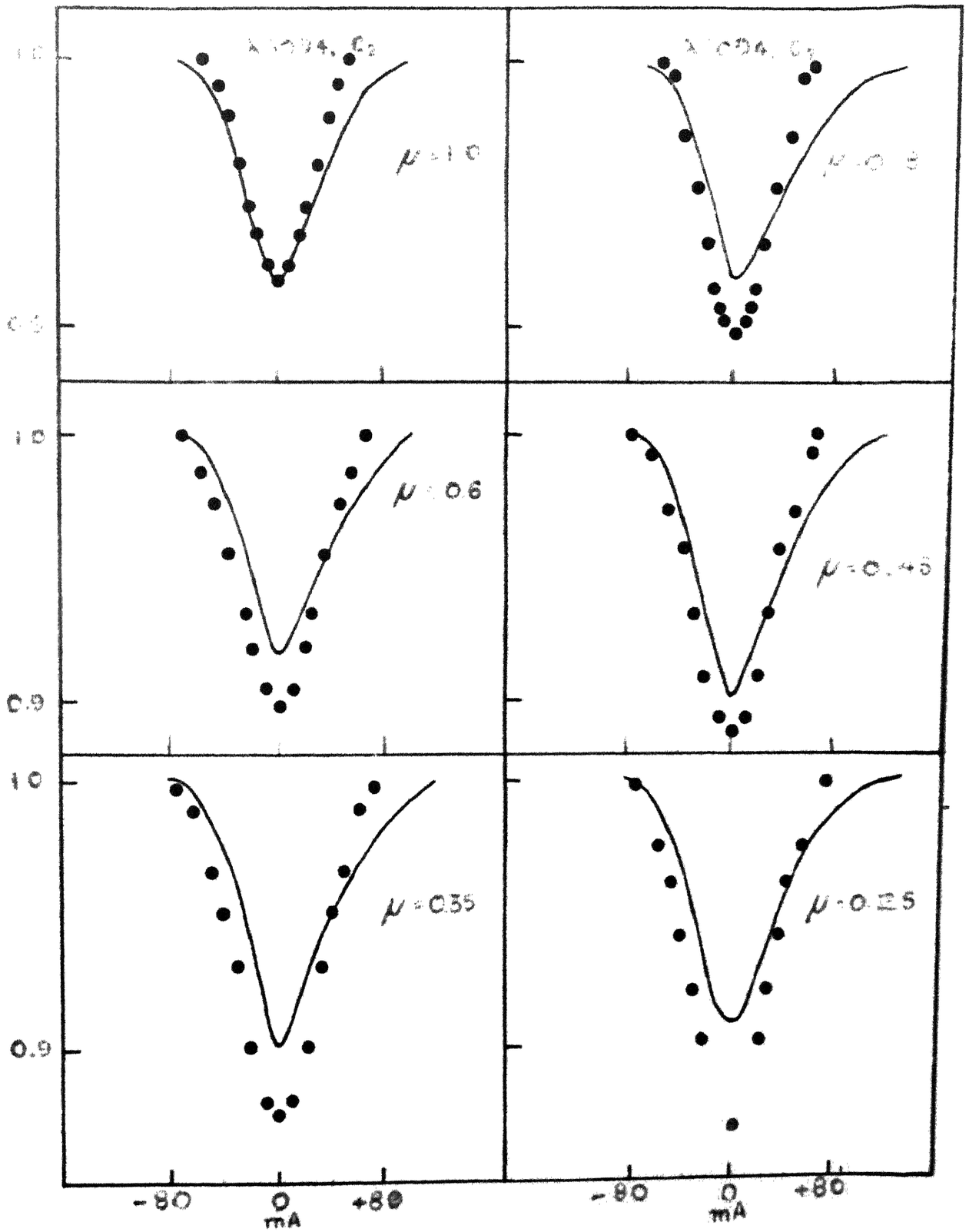
1.0
0.9
μ = 1.0
μ = 0.8
μ = 0.6
μ = 0.45
μ = 0.35
μ = 0.25
-80
0
+80
mA

in Figure VI-6. It is also interesting to note that the variation of the fitting factors from centre to limb is very linear.

Exactly analogous calculations were carried out for the CH lines 4210.970A, 4281.974A and C_2 line 5147.106. The values ξ_{rad}=4.0 km/sec. and ξ_{tan}= 5.05 km/sec. seemed to be an optimum combination in every case, for the singlet assumption (Figure VI-7 to VI-9). Ofcourse, for each of these lines the computed profiles become deeper and broader than the observed lines. Although the trends of centre-limb variation of both computed and observed central intensities are similar, they are by no means identical (Figure VI-5).

Detailed profiles were computed at the centre of the disc for the 4281.974A C_2 line, using Schnalberger's turbulence model. The line profile was too narrow. It is unlikely that a detailed doublet profile calculation for Schnalberger's model would have improved the situation very much. Figure VI-10 sets out the profile calculations for Schnalberger's model as compared with those calculated for the singlet depth - independent model.

Using the approach of varying fitting factors for different disc positions, once again strikingly good profile fits were obtained for the anisotropic turbulence

FIGURE VI-6a and 6b.

Computed and observed profiles with
different fitting factors at different μ positions.

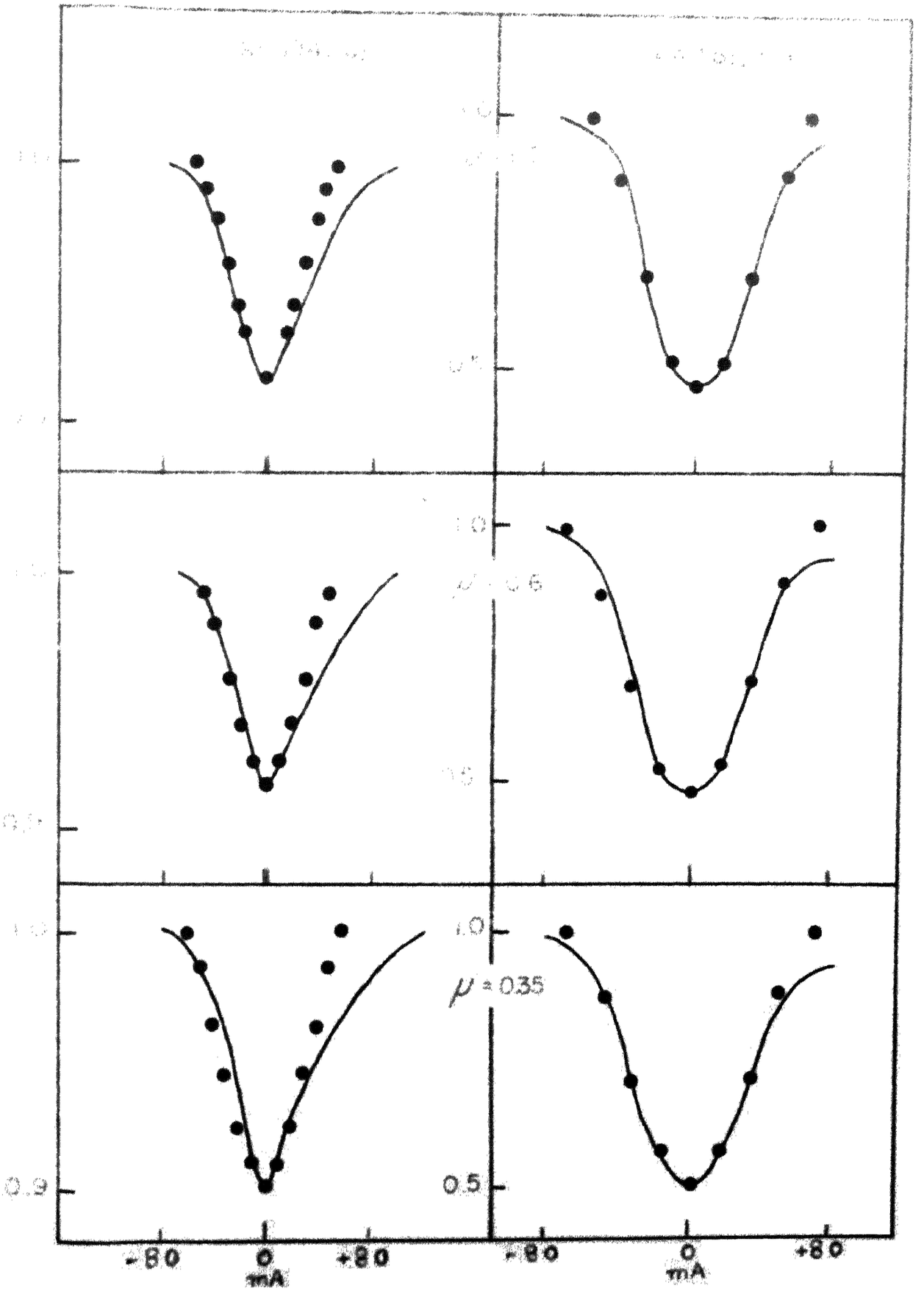
1.0
0.9
1.0
0.5
μ = 0.35
-80
0
+80
mA
-80
0
+80
mA

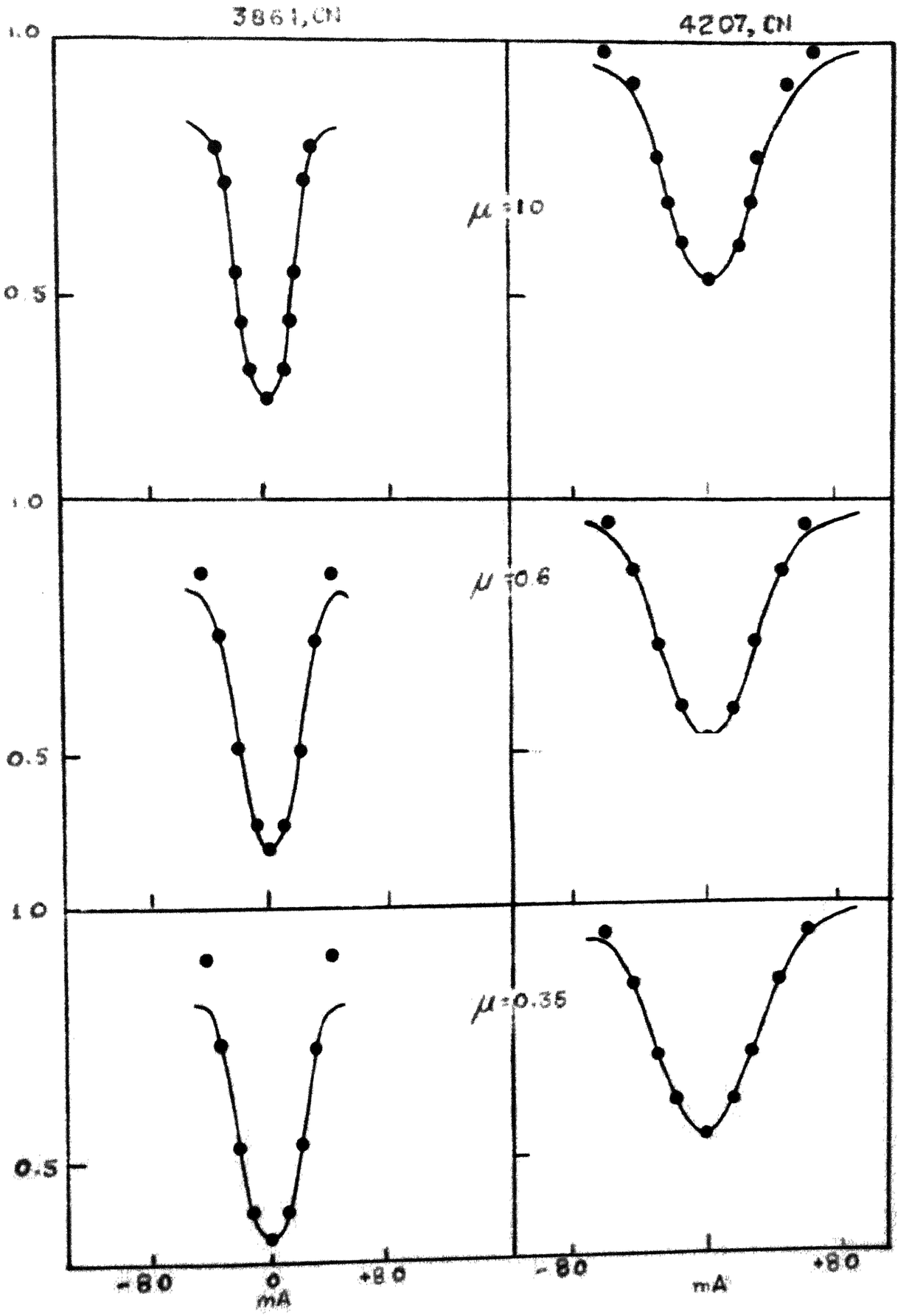
3861, CN
4207, CN
1.0
0.5
1.0
μ=1.0
μ=0.6
0.5
1.0
μ=0.35
0.5
-80
0
+80
mA
-80
+80
mA

FIGURE VI-7.

Computed and observed profiles for
CH 4210A on the singlet assumption.

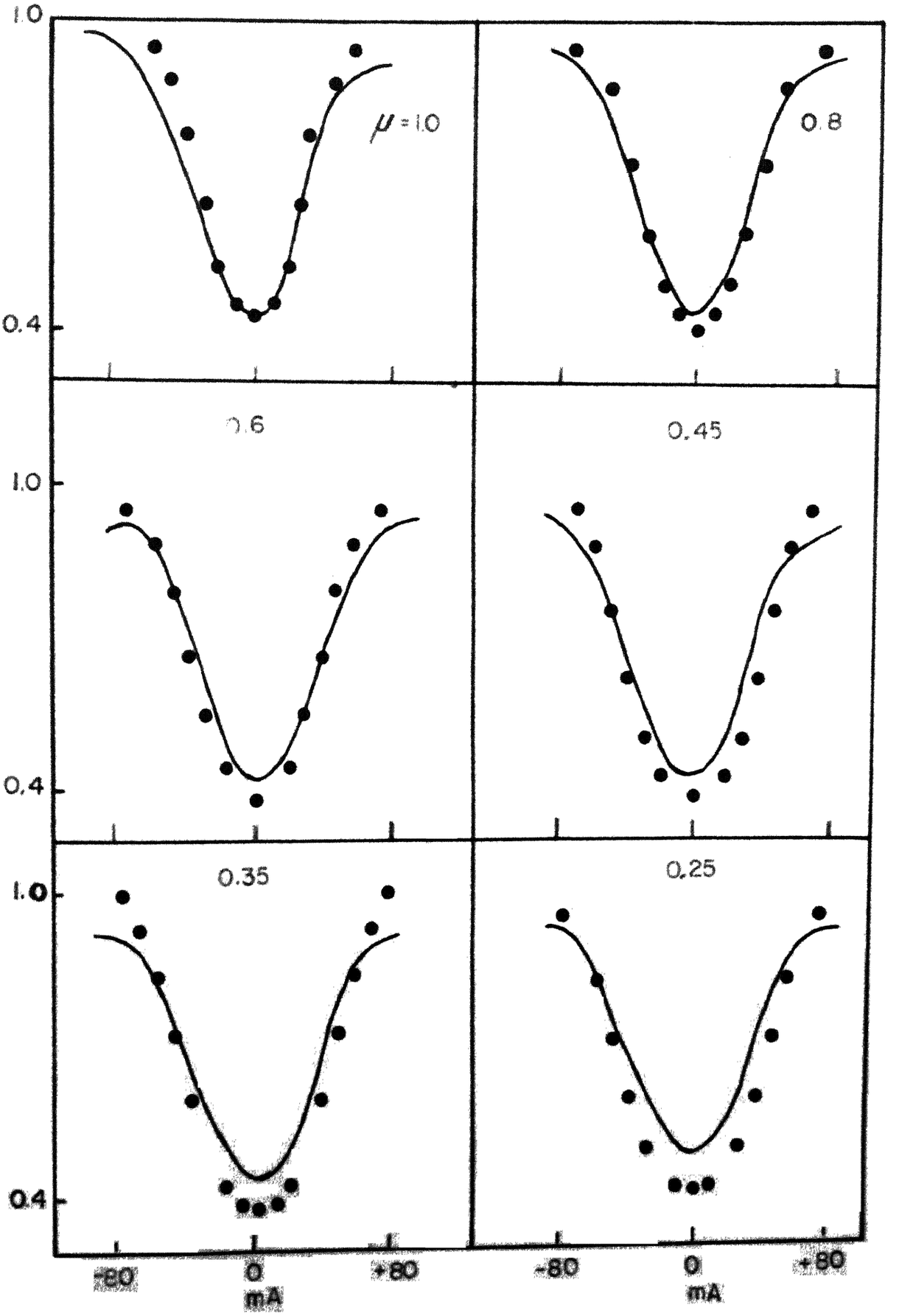
1.0
0.4
μ = 1.0
0.8
0.6
0.45
1.0
0.4
0.35
0.25
1.0
0.4
-80
0
+80
mA
-80
0
+80
mA

FIGURE VI-3.

Computed and observed profiles for C.I 4291A on the singlet assumption.

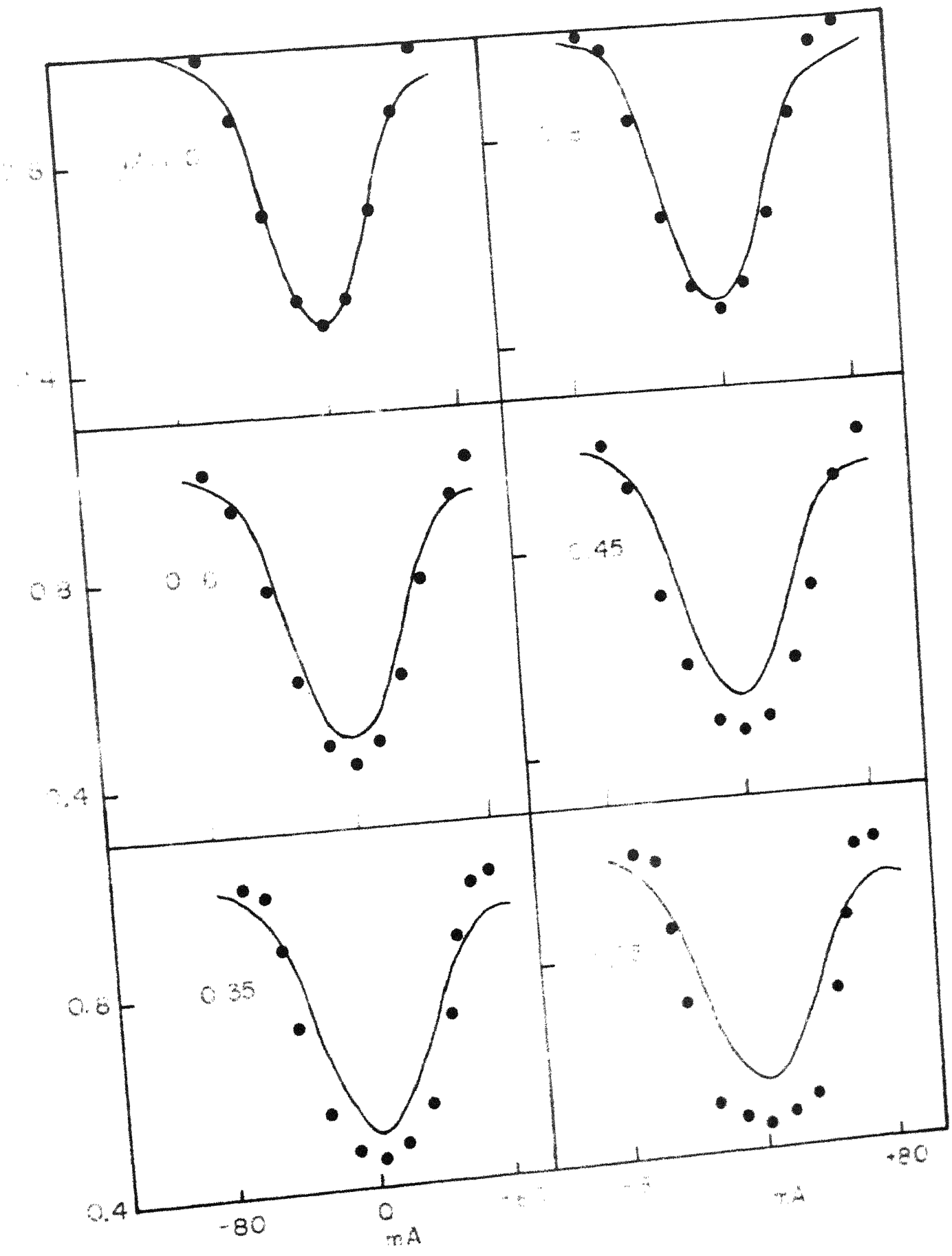
0.45
0.35
0.4
0.6
0.4
-80
0
mA
+80

FIGURE VI-3.

Computed and observed profiles for C_2 5147 on the singlet assumption.

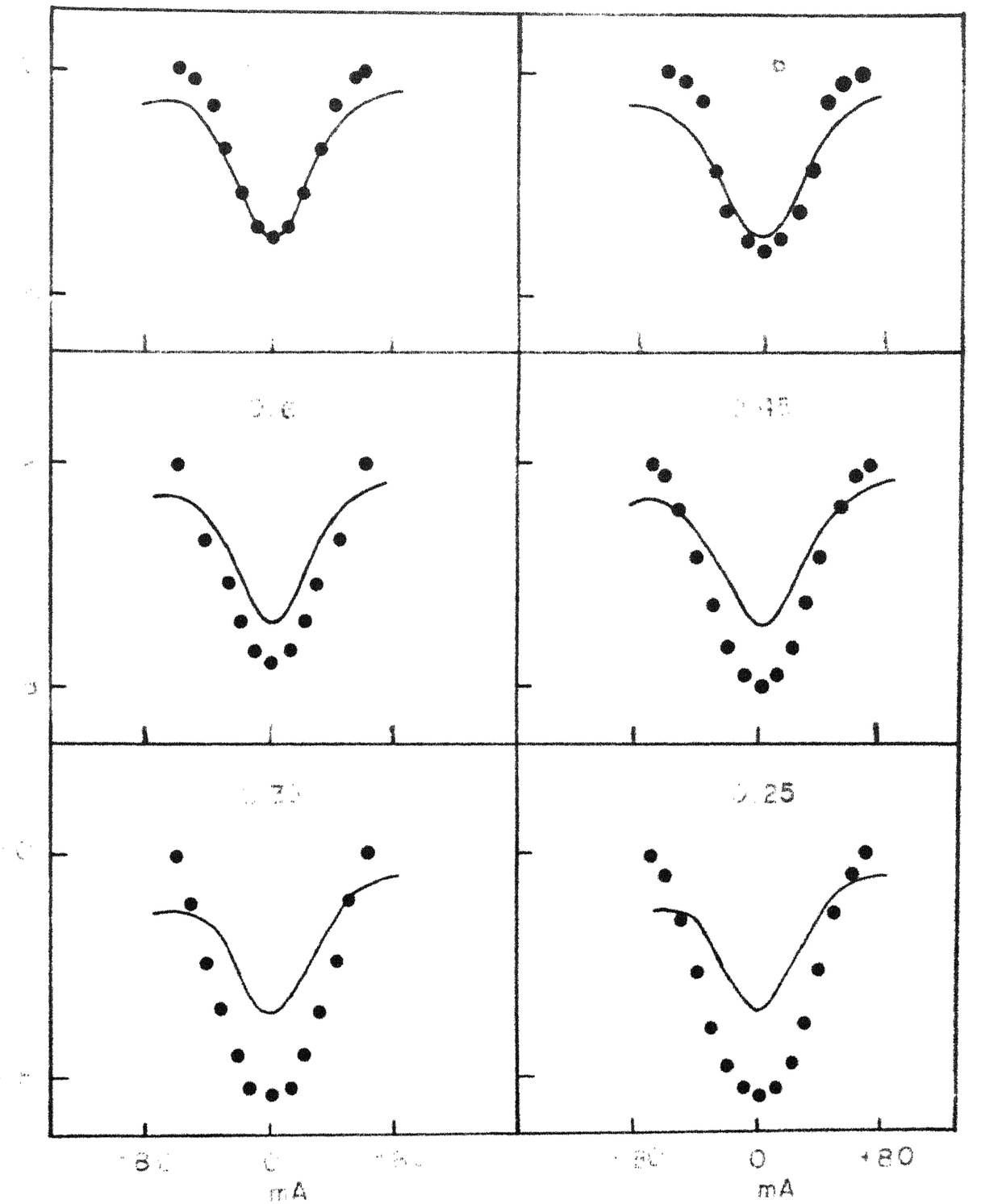
mA
mA
+20

FIGURE VI-12.

(a) Observed and computed profile for GI 4231A with depth-independent and anisotropic turbulence model.

(b) Observed and computed profile for GI 4231A with Schmalbergern depth-dependent and isotropic turbulence model.

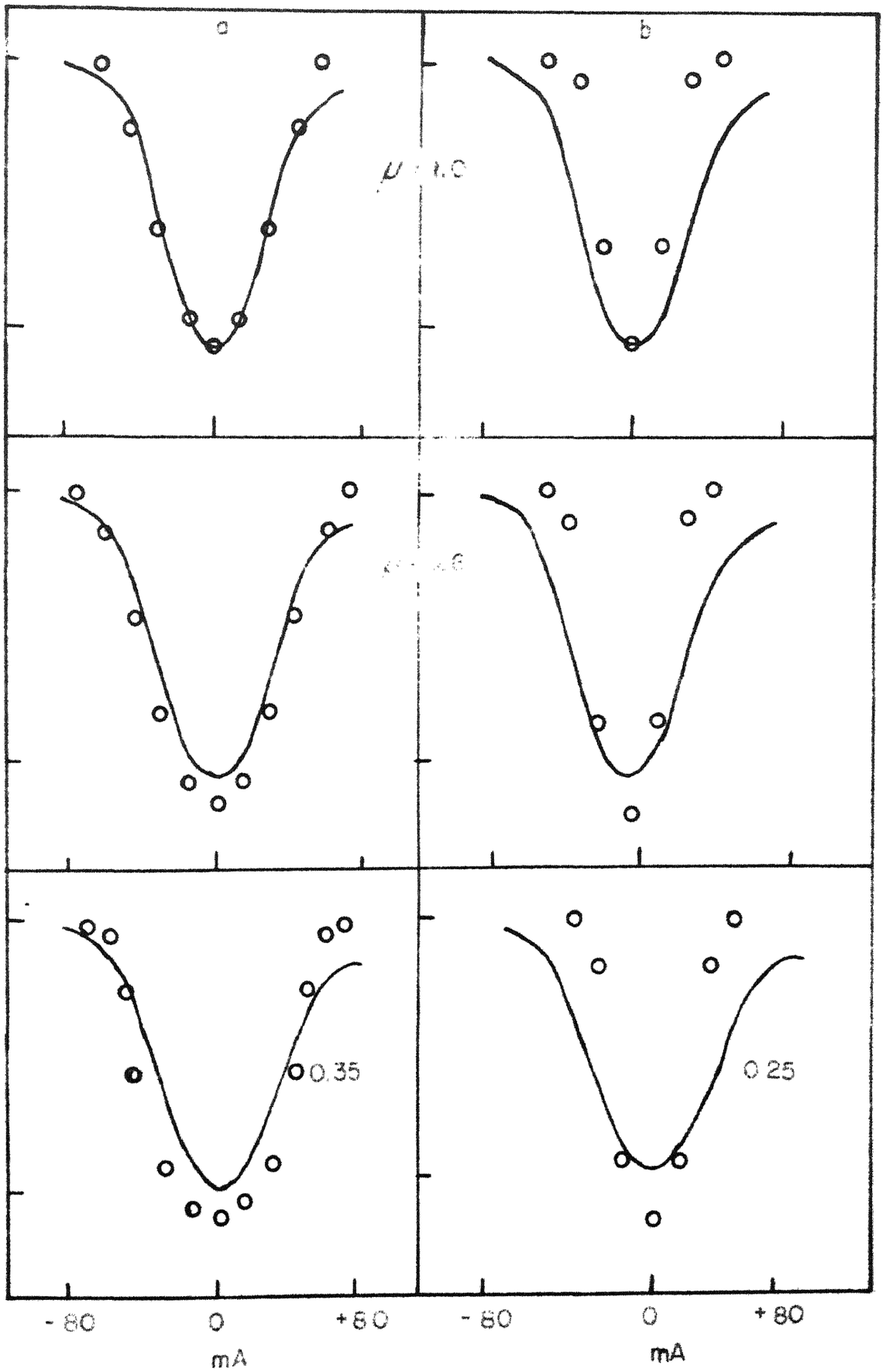
a
b
0.35
0.25
- 80
0
+ 80
mA
- 80
0
+ 80
mA

model with ξ_{max}=4.0 km/sec. and ξ_{base}=3.05 km/sec. The normalised variation of fitting factors for all the six lines is presented in figure VI-11. These variations are extremely striking, being parallel to each other for C_1 and C_2 lines, while the two Ca lines are parallel to each other.

The results presented so far draw attention to three facts. First of all the calculations for 3968.50Å and 4227.40 Å of Ca and 5004.02Å of C_2 have established beyond doubt that at the centre of the disc the radial turbulent velocity is 3.0 km/sec. The derived tangential velocity of 3.5 km/sec. is less certain, although it appears to be the best value capable of describing the centre-limb variation of the profiles, at least to a limited extent. The second result of interest is that calculations based on the singlet assumption lead certainly to larger velocities than for the doublet calculations, but the same value of 4.0 km/sec. seems to fit the observations uniformly well for all the lines, although the separations (which are not known) for each of these lines are not likely to be identical. In order to understand this result, it is necessary to recall, that <u>although the separation between the two lines is extremely critical in obtaining an absolute fit of a computed profile with the observed profile, for any given separation there is one unique value for the turbulent velocity giving the best over-all relative fit.</u>

FIGURE VI-11.

The variation of normalized fitting factors for central intensities from centre to limb.

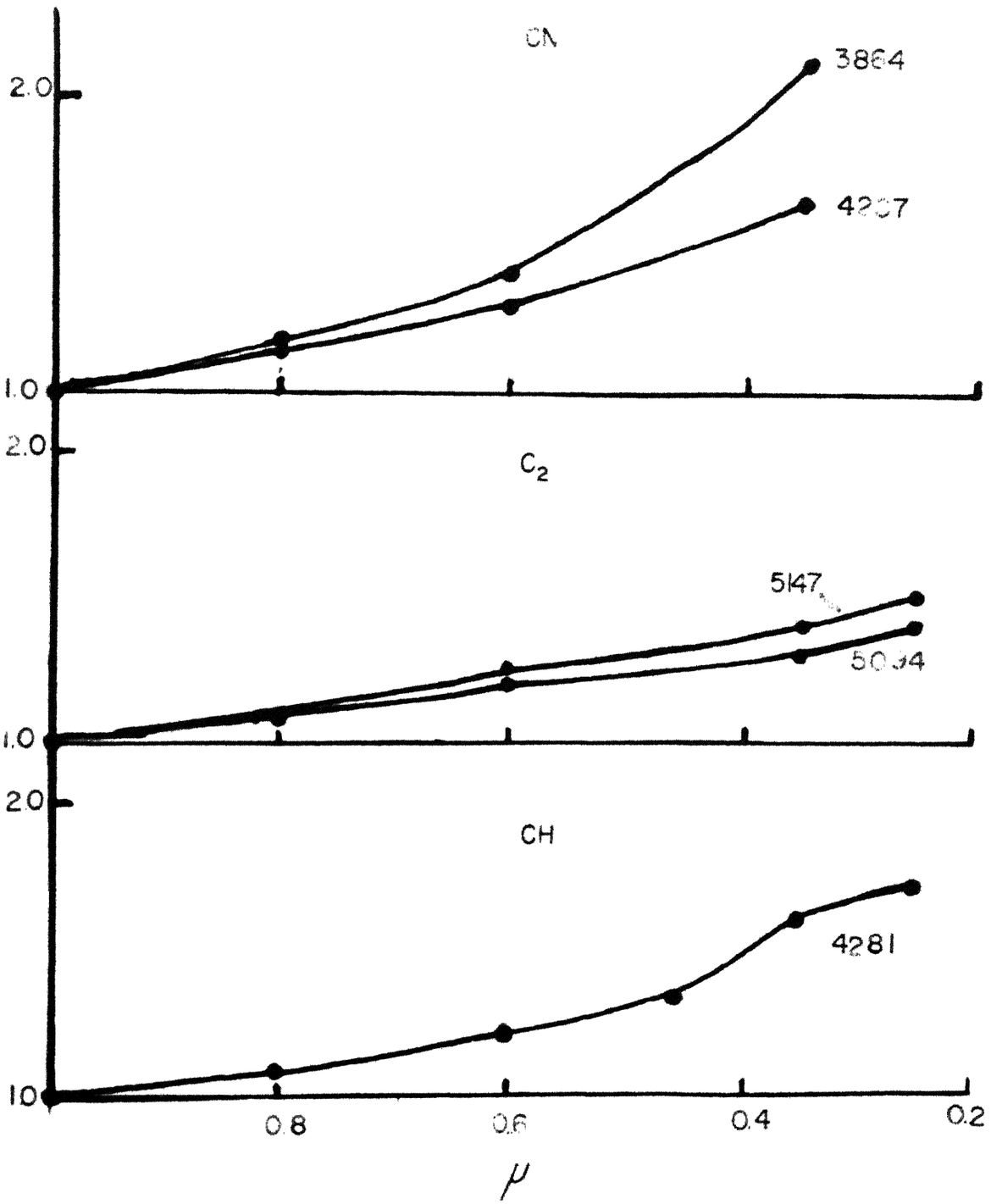
CN
3864
4207
2.0
1.0
2.0
C2
5147
5034
1.0
2.0
CH
4281
10
0.8
0.6
0.4
0.2
μ

Also it must be emphasized that the line asymmetries of the lines used in this investigation probably have values greater than 3%, but less than 10%. Both 4237.15Å and 5154.07Å also give best fits for $\xi_{rad.}$ = 3.5 km/sec. and $\xi_{tan.}$ = 3.25 km/sec. under the simplest assumptions. This suggests very strongly, the equivalence of the doublet emmission results with a 3.5 km/sec. and 3.5 km/sec. combination, and the singlet emmission results with 4.5 km/sec. and 3.25 km/sec. It is also very instructive to note that the ratio of $\xi_{rad.}/\xi_{tan.}$ has remained the same in going from the doublet to the singlet emmission. It must, however, be pointed out that these conclusions are strictly valid for doublet lines whose intensities are almost the same, as is true for every case of low excitation doublets of relatively high rotational quantum number. These deductions will not be valid in their entirety in discussions of atomic hyperfine structure where there is a wide range of intensities of the component lines.

The behaviour of varying fitting factors providing such very good fits with the observed profiles for the same combination of radial and tangential turbulent velocities and the fact that these centre-limb variations for all the lines are very nearly parallel to each other seems extraordinarily

important, and as having a direct bearing on the problem of centre-limb variations of equivalent widths of the C_2, CN and CH.

The fitting factors normally used to fit predicted and observed profiles at the centre of the disc are generally interpreted in terms of a combination of uncertainties in abundance per a tomic oscillator strengths. The abundance parameter in the molecular case enters indirectly in the partial pressures. It is obvious that the oscillator strength and abundance must remain constant and, therefore, the variation in fitting factors can only be interpreted as a variation in two other factors that enter the calculation of partial pressures. These are the temperature structure at the outermost layers of the sun and the amount of free carbon available for the formation of C_2, CN and CH.

The basis for assuming a LTE source function in calculation of rotational lines is perfectly valid, as has often been proved by the derivation of consistent rotational temperatures and the prediction of correct equivalent widths for the centre of the disc (Cowley 1964).

But the basis for assuming a LTE configuration for dissociation equilibrium calculations to obtain partial pressures is open to question. The values 3.0 kv/sec. and

3.6 km/sec. obtained for turbulent velocities immediately point out that molecules are formed in layers of the sun where acoustic propagation of energy is already important. It is not unreasonable to expect the atmosphere to have a 'dissociation temperature' (a point also raised by Oster and Prunderie 1960) as distinct from the electron temperature of the atmosphere. Newkirk (1957) has reached the interesting conclusion that the de Jager (1954) model with hyper-dissociation, where the temperature of dissociation is different from the electron temperature, explains the observed centre-limb variations of CO as well as do the Aller-Pierce model or the Minnaert model. The explanation of the CO molecule observations on the basis of lack of dissociation equilibrium is crucial for any attempt at explaining C_2, CH and CN molecule observations. CO with its high dissociation potential and high concentration at the very highest layers of the sun, is capable of depleting the free carbon supply available, to a significant extent, and thus affect the partial pressures of other carbon constituent molecules. From the variation of fitting factors alone, obtained in this investigation it is difficult to reach any positive conclusions, but it is very certain that this variation has definite physical significance, even though a quantitative interpretation seems remote at the present stage.

In order to arrive at the mean depths of formation of the C_2, CH and CH lines, contribution functions defined as the integrand of the expression

$$r_{\Delta\lambda} = K \int_{-\infty}^{+\infty} \frac{G}{\mu} \frac{\rho}{K_e} \frac{N_{ab}}{\Delta\lambda_D} \psi \, e^{-\Delta\lambda/\Delta\lambda_D} \, d(\log \tau)$$

with G as the weighting function given by

$$G = \frac{\mu e^{-\tau/\mu} \{ b + c [E_1(\tau + \tau/\mu) - E_1(\tau)] \}}{a + b\mu + c[1 - \mu \ln(1 + \mu^{-1})]}$$

and ψ the saturation function is given by

$$\psi = \exp - K \int_{-\infty}^{\tau} \rho \frac{N_{ab}}{\mu} \frac{1}{K_0 \Delta\lambda_D} \exp -(\Delta\lambda/\Delta\lambda_D)^2 \, d(\log \tau)$$

were determined. The contribution functions at the centre of the line were calculated for the 3864.307A CH line, 4281.774A CH line and the 5094.02eA C_2 line and are presented in Figure VI-12. The mean depths of formation of the three lines are:

CH;	$\bar{\tau} = 0.04$
C_2;	$\bar{\tau} = 0.06$
CH;	$\bar{\tau} = 0.10$

FIGURE VI-12.

Contribution functions for CH 3884A, CH 4281A and C_2 5094A.

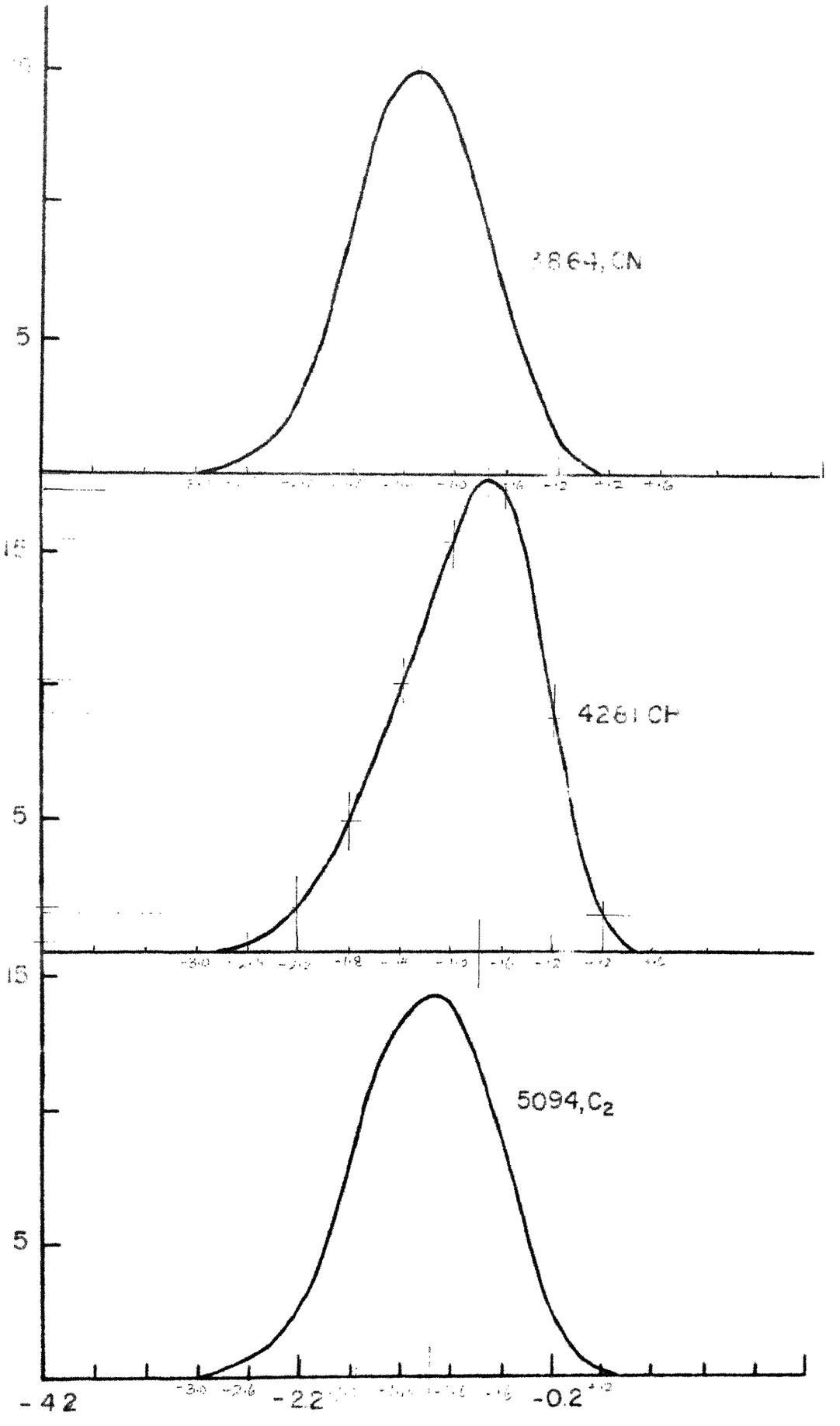
3864, CN
4281 CH
5094, C_2
5
5
5
-4.2
-2.2
-0.2
log τ

Thus, the velocities derived refer to these regions of the atmosphere. Further, the remarks regarding the possible lack of dissociation equilibrium must relate to these layers.

Summarising, the results presented in this investigation point out that the radial turbulent velocity for optical depths ranging from 0.04 to 0.10 is 3.0 km/sec. This value of velocity has been derived from lines having different Rowland intensities and on the basis of detailed doublet profile calculations. A less certain value of 3.6 km/sec. has been derived for the tangential velocity, a value chosen on the basis of general agreement in the trends of centre-limb variation of the observed lines. These values of velocities have received additional confirmation from singlet profile calculations, standardised with the doublet profile calculations. A very interesting variation of the fitting factors is calculated from centre to limb, to fit observed and computed central intensities. The striking similarity of these variations from line to line seems to be suggestive of important physical significance regarding the presence of as yet unknown factors affecting the dissociation equilibrium, although quantitative confirmations are lacking at present.

CHAPTER VII

SIGNIFICANCE OF THE MOLECULAR MODELS IN THE SOLAR ATMOSPHERE.

The investigation reported in this thesis addressed itself to the problem of using molecular lines effectively in the determination of certain physical parameters in the topmost layers of the photosphere, within the framework of a set of basic assumptions. In the light of the observed results presented in chapter IV and the comparative study of observed and predicted results described in chapter VI, the validity of these assumptions should be examined.

7.1. Local thermodynamic equilibrium.

In the molecular problem the concept of local thermodynamic equilibrium enters the picture in two distinct aspects. In the mode of molecular line formation the postulation of local thermodynamic equilibrium is equivalent to assuming the source function in the line being identical with the Planck function at the local electron temperature. As has been pointed out several times by various workers the closely packed nature of the rotational lines ensures the validity of this postulate and the consistent values derived for the rotational temperatures confirms it fully. In this investigation also

the assumption of LTE has led to similarly consistent results and fixed correctly the values of radial velocity, giving very good agreement between observed and predicted profiles for the centre of the disc. Similar calculations of equivalent widths of selected CH lines by Cowley (1964) also lead him to the same conclusion.

In the treatment of dissociation equilibrium, the LTE postulate is implicitly assumed, even in the definition of the dissociation constant. Although observations agree with predictions at the centre, the wide deviations of predicted and observed profiles at other disc positions suggest strongly that one must look for non-equilibrium effects in the higher layers of the sun, that would seriously affect the dissociation constants and partial pressures of the C_2, CH and CN molecules. Other studies which include the region of molecular line formation also show that superthermic phenomena are already important in this region. Calculations of concentration profiles on molecules with heights, in region where the vibrational excitation temperatures are different from the dissociation temperature and the local kinetic temperature are probably required, but this would involve the knowledge of vibrational relaxation times and rate constants at solar temperatures, which are not available. However, the dissociation temperature structure of the outer layers could be modified empirically,

so that partial pressures thus derived would explain the centre-limb variations of CO, C_2, CN and CH simultaneously. It is essential that CO be the molecule with which the fitting procedure for the empirical dissociation temperature structure be carried out, because it is CO, with its large dissociation potential of 11.09 e.v. and highly localised concentration around optical depth $\bar{\tau}$ =.01, that is the crucial molecule. The smallest factor causing a decrease in the dissociation of CO would result in sufficiently serious depletion of free carbon for the formation of the other carbon molecules. That the answer to the poor agreement between predicted and observed profiles lies some where in this direction is made evident by the interesting behaviour of the fitting factors for observed central intensities from central to limb.

Although deviations from conventional dissociation equilibrium strike as being the one single factor capable of a comprehensive explanation, this may not be the sole cause for disagreement between the observed and theoretical profiles. As has been pointed out by Laborde carbon depletion could be brought about by the presence of polyatomic molecules or the centre-limb variations may be interpreted in terms of non-LTE methodology referred to the populations of the 'electronic' levels rather than the rotational

levels (Pecker and Praderie 1960). However, these considerations have not resolved the existing discrepancy, although they did improve the situation a little.

It is seen that theoretical profiles are consistently deeper than the observed ones, on going from centre to limb. All three molecules CH, OH and C_2 have been observed in emission. What role does chromospheric emission play in raising the central intensities? Investigation of this emission may answer in part, the high central intensities at the limb.

In any event, it would be erroneous to conclude on the basis of rotational temperatures alone, that non-LTE effects are not necessarily indicated in the region of molecular line formation. An empirical examination of the dissociation temperature structure might well be of significance in testing the equilibrium approximations in these regions.

7.2. Is a line profile analysis of molecules justified?

In the outline of the problem of calculating molecular line profiles, three sources of uncertainty were pointed out. These are the uncertainties in, the oscillator strengths of the electronic transitions, dissociation potentials and the precise separations between the very

close spin doublets. The value of carrying through precise line profile calculations may be questioned, considering the above listed uncertainties in the physical constants. But the fact that it has been possible to derive a consistent value for velocities, after accounting suitably for all the factors entering the problem, proves the effectiveness of such detailed, if somewhat laborious, analyses. It also throws into prominence the urgent need for making high resolution laboratory studies of spin doubling for those molecules and the evaluations of accurate f values. With these areas of uncertainty removed, profile analyses can be undertaken with more confidence on a comprehensive scale.

In conclusion, it must be said that the original objectives of the investigation of deriving the temperature and velocity structure have only been partially achieved, in that large uncertainties still remain. But the positive result reached for the value of the turbulent radial velocity, together with the interesting feature of fitting factor variations have strengthened the original conviction that molecules remain the best agents for elucidating the physical structure of the very high photosphere and the very low chromosphere.

REFERENCES

Adam, M.G.,	1938,	M.N., 98, 544.
Allen, C.W.,	1949,	M.N., 109, 343.
Aller, L.H.,	1953,	Astrophysics, Vol.I.
Babcock, H.D.,	1945,	Ap.J., 102, 154.
Birge, R.T.,	1922,	Ap.J., 55, 273.
Blackwell, D.E.,	1953,	Vistas in Astronomy 1,726.
Blitzer, L.,	1940,	Ap.J., 91, 421.
Bracewell, R.N.,	1955,	J.Opt.Soc.America, 45,873.
Broderson, S.,	1954,	J.Opt.Soc.America,44, 22.
Budo, A.,	1937,	Z. Physik, 105, 579.
Chandrasekhar, S., and Breen, F.H.,	1946,	Ap.J., 104, 444.
Cowley, C.R.,	1964,	Ap.J., 139, 731.
Jager, C. de.,	1952,	Rech.Astr. Obs. Utrecht, Vol.13, Part I.
Jager, C. de., and Nevon, L.,	1957,	Mem. Soc. Roy. Sc. Liege, (4), 18, 357.
Gingerich, O.J.,	1961,	Thesis, Harvard University. Ap.J. 134, 658
Goldberg, L.,	1958,	Ap.J., 127, 308.
Goldberg, L., and Muller, E.A.,	1953,	Ap.J., 118, 397.
Goldberg, L., Aller, L.H., and Muller, E.A.,	1959	Ap.J., Suppl. Vol.V, 1.
Hourlinger,	1918,	Lund thesis. ~~Ap.J. Suppl.~~
Horaberg, G.,	1951,	Spectra of ~~Diatamic~~ Diatomic molecules.

Hulst, H.C. van de.,	1946,	B.A.N., 10, 79.
Hunaerts, J.,	1947,	Ann. d'Ap., 10, 237.
Johnson, H.C.,	1927,	Phil. Trans. Roy. Soc. A, 226, 157.
Labordo, G.,	1961,	Ann. d'Ap. 24, 89.
Lyddane, R.H., Rogers, F.T., and Roach, F.E.,	1941,	Phys. Rev. 60, 281.
Michard, R., and Evans, J.W.,	1962a, Ap.J 135, 812. 1962b, Ap.J 136, 487. 1962c, Ap J 136, 493.	
Minnaert, M.,	1940,	B.A.N. 11, 51.
Minnaert, M.,	1953,	The Sun. (ed.G.P.Kuiper)
Newkirk, G.A.,	1957,	Ap.J., 125, 571.
Nomura, T. and Nomura, H.	1960,	Ap.J., 131, 8.
Parker, J.H.	1955,	Ap.J., 121, 731.
Pecker, J.C.,	1949,	Ann. d'Ap., 12, 9.
Pecker, J.C.,	1957a,	Liege Colloque International d'Astrophysique Page 332.
Pecker, J.C.,	1957b,	Comptes Rendus 245, 499.
Pecker, J.C., and Athay, R.G.,	1955,	Ap.J., 121, 391.
Pecker, J.C., and Pecker, C.,	1949,	Ann.d'Ap., 12, 9.
Pecker, J.C., and Peyturaux, R.,	1948,	Ann.d'Ap., 11, 90.
Pecker, J.C., and Praderie, F.,	1960,	Ann.d'Ap., 23, 622.
Pierce, A.K., and Waddell, J.,	1961,	Mem. R. Astr. Soc., 68, 89.
Richardson, R.S.,	1931,	Ap.J., 73, 216.
Richardson, R.S.,	1932,	P.A.S.P., 44, 250.
Richardson, R.S.,	1933,	Ap.J., 77, 195.

Roach, F.E.,	1939,	Ap.J., 89, 99.
Rogerson, J.B.,	1957,	Ap.J., 125, 275.
Russell, H.N.,	1934,	Ap.J., 79, 317.
Schmalberger, D.C.,	1963,	Ap.J., 138, 693.
Stanger, P.,	1963,	A.J. 68, 79.
Sugiyoto, Z.,	1957,	M.N., 117, 2.
Thomas, D.V.,	1958,	M.N., 118, 458.
Thomas, R.N., and Athay, R.G.,	1961,	Physics of the Solar Chromosphere.
Unno, W.,	1959,	Ap.J., 129, 375.
Waddell, J.,	1958,	Ap.J., 127, 284.
Waddell, J.,	1962,	Ap.J., 136, 223.
Waddell, J.,	1963,	Ap.J., 137, 1210.
Wohlan, and Wohlan,	1956,	P.A.S.P., 68, 358
White, J.U.,	1940,	J.Chem. Phys., 8, 79.
White, O.R.,	1961,	Thesis, University of Colorado.
White, O.R.,	1962,	Ap.J., Suppl.VII, 333.
Wilkinson, P.G.,	1963,	Ap.J., 138, 779.

Appendix I

Weighting functions for Pierce-Waddell [illegible] Model

λ = 3800A

log τ_0	μ=0.25	0.35	0.45	0.60	0.80	1.00
-5.00	0.7879	0.8323	0.8606	0.8801	0.9110	0.9258
-4.80	0.7879	0.8323	0.8606	0.8801	0.9109	0.9258
-4.60	0.7878	0.8323	0.8606	0.8800	0.9109	0.9258
-4.40	0.7878	0.8322	0.8605	0.8800	0.9109	0.9258
-4.20	0.7877	0.8322	0.8605	0.8800	0.9109	0.9257
-4.00	0.7876	0.8321	0.8604	0.8799	0.9108	0.9257
-3.80	0.7873	0.8319	0.8603	0.8798	0.9107	0.9256
-3.60	0.7870	0.8316	0.8600	0.8796	0.9106	0.9255
-3.40	0.7864	0.8312	0.8597	0.8794	0.9104	0.9254
-3.20	0.7856	0.8306	0.8592	0.8790	0.9101	0.9251
-3.00	0.7842	0.8295	0.8584	0.8783	0.9096	0.9247
-2.80	0.7821	0.8279	0.8570	0.8773	0.9088	0.9240
-2.60	0.7787	0.8253	0.8549	0.8757	0.9075	0.9230
-2.40	0.7733	0.8213	0.8516	0.8731	0.9055	0.9214
-2.20	0.7649	0.8148	0.8464	0.8690	0.9024	0.9188
-2.00	0.7518	0.8047	0.8382	0.8626	0.8974	0.9147
-1.80	0.7315	0.7890	0.8254	0.8525	0.8896	0.9083
-1.60	0.7006	0.7649	0.8056	0.8369	0.8773	0.8982
-1.40	0.6544	0.7282	0.7752	0.8127	0.8583	0.8826
-1.20	0.5878	0.6739	0.7295	0.7759	0.8291	0.8584
-1.00	0.4961	0.5968	0.6633	0.7204	0.7852	0.8216
-0.80	0.3825	0.4937	0.5715	0.6517	0.7211	0.7672
-0.60	0.2525	0.3687	0.4541	0.5472	0.6317	0.6902
-0.40	0.1336	0.2307	0.3146	0.4148	0.5156	0.5954
-0.20	0.0499	0.1131	0.1797	0.2713	0.3714	0.4696
0.00	0.0108	0.0375	0.0756	0.1407	0.2257	0.3008
0.20	0.0010	0.0069	0.0222	0.0521	0.1070	0.1655
0.40	0.0000	0.0004	0.0025	0.0109	0.0331	0.0646

Weighting functions at Six μ positions.

λ = 4200A

log τ	μ=0.25	μ=0.35	μ=0.45	μ=0.60	μ=0.80	μ=1.00
-5.00	0.7487	0.7963	0.8274	0.8583	0.8849	0.9026
-4.80	0.7487	0.7962	0.8274	0.8583	0.8848	0.9026
-4.60	0.7487	0.7962	0.8273	0.8583	0.8849	0.9026
-4.40	0.7486	0.7962	0.8273	0.8583	0.8849	0.9026
-4.20	0.7485	0.7961	0.8272	0.8582	0.8848	0.9025
-4.00	0.7484	0.7960	0.8272	0.8582	0.8848	0.9025
-3.80	0.7482	0.7958	0.8270	0.8581	0.8847	0.9024
-3.60	0.7478	0.7956	0.8268	0.8579	0.8845	0.9023
-3.40	0.7473	0.7951	0.8265	0.8576	0.8843	0.9021
-3.20	0.7464	0.7945	0.8259	0.8572	0.8840	0.9019
-3.00	0.7451	0.7934	0.8251	0.8565	0.8835	0.9014
-2.80	0.7429	0.7918	0.8237	0.8554	0.8826	0.9007
-2.60	0.7395	0.7891	0.8215	0.8537	0.8813	0.8996
-2.40	0.7341	0.7850	0.8181	0.8511	0.8792	0.8979
-2.20	0.7257	0.7784	0.8128	0.8468	0.8759	0.8952
-2.00	0.7125	0.7682	0.8044	0.8402	0.8707	0.8909
-1.80	0.6922	0.7523	0.7912	0.8298	0.8625	0.8841
-1.60	0.6613	0.7278	0.7709	0.8135	0.8496	0.8735
-1.40	0.6153	0.6908	0.7399	0.7886	0.8298	0.8569
-1.20	0.5495	0.6363	0.6936	0.7507	0.7994	0.8315
-1.00	0.4604	0.5595	0.6267	0.6951	0.7539	0.7931
-0.80	0.3504	0.4582	0.5353	0.6164	0.6881	0.7367
-0.60	0.2266	0.3378	0.4203	0.5124	0.5977	0.6573
-0.40	0.1170	0.2063	0.2853	0.3819	0.4829	0.5529
-0.20	0.0424	0.0986	0.1593	0.2448	0.3407	0.4172
0.00	0.0089	0.0318	0.0653	0.1240	0.2026	0.2737
0.20	0.0008	0.0057	0.0172	0.0454	0.0952	0.1495
0.40	0.0000	0.0003	0.0021	0.0097	0.0292	0.0592

Weighting functions at six μ positions.

λ = 5100A

$\log \tau_0$	μ=0.25	μ=0.35	μ=0.45	μ=0.60	μ=0.80	μ=1.00
-5.00	0.6743	0.7219	0.7543	0.7878	0.8182	0.8396
-4.80	0.6743	0.7219	0.7543	0.7878	0.8182	0.8396
-4.60	0.6743	0.7219	0.7543	0.7878	0.8182	0.8395
-4.40	0.6742	0.7218	0.7542	0.7878	0.8182	0.8395
-4.20	0.6741	0.7217	0.7542	0.7877	0.8181	0.8395
-4.00	0.6740	0.7216	0.7541	0.7876	0.8181	0.8394
-3.80	0.6738	0.7215	0.7539	0.7875	0.8180	0.8394
-3.60	0.6734	0.7212	0.7537	0.7873	0.8178	0.8392
-3.40	0.6729	0.7207	0.7533	0.7870	0.8176	0.8390
-3.20	0.6720	0.7200	0.7527	0.7866	0.8172	0.8387
-3.00	0.6706	0.7189	0.7518	0.7858	0.8166	0.8382
-2.80	0.6684	0.7172	0.7504	0.7847	0.8157	0.8374
-2.60	0.6649	0.7145	0.7481	0.7828	0.8142	0.8361
-2.40	0.6595	0.7101	0.7445	0.7799	0.8118	0.8341
-2.20	0.6510	0.7033	0.7388	0.7752	0.8080	0.8310
-2.00	0.6377	0.6927	0.7298	0.7679	0.8022	0.8260
-1.80	0.6172	0.6762	0.7159	0.7566	0.7929	0.8181
-1.60	0.5862	0.6510	0.6945	0.7389	0.7785	0.8059
-1.40	0.5405	0.6130	0.6619	0.7119	0.7564	0.7870
-1.20	0.4758	0.5578	0.6138	0.6714	0.7227	0.7581
-1.00	0.3902	0.4814	0.5454	0.6126	0.6750	0.7150
-0.80	0.2879	0.3835	0.4543	0.5314	0.6026	0.6529
-0.60	0.1760	0.2726	0.3447	0.4282	0.5091	0.5682
-0.40	0.0845	0.1545	0.2193	0.3020	0.3773	0.4621
-0.20	0.0279	0.0677	0.1131	0.1804	0.2602	0.3273
0.00	0.0052	0.0196	0.0418	0.0831	0.1420	0.1983
0.20	0.0004	0.0034	0.0105	0.0231	0.0642	0.1048
0.40	0.0000	0.0002	0.0012	0.0058	0.0189	0.0531

```
C       NIRUPAMA  SUBRAHMANYAM
C       SYNTHETIC MOLECULAR LINE PROFILES  I
C       CALCULATION OF CONTINUOUS ABSORPTION COEFFICIENT
        DIMENSION TABS (34,10), ABCOF (34,10)
1       FORMAT (7E11.4)
        READ, ( (TABS (1,J), 1=1,34), J=1,10)
2       FORMAT (5E11.4)
        CONS=6.2444E-03*1.6734E-24
        B1=1.440
        B2=5040.*31.31
        DO 24 J=5,10
        DO 25 1=6, 34
        ALPHA=TABS(1,J)**3*(1.-EXPF(-B1/(TABS (1,J)* TABS (1,2) )))
        X1=B2/TABS (1,2)
        X =EXPF (-X1)
        TERM2=EXPF(B2/(81.*TABS (1,2)))/(2.*X1)
        SUM=0.
        DO 23 N=3,9
        FN=N
        TERM1=EXPF(B2/(FN*FN*TABS(1,2)))/FN**3.
23      SUM=SUM+TERM1
        SUM=SUM+TERM2
        SUM=SUM*ALPHA*CONS*X
        HMIN=TABS(1,J)*TABS(1,4)
        ABCOF (1,J)=SUM+HMIN
        RATIO=ABCOF(1,J)/ABCOF(1,5)
25      PUNCH2, (TABS(1,L), L=1,3), ABCOF (1,5), RATIO
        END
GO
```

```
C       NIRUPAMA  SUBRAHMANYAM
C       SYNTHETIC MOLECULAR LINE PROFILES  II
C       CALCULATION OF PARTIAL PRESSURES
        DIMENSION FMOL (4,8), TMODL (34,5), Z(8), FK (29, 8)
        READ3, ( (FMOL (1,J), J=1,8), 1=1, 4)
3       FORMAT (8E10.5)
        READ2, ((TMODL (1,J), J=1,5), 1=1,34)
2       FORMAT (5E11.4)


        BOLTK=1.3804E-16/1.602E-12
        CON1=1.440
        CON2=2.624E04
        R=1.2
        DO 101 K=6, 34
        KK=K-5
        DO 100 J=1,8
        Z (J) =CON1*FMOL (1,J)*(1.-EXPF(-CON1*FMOL(2,J)/TMODL(K,2)))
        Z(J)=TMODL (K,2)/Z(J)
        CON=CON2*FMOL(3,J)
        FK(KK,J)=CON*TMODL(K, 2)**2.5/Z(J)
        F=EXPF(-FMOL(4,J)/(BOLTK*TMODL(K,2)))
100     FK(KK,J)=FK(KK,J)*F
        FPH=TMODL(K,3)/R
        FPO=FPH*9.12E-04
        FPN=9.550E-05*FPH
        FPC=FPH*5.248E-04
        PH=-FK(KK,1)/4.+SQRTF(FK(KK,1)**2+8.*FPH*FK(KK,1))/4.
        A=FK(KK,3)*2.
        B+FK(KK,2)*(PH+FK(KK,3))
        C=FK(KK,3)**2*FK(KK,2)*FPN*4.
        PN=-B/(2.*A)+SQRTF(B**2+2.*C)/(12.*A)
        A=FK(KK,7)*(PH+FK(KK,5))
        B1=FK(KK,5)*FK(KK,7)*(FK(KK,4)+FPC-FPO)
        B2=FK(KK,4)*PH*(FK(KK,5)+FK(KK,7)+PH)*FPO
        B=B1+B2
        C=FK(KK,4)*FK(KK,5)*(FK(KK,7)+PH)*FPO
        PO=-B/(2.*A)+SQRTF(B**2+4.*A*C)/(2.*A)
```

```
      PC=FPC/(1.+PH/FK(KK,7)+PO/FK(KK,4))
      PCH=PC*PH/FK(KK,7)*R/TMODL (K,3)
      PCO=PC*PO/FK(KK,4)*R/TMODL(K,3)
      PCN=PC*PN/FK(KK,6)*R/TMODL(K,3)
      PC2=PC*PC/FK(KK,8)*R/TMODL(K,3)
      PUNCH7, PC, PO, PCO, K
      PUNCH6, Z(7), PCH,K
      PUNCH6, Z(6), PCN, K
101   PUNCH6, Z(8), PC2, K
7     FORMAT (3E11.4,13)
6     FORMAT(2E14.5,13)
      STOP
      END
GO
```

```
C       NIRUPAMA SUBRAHMANYAM
C       CALCULATION OF SYNTHETIC MOLFCULAR LINF PROFILES  III
C       CALCULATION OF CONTINUUM INTENSITY
        DIMENSION TMODL (26,5), C(6), Y (26)
2       FORMAT (6F5.2)
3       READ2, (C(K), K=1,6)
        N=0
9       READ3, ((TMODL(1,J),J=1,5),1=1,26)
        CONS1=3.974E-16
        CONS2=1.440
        RMOD=.4343
        ARG=.2
        DO 36 K=1,6
        FINT=0.
        TLINI=.5*TMODL (2,5)*10.**TMODL (2,1)+TMODL (5,5)*10.**TMODL(5,1)
        TLIN2=TMODL (3,5)*10.**TMODL(3,1)+TMODL(4,5)*10.**TMODL(4,1)
        TLIN3=TMODL(3,5)*10.**TMODL(3,1)-TMODL(2,5)*10.**TMODL(2,1)
        TLIN4=TMODL(4,5)*10.**TMODL(4,1)-TMODL(5,5)*10.**TMODL(5,1)
        TLIN=TLINI+TLIN2-(TLIN3+TLIN4)/12.
        DO 34 1=6,34
        11=1-1
        TERMI=TMODL(11,5)*10.**TMODL(11,1)*.5
        TERM2=TMODL(1,5)*10.**TMODL(1,1)*.5
        KK=1-2
        TERM3=TMODL(11,5)*10.**TMODL(11,11)-TMODL(1,5)*10.**TMODL(1,1)
        TERM4=TMODL(KK,5)*10.**TMODL(KK,1)-TMODL(11,5)*10.**TMODL(11,1)
```

```
      TLIN=TLIN+TERM1+TERM2-(TERM3-TERM4)/12.
      TC=TLIN*ARG/FMOD
      F=EXPF(-TC/C(K))*10.**TMODL (1,1)
      E1=EXPF(CONS2/(TMODL(1,5)*TMODL(1,2)))-1.
      E=CONS1/((TMODL(1,5)**3)*E1)
      Y(1)=E*F*TMODL(1,5)

34    FINT=FINT+Y(1)
      CORR=-.5*(Y(6)+Y(34)
      DIFF=(Y(7)+Y(33)-Y(6)-Y(34))/12.
      FINT=(FINT+CORR-DIFF)*ARG/(C(K)*FMOD)
4     FORMAT(E11.4,F5.2,E11.4)
36    PUNCH4,TMODL(1,5),C(K),FINT
      N=N+1
      IF(N-3)9,9,10
10    CONTINUE
      END
GO
```

```
C       NIRUPAMA SUBRAHMANYAM
C       SYNTHETIC MOLECULAR LINE PROFILES  V
C       CALCULATION OF MULTIPLET PROFILES
        DIMENSION E(34)
        DIMENSION BLEND (3,4)
        DIMENSION TABPP(29,3),TMODL(34,5),TCONT(6,3)
        DIMENSION ETA(34), Y(34), TL(34)
        READ101,RLO
101     FORMAT(E12.7)
        READ100,BK,FMAS,OS
100     FORMAT(E10.5,E9.4,E8.3)
        READ7,((TABPP(I,J),J=1,3),1=1,29)
7       FORMAT(2E14.5,13)
        READ8,((TCONT(I,J),J=1,3),1=1,6)
8       FORMAT(E11.4,F5.2,F11.4)
        READ20,((TMODL(I,J),J=1,5),1=1,34)
20      FORMAT(5E11.4)
        RFAD12,((BLEND(I,J),J=1,4),1=1,2)
        READ13,SP
13      FORMAT(E7.2)
        READ1,L
81      READ1,I
1       FORMAT (I2)
        READ13, DELL
        READ15,CN
15      FORMAT(I4)
V/1
```

```
12      FORMAT(4E10.5)
47      READ85,RADT,TANT
85      FORMAT(2E10.4)
82      READ28,FAC
28      FORMAT(F7.2)
        CONST=4.989E-13
        CONS1=3.974E-16
        CONST=CONST*FLO**2*OS
        CONS2=1.440
        CONS1=CONS1/FLO**3
        CONS2=CONS2/FLO
        FMOD=.4343
        ARG=.2
        SCALE=ARG/FMOD
        TN=0.
        TURB=TANT**2-TCONT(I,2)**2*(TANT**2-RADT**2)
73      N=0
        DO 71 K=6,34
        FLINE=0.
        KK=K-5
        E(K)=CONS1/(EXPF(CONS2/TMODL(K,2))-1.1)
        THERM=FMAS*TMODL(K,2)
        DELD=SQRTF(THERM+TURB)*FLO/3.E10
        FN=TABPP(KK,2)/(FAC*TABPP(KK,1))
        DO 16M=1,L
        FN=FN*BLEND(M,1)*EXPF(-BLEND(M,3)*BK/TMODL(K,L))*BLEND(M,2)
```

```
      DELL=DELL-BLEND(M,4)
      D=(DELL/DELD)**2
      DELL=DELL+BLEND(M,4)
      FTERM=FN*CONST*FXPF(-D)/DFLD
16    FLINF=FLINF+FTERM
      ETA(K)=FLINE/TMODL(K,4)+TMODL(K,5)
71    CONTINUE
      TLINI=(ETA(6)*10.**TMODL(6,1)+ETA(9)*10.**TMODL(9,1))*.5
      TLIN2=ETA(7)*10.**TMODL(7,1)+ETA(8)*10.**TMODL(8,1)
      TLIN3=TLIN2/12.
      TLIN4=TLINI/6.
      TLINE=TLINI+TLIN2-TLIN3+TLIN4
      RINT=0.
      DO 72 K=10,34
      KK=K-1
      JJ=K-2
      TLINI=.5*(ETA(KK)*10.**TMODL(KK,1)+ETA(K)*10.**TMODL(K,1))
      TLIN2=(ETA(JJ)*10.**TMODL(JJ,1)-2.*ETA(KK)*10.**TMODL(KK,1))/12.
      TLIN3=ETA(K)*10.**TMODL(K,1)/12.
      TLINF=TLINE+TLINI+TLIN2+TLIN3
      TL(K)=TLINF*SCALE
      IF(TL(K)-150.)24,24,25
      EXPT=EXPF(-TL(K)/TCONT(1,2))
      F=10.**TMODL(K,1)*EXPT*ETA(K)
```

```
      Y(K)=E(K)*F/TCONT(1,2)
      GO TO 14
25    Y(K)=0.
14    Z=Y(K)*SCALE
72    RINT=RINT+Y(K)
      CORR=-.5*(Y(10)+Y(34))
      DIFF=(Y(34)+Y(10)-Y(33)-Y(11))/12.
      RINT=(RINT+CORR+DIFF)*ARG/FMOD
      RINT=RINT/TCONT(1,3)
41    PUNCH17,RINT,DELL,TCONT(1,2)
17    FORMAT(3E11.4)
      TN=TN+1.
      DELL=DELL-SP
      IF(TN-CN.)73,73,74
74    CONTINUE
74    CONTINUE
      GO TO 81
46    STOP
      END
GO
```

```
      Y(K)=E(K)*F/TCONT(1,2)
      GO TO 14
25    Y(K)=0.
14    Z=Y(K)*SCALE
72    RINT=RINT+Y(K)
      CORR=-.5*(Y(10)+Y(34))
      DIFF=(Y(34)+Y(10)-Y(33)-Y(11))/12.
      RINT=(RINT+CORR+DIFF)*ARG/FMOD
      RINT=RINT/TCONT(1,3)
41    PUNCH17,RINT,DELL,TCONT(1,2)
17    FORMAT(3E11.4)
      TN=TN+1.
      DELL=DELL-SP
      IF(TN-CN.)73,73,74
74    CONTINUE
74    CONTINUE
      GO TO 81
46    STOP
      END
GO
```